Deposit & Copying of Dissertation Declaration

UNIVERSITY OF CAMBRIDGE

Board of Graduate Studies

Please note that you will also need to bind a copy of this Declaration into your final, hardbound copy of thesis - this has to be the very first page of the hardbound thesis.

1 Surname (Family Name)	Forenames(s)	Title
Wylde	George William	Mr

2 Title of Dissertation as approved by the Degree Committee

Mechanotransduction at the nuclear envelope: the role of forces in facilitating embryonic stem cell fate decisions

In accordance with the University Regulations in *Statutes and Ordinances* for the PhD, MSc and MLitt Degrees, I agree to deposit one print copy of my dissertation entitled above and one print copy of the summary with the Secretary of the Board of Graduate Studies who shall deposit the dissertation and summary in the University Library under the following terms and conditions:

1. Dissertation Author Declaration

I am the author of this dissertation and hereby give the University the right to make my dissertation available in print form as described in 2. below.

My dissertation is my original work and a product of my own research endeavours and includes nothing which is the outcome of work done in collaboration with others except as declared in the Preface and specified in the text. I hereby assert my moral right to be identified as the author of the dissertation.

The deposit and dissemination of my dissertation by the University does not constitute a breach of any other agreement, publishing or otherwise, including any confidentiality or publication restriction provisions in sponsorship or collaboration agreements governing my research or work at the University or elsewhere.

2. Access to Dissertation

I understand that one print copy of my dissertation will be deposited in the University Library for archival and preservation purposes, and that, unless upon my application restricted access to my dissertation for a specified period of time has been granted by the Board of Graduate Studies prior to this deposit, the dissertation will be made available by the University Library for consultation by readers in accordance with University Library Regulations and copies of my dissertation may be provided to readers in accordance with applicable legislation.

3 Signature	Date
	20th October 2017

Corresponding Regulation

Before being admitted to a degree, a student shall deposit with the Secretary of the Board one copy of his or her hard-bound dissertation and one copy of the summary (bearing student's name and thesis title), both the dissertation and the summary in a form approved by the Board. The Secretary shall deposit the copy of the dissertation together with the copy of the summary in the University Library where, subject to restricted access to the dissertation for a specified period of time having been granted by the Board of Graduate Studies, they shall be made available for consultation by readers in accordance with University Library Regulations and copies of the dissertation provided to readers in accordance with applicable legislation.

Mechanotransduction at the nuclear envelope: the role of forces in facilitating embryonic stem cell fate decisions

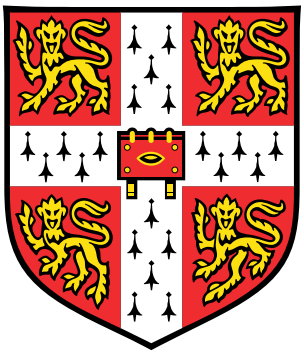

George W. Wylde

Department of Physics
University of Cambridge

This dissertation is submitted for the degree of
Doctor of Philosophy

Christ's College January 2017

Mechanotransduction at the nuclear envelope: the role of forces in facilitating embryonic stem cell fate decisions

George W. Wylde

Summary

While a large body of work has focused on the transcriptional regulation of cellular identity, the role of the mechanical properties of cells and the importance of their physical interactions with the local environment remains less well understood.

In this project, we explored the impact of cytoskeleton-generated forces exerted on the nucleus in the context of early embryonic stem (ES) cell fate decisions. We chose to perturb force generating components in the cytoskeleton notably the molecular motor non-muscle myosin II - and key structural and chromatin binding proteins in the nuclear envelope, notably, the lamins (LMNA), Lamin B receptor (LBR) and components of the LINC complex (nesprins/KASH). The structural proteins in the nuclear envelope regulate both the mechanical response of the nucleus to force and the stabilization of peripheral heterochromatin (repressed genes). Our hypothesis is that reducing forces transmitted directly to chromatin or increasing tethering of peripheral heterochromatin to the nuclear envelope would restrict access to lineage specific genes sequestered at the nuclear lamina and thereby either impair, or delay, differentiation.

We found phenotypes in the capacity of mouse ES cells to specify to the neural lineage following our perturbations: overexpression of LMNA, LBR and KASH proteins resulted in a significant fraction of cells that did not express the neuroectoderm marker Sox1 after four days of differentiation, while inhibiting non-muscle myosin II delayed Sox1 expression in the entire population. Overexpression of LMNA and LBR did not affect the ability of the cells to exit the naive pluripotent state, which raises the possibility that the perturbations are halting the cells in a formative phase prior to lineage specification. Future work will focus on looking at genome-wide transcriptional changes accompanying differentiation combined with an analysis of spatial information of differentially regulated genes.

Declaration

I hereby declare that except where specific reference is made to the work of others, the contents of this dissertation are original and have not been submitted in whole or in part for consideration for any other degree or qualification in this, or any other university. This dissertation is my own work and contains nothing which is the outcome of work done in collaboration with others, except as specified in the text and Acknowledgements. This dissertation contains fewer than 60,000 words including appendices, bibliography, footnotes, tables and equations and has fewer than 150 figures.

George W. Wylde
January 2017

Acknowledgements

First and foremost, I would like to thank my supervisor Dr. Kevin Chalut. Kevin has been a guide and mentor throughout my masters and PhD and I am incredibly grateful for the opportunities he has given me to grow, both personally and professionally. He has mastered the difficult balancing act of giving enough freedom to experiment - both literally and figuratively - without taking his hands off the wheel, and he has always been there to chat - even if the news is the amazing discovery I found last week was a result of mixing up my variables in the analysis...

I would also like to say how grateful I am to the members, past and present, of the Chalut lab - who have supported me with their insights and for all the time they have given to the project. Particular thanks go to the lab wizard - Christophe Verstreken, and to Céline Labouesse, for their advice, company in tissue culture at odd hours of the day, and for their papier-mâché skills.

I am also indebted to Lawrence Bates who, having acquired the unfortunate reputation as a safe pair of hands, had dug me out of numerous technical (I didn't have the correct reagent) and epistamological (I wasn't sure what I was doing) holes, and to Carla Mulas for her rigorous scientific advice.

I would also like to express gratitude to my examiners - Dr. Kristian Franze and Dr. Joe Swift, for their critical appraisal of this project, and to say that I thoroughly enjoyed the resulting discussion.

Finally, I would like to honour my mother and father - without their continued support and encouragement over the years, none of this would have been possible.

Abstract

While a large body of work has focused on the transcriptional regulation of cellular identity, the role of the mechanical properties of cells and the importance of their physical interactions with the local environment remains less well understood.

In this project, we explored the impact of cytoskeleton-generated forces exerted on the nucleus in the context of early embryonic stem (ES) cell fate decisions. We chose to perturb force generating components in the cytoskeleton notably the molecular motor non-muscle myosin II - and key structural and chromatin binding proteins in the nuclear envelope, notably, the lamins (LMNA), Lamin B receptor (LBR) and components of the LINC complex (nesprins/KASH). The structural proteins in the nuclear envelope regulate both the mechanical response of the nucleus to force and the stabilization of peripheral heterochromatin (repressed genes). Our hypothesis is that reducing forces transmitted directly to chromatin or increasing tethering of peripheral heterochromatin to the nuclear envelope would restrict access to lineage specific genes sequestered at the nuclear lamina and thereby either impair, or delay, differentiation.

We found phenotypes in the capacity of mouse ES cells to specify to the neural lineage following our perturbations: overexpression of LMNA, LBR and KASH proteins resulted in a significant fraction of cells that did not express the neuroectoderm marker Sox1 after four days of differentiation, while inhibiting non-muscle myosin II delayed Sox1 expression in the entire population. Overexpression of LMNA and LBR did not affect the ability of the cells to exit the naive pluripotent state, which raises the possibility that the perturbations are halting the cells in a formative phase prior to lineage specification. Future work will focus on looking at genome-wide transcriptional changes accompanying differentiation combined with an analysis of spatial information of differentially regulated genes.

Contents

List of Figures

Outline

Chapter One introduces, motivates and presents the background knowledge pertinent to the this project. I will give an overview of the components, structure and organisation of the nucleus, focusing on the higher-level regulation of transcription at the nuclear envelope in the context of embryonic stem cell differentiation. Secondly I will describe mechanotransduction and how forces might directly influence nuclear dynamics and facilitate transcriptional changes.

Chapter Two will present data from the start of the project exploring chromatin mobility. The hypothesis and goals of the project will also be introduced and discussed.

Chapter Three presents the materials and general methods used throughout the project. Methods that are specific to individual Chapters are discussed within the Chapters themselves.

Chapter Four examines nuclear shape changes and outlines our methods for their characterisation. We explore which elements in the actomyosin cytoskeleton are responsible for driving nuclear shape changes and determine whether there is a relationship between local distributions of actin and fluctuations in the nuclear envelope.

Chapter Five introduces the perturbations of the nuclear envelope. I will explore how the perturbations affect nuclear shape, dynamics and look at whether they can modulate the distributions of epigenetic histone modifications, primarily focusing on repressive histone modifications at the nuclear periphery.

Chapter Six presents data that explores how our perturbations of the nuclear envelope and nuclear shape changes influences the capacity of embryonic stem cells to specify to the neural lineage. I also explore whether the perturbations affect the ability to exit the naive pluripotent state.

Chapter Seven presents data from current work followed by an overall discussion of what was achieved in the project and to what extend the goals have been met. I tie together and provide a summary of each Chapter and discuss the future directions in which the work can be developed.

Chapter 1

Introduction and background

Embryonic stem (ES) cells possess the capacity to self-renew and to become any cell type in the body. The potential to exploit these properties makes them a powerful tool. Firstly, embryonic stem cells can be used to model disease; they can be genetically modified in-vitro and re-introduced into the developing embryo to create model organisms. The genetic modifications create the diseased state in the organism (e.g. mouse), mimicking that of humans. Such model organisms provide a powerful platform with which to study disease and devise treatments. Secondly, embryonic stem cells can be used to study embryogenesis, knowledge of which is invaluable for both understanding abnormal developmental processes and manipulating cell fate for therapeutic purposes. To this end, embryonic stem cells have enormous potential to enhance the field of regenerative medicine. Lastly, embryonic stem cells can provide an unlimited source of specialised adult cells with which to discover and test new drugs.

A thorough understanding of how embryonic stem cells regulate themselves and determine their fate is a key research goal. One approach has been to dissect the genetic regulatory networks that define embryonic stem cell identity and underpin fate transitions. A decade ago, this led to the discovery of four key transcription factors which, when expressed in somatic cells, reprogram them back into an embryonic stem cell like state (Takahashi & Yamanaka, 2006). With the development of next generation sequencing technologies, coupled with advances in bioinformatics, attention has turned to acquiring data of global transcriptional changes during development at the resolution of individual cells (Wen & Tang, 2016). These studies promise to provide deep insights into the temporal dynamics of embryonic stem cell differentiation (Semrau *et al.* , 2016) (Guo *et al.* , 2017).

A second approach is to explore how embryonic stem cells interact with their surroundings. An embryonic stem cell is not an isolated unit; it must be able to receive biochemical and biophysical cues from the local environment and respond at both the protein and transcriptional levels. While biochemical signalling pathways have been extensively studied, the mechanisms by which the cell transduces and responds to forces, generated and applied both internally and externally, are not as well understood. Mesenchymal stem cells have been shown to sense the physical properties of the local micro-environment - such as stiffness and geometry - by actively exerting forces on the surrounding matrix which, in turn, can direct their fate (McBeath *et al.* , 2004) (Engler *et al.* , 2006). The mechanisms through which forces manipulate cell fate, however, have remained largely elusive. Recent work has highlighted the importance of forces acting on the nucleus: it has been shown that applying mechanical strain to human epidermal multipotent stem/progenitor cells can block the expression of lineage commitment genes by directly reorganising chromatin. This reorganisation is mediated by mechanically sensitive components of the nuclear envelope (Le *et al.* , 2016).

The organisation of chromatin and the structure of the nuclear envelope in embryonic stem cells, however, differs from that of more specialised stem cells and somatic cells. Embryonic stem cells possess a more open and dynamic chromatin structure (Meshorer *et al.* , 2006) (Gaspar-Maia *et al.* , 2011). Major structural proteins, e.g. Lamin A and C, which are implicated in mechanical sensing (Swift *et al.* , 2013) (Buxboim *et al.* , 2014), are also expressed at low levels and largely absent from the nuclear envelope (Constantinescu *et al.* , 2006) (Eckersley-Maslin *et al.* , 2013). It is unknown whether embryonic stem cells possess similar mechanical sensing pathways and, given the differences in nuclear organisation, what effect they might have on the function of the cells if they are present. The goal of this project is, therefore, to explore the role of forces acting on the nuclei of embryonic stem cells in the context of embryonic stem cell fate decisions.

1.1 Embryonic stem cells

Mouse embryonic stem cells are isolated from the inner cell mass of the pre-implantation blastocyst at embryonic day 3.5 (E3.5) and can be maintained in *in vitro* culture (Evans & Kaufman, 1981) (Martin, 1981). ES cells are characterised by their capacity to indefinitely self-renew and to form

chimeras, contributing to all somatic cell lineages and the germ line, a property known as pluripotency (Nichols & Smith, 2012). *In vitro* culture of embryonic stem cells provides several advantages over *in vivo* studies, an important proponent of which is the ability to fine-tune the local microenvironments in which the cells reside. This has allowed the processes that govern the establishment, regulation and subsequent exit from the pluripotent state to be more readily explored. Advances in mouse ES cell culture have led to the development of the medium known as 2i (Ying *et al.* , 2008): by combining chemically-defined base medium (N2B27) with inhibitors of mitogen-activated protein kinase (MAPK) and glycogen synthetase kinase-3 (GSK3) signalling pathways, mouse embryonic stem cells are restricted to a transcriptionally homogeneous naive pluripotent state. Additionally, activation of the transcription factor STAT3 by adding leukaemia inhibitory factor (LIF) enhances mouse ES cell proliferation and inhibits differentiation (Ying *et al.* , 2003).

Differentiation is a tightly regulated process that relies on external chemical and physical cues from neighbouring cells and the extracellular matrix. *In vitro*, mouse ES cell differentiation is coupled to changes in cell morphology that accompany global transcriptional changes. Figure 1.1 outlines the model of the initial phases of mouse ES cell differentiation, prior to lineage specification:

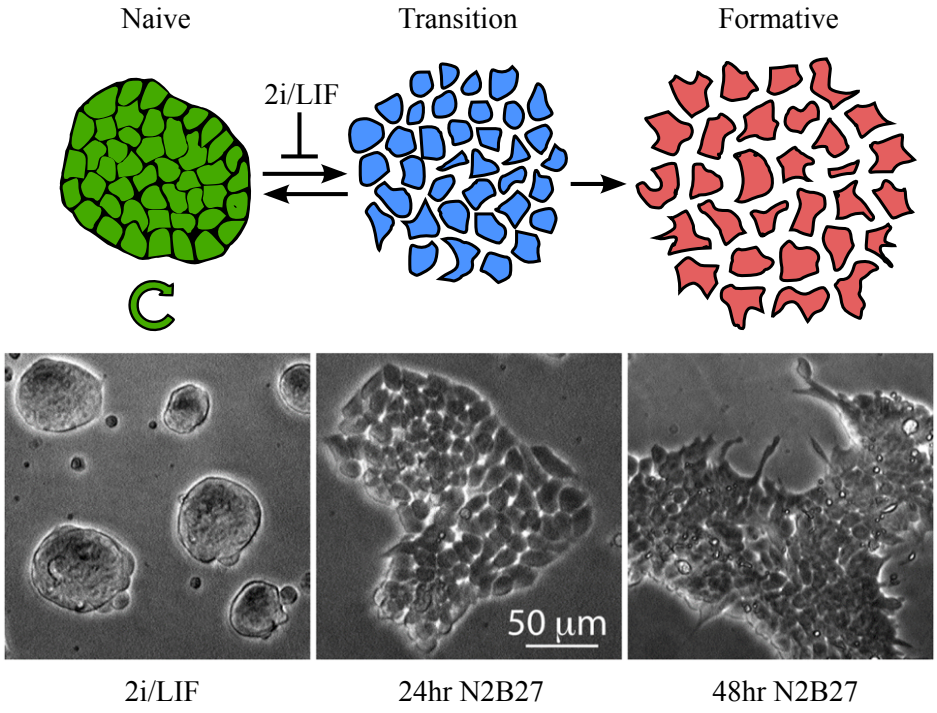

Figure 1.1: Mouse ES cell differentiation and morphology. ES cells are restricted to the naive pluripotent state by culturing in 2i/LIF where colonies are round and tight. During differentiation, the colonies break apart and flatten; after 24hrs in N2B27 the cells are transiting between the naive phase and the formative phase which represents the final timepoint that naive pluripotency can be recovered by adding 2i/LIF. After 48hrs in N2B27 the cells are in the formative phase prior to lineage specification.

Upon removal of the 2i inhibitors and LIF, mouse ES cells start to disassemble their naive pluripotency network, shutting down naive pluripotency factors such as Nanog and Klf4. This process is largely complete after 24 hours and the cells are in a transition phase after which the naive state can no longer be recovered by re-introducing the 2i inhibitors. The cells then enter a formative phase, transiently expressing factors such as Pou3f1 and Otx2, where they gain the capacity to rapidly respond to differentiation signals. The end of the formative phase is marked by linage commitment and a functional loss of germ-line capacity, which occurs roughly 72 hours after 2i/LIF withdrawal. Neural lineage commitment is marked by expression of the transcription factor Sox1. This is the default lineage that ES cells will commit to when cultured in N2B27 *in vitro*. It is worth mentioning that the cells may be restricted to the pluripotent state by culturing in 2i without LIF and that this speeds up exit from naive pluripotency by 12 hours.

1.2 The organisation of the nucleus

The nucleus is a complex and highly organised organelle. At a fundamental level the bulk of the nucleus is made up of negatively charged DNA wrapped around positively charged proteins called histones. The DNA and associated proteins, collectively known as chromatin, can compact by coiling around itself at multiple length scales (heterochromatin), or unwind where it can be easily accessed by the transcriptional machinery of the nucleus (euchromatin). Chromosome conformation capture technology has revealed that chromosomes exhibit the properties of a fractal globule, possessing conserved internal structure with DNA organised into domains on the megabase scale (Lieberman-Aiden *et al.* , 2009). Increasing the resolution to look at individual cells (single cell Hi-C) has found that, while intra-chromosomal domain structure is well conserved, there is significant variability in the organisation of chromosome territories between cells (Nagano *et al.* , 2014). A recent study has shown that the chromatin in human embryonic stem cells undergoes significant re-organisation during lineage specification. While chromosomal domain boundaries remain intact there is significant re-structuring both within and between domains (Dixon *et al.* , 2015).

1.2.1 Histone structure and modifications

Histone proteins are an integral component in the organisation and structure of DNA and form a template upon which information can be stored and passed to daughter cells. Information is encoded by modifying the structure of histone proteins which, in turn, influences whether the gene that they are bound to is transcribed, or repressed. Histone proteins form nucleosomes, which comprise a core histone 3/histone 4 (H3/H4) tetramer flanked by two histone 2A-histone 2B (H2A-H2B) dimers, around which the DNA is wrapped - a diagram of which is shown below in Figure 1.2. Every histone possesses an amino acid tail which protrudes from the nucleosome that can be enzymatically modified. The most prevalent types of histone modification are the acetylation and methylation of lysine (K) residues. Histone acetylation is enriched in open chromatin regions and at active sites of transcription while histone methylation, dependent on the number of methyl groups and on which residue, is associated with both transcriptional activation and repression. Histone ubiquitination has been implicated in both the regulation of transcription and the DNA damage response (Cao & Yan, 2012). The most highly modified histone is H3 which can drive both gene repression

and heterochromatin formation through methylation of H3K9 and H3K27 (H3K9me2/3 and H3K27me3) or gene activation by methylation of H3K4 (H3K4me1/3) (Bannister & Kouzarides, 2011).

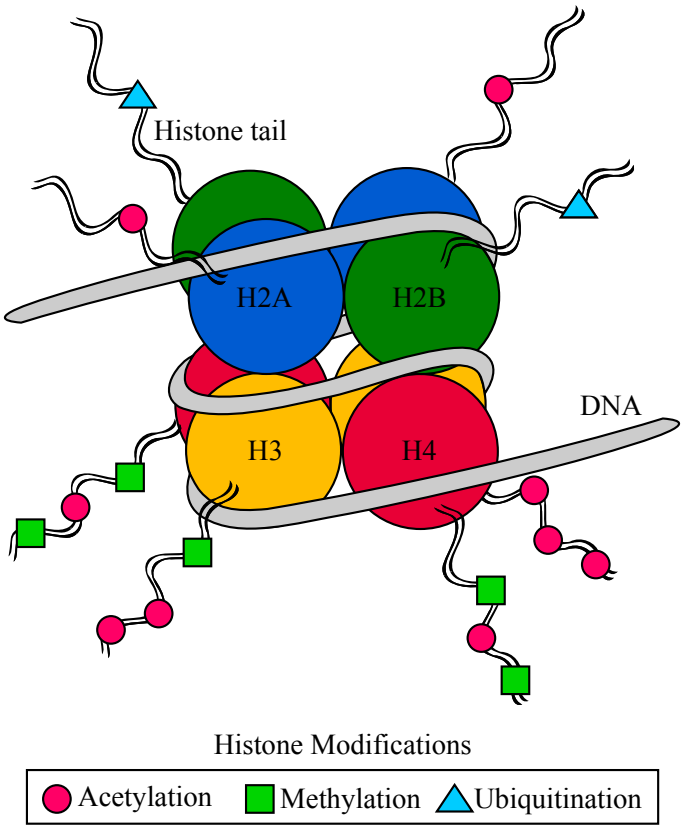

Figure 1.2: Nucleosome structure and histone modifications.

The information contained within the distribution of histone modifications is passed on to daughter cells during cell division. In contrast to semi-conservative replication, the method by which the genetic code is copied with one DNA strand acting as the template for the new strand, the inheritance of histone modifications is a complicated affair with multiple mechanisms. When the DNA is copied, parental histones are segregated and deposited onto both the template DNA and the newly synthesised strand (Annunziato, 2015). Histones are released ahead of the replication fork and deposited behind with the help of a network of histone chaperone proteins. During DNA replication, histone chaperone proteins ensure the correct interactions between histones and DNA and guide chromatin assembly (Burgess & Zhang, 2014). One mechanism of epigenetic inheritance of histone modifications is the dilution model: prior to DNA synthesis, sequences of DNA are en-

riched in their constituent histone modifications - in particular sequences containing H3K4me3 and/or H3K27me3 (Lanzuolo *et al.* , 2012). These modifications are then diluted out when the histones are segregated at the replication fork. This ensures that the distribution of histone modifications is passed on accurately, and that both template and newly synthesised DNA are not without the requisite modifications for any length of time - which might otherwise alter their regulation. Another mechanism relies on the recruitment of histone modifying enzymes to the replication fork, mediated through interactions with the replication machinery (Moldovan *et al.* , 2007). These enzymes then re-establish the histone modifications during DNA synthesis (Peng *et al.* , 2015) (Lowe *et al.* , 2016). Finally, propagation of DNA methylation during replication, through DNA methylases recruited to the replication fork, act as a template on which histone modifying enzymes are recruited and subsequently act to re-establish the post-translational histone modifications (Zhang *et al.* , 1999) (Liao *et al.* , 2015).

1.2.2 The nuclear lamina

In the vast majority of cell types the heterochromatin resides at the nuclear periphery where it interacts with the nuclear lamina. The nuclear lamina is formed from a network of intermediate filament proteins that forms scaffold beneath the nuclear envelope. The primary constituents of the nuclear lamina are A-type (LMNA) and B-type (LMNB1 and LMNB2) lamins. Lamins A and C are created by alternate splicing of the *Lmna* gene and are developmentally regulated whereas the B-type lamins are ubiquitously expressed in all cell types. It has been shown that the A-type lamins regulate nuclear mechanics and contribute to nuclear stiffness, whereas the B-type lamins contribute to nuclear integrity, but not to stiffness (Lammerding *et al.* , 2006). In a later study it was found that the levels of LMNA scale with tissue elasticity: cells that undergo high strain rates, e.g. muscle and connective tissue, express LMNA at high levels. It is thought that, because LMNA stiffens the nucleus, high levels of LMNA protect the nucleus from rapid deformation and subsequent DNA damage (Swift *et al.* , 2013). It was originally thought that ES cells do not express LMNA (Constantinescu *et al.* , 2006); however, it has been shown by the authors in Eckersley-Maslin *et al.* (2013) that LMNA is present, but expressed at low levels. Nevertheless, in ES cells, the B-type lamins are the dominant lamins and their nuclei are correspondingly soft.

The lamins play an integral role in orchestrating higher-order chromatin organisation, regulating transcription and DNA replication (Prokocimer *et al.* , 2009). In particular, the lamins are implicated in binding peripheral heterochromatin, anchoring it to the nuclear envelope where transcriptional repression is stabilised (Peric-Hupkes & van Steensel, 2010). Studies have shown that proximity to the nuclear envelope plays an active role in repressing genes; movement of regions of chromatin to and from the nuclear envelope allows genes to be reversibly silenced (Finlan *et al.* , 2008) (Reddy *et al.* , 2008) (Zullo *et al.* , 2012). Figure 1.3 depicts two mechanisms proposed by Solovei *et al.* (2013) for tethering peripheral heterochromatin; a lamin b receptor tether (LBR) that interacts with B-type lamins and an A-type lamin tether. As ES cells are largely deficient in LMNA, the LBR tether might act as the primary mechanism.

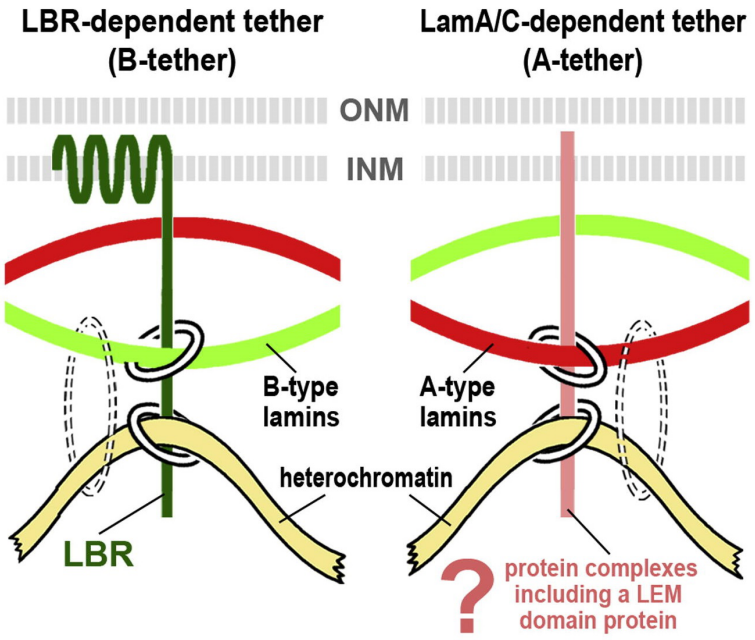

Figure 1.3: Mechanisms of heterochromatin tethering to the nuclear envelope. The nuclear lamins are thought to be responsible for anchoring heterochromatin to the nuclear envelope through independent A-type and B-type lamin mechanisms. ES cells do not express A-type lamins which would make the proposed LBR tether the dominant mechanism. Solid circles represent binding interactions. The dotted circles indicate that direct chromatin binding of B-type and A-type lamins is not sufficient for, but might synergistically enhance, heterochromatin tethering. Figure taken from Solovei *et al.* (2013).

1.2.3 Lamin associated domains and differentation

Chromatin interacts with the nuclear lamina in regions termed lamin associated domains (LADs). LADs are enriched with the repressive histone modifications H3K27me3, H3K9me2 and H3K9me3, which are necessary for the binding of chromatin to the nuclear lamina, facilitated by the recruitment of lamin/chromatin binding proteins (Guelen *et al.* , 2008)(Kind *et al.* , 2013)(Harr *et al.* , 2015).

The technique known as Dam-ID has allowed the interactions between the nuclear lamina and the LADs to be mapped dynamically. Dam-ID relies on the fusion of DNA adenine methyltransferase (Dam), absent in eukaryotes, to a protein of interest (Vogel *et al.* , 2007). Whenever the fusion

protein is in close proximity to DNA, the palindromic sequence GATC is methylated. The genome is then sequenced and regions that are enriched in DNA methylation are known to have been in close proximity/interacted with the fusion protein. A challenge to this technique is that any freely diffusing Dam (there will always be some) will methylate everywhere in the genome. This can be controlled for by expressing freely diffusing Dam in a control population and using the results to normalise the data. The authors in Peric-Hupkes *et al.* (2010), fusing Dam with lamin B1, explore how the LADs change dynamically during ES cell neural differentiation - Figure 1.4. In the naive pluripotent state they show that the nuclear lamina is enriched in repressed neural lineage genes while the pluripotency genes are internalised in the nucleus. During differentiation this organisation reverses: the pluripotency genes become enriched at the nuclear envelope and are concomitantly silenced, while the lineage genes are unlocked and move inwards. The authors also find that not every gene is expressed when unlocked from the nuclear lamina, but can be poised for transcription at a later stage in the differentiation process.

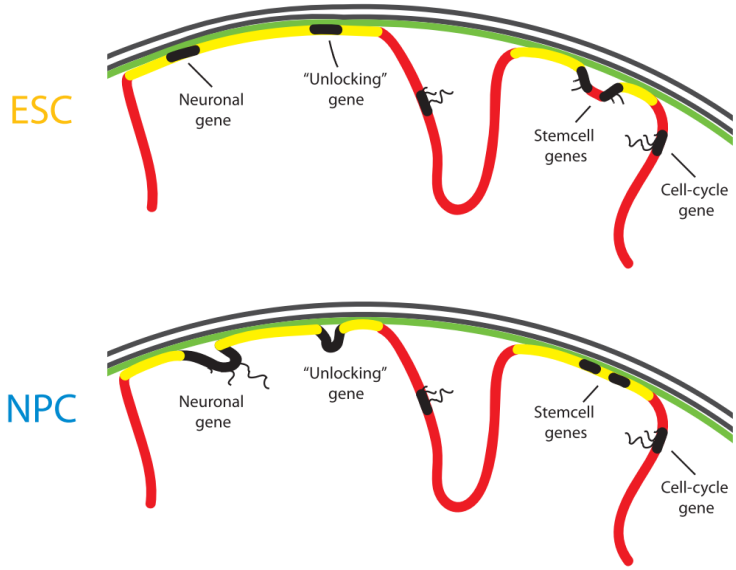

Figure 1.4: Lineage and pluripotency gene positioning at the nuclear envelope during neural differentiation. Neural lineage genes are locked at the nuclear periphery in the pluripotent state. During differentiation into neural precursor cells (NPCs) the stem cell genes are silenced and are sequestered to the nuclear lamina while the neural genes are unlocked and move inwards, where they are transcribed or poised for activation at a later stage of differentiation. Figure taken from Peric-Hupkes *et al.* (2010).

1.3 The cytoskeleton

The ability of a cell to generate and respond to forces necessary for interacting with the physical properties of the local micro-environment is governed, in part, by the complex and dynamic interactions of a set of regulatory proteins and filamentous polymers in the cytoplasm, known collectively as the cytoskeleton. The cytoskeleton is not a rigid structure: it is highly adaptable and is continuously being re-organised in order to meet the needs of the cell, both external - responding to cues in the environment (e.g. the need for movement/migration) - and internal - providing structure and maintaining cellular compartments/organisation (Fletcher & Mullins, 2010).

The filamentous polymers that make up the cytoskeleton fall into one of three categories - microtubules, actin filaments and intermediate filaments, with each possessing distinct physical properties. The most rigid of the polymers are the microtubules, which have a persistence length in the region

of 4-8 mm (Gittes *et al.* , 1993) (Janson & Dogterom, 2004) and are capable of bearing compressive loads (Brangwynne *et al.* , 2006). Persistence length is a mechanical property which provides a measure of polymer stiffness - it is defined as the length at which correlations in the direction of the tangent to the polymer are lost. During mitosis and meiosis, microtubules form a crucial component in the cellular replication machinery where they are involved in the alignment and separation of chromosomes (Inoué & Salmon, 1995) while, during interphase, they provide the backbone for inter-cellular trafficking. Microtubules possess complex growth dynamics: they switch from slowly assembling to rapidly disassembling during an event known as a 'catastrophe' (Mitchison & Kirschner, 1984). By altering the kinetics of polymerisation, depolymerisation and the rate of catastrophe, the cell controls the structure and organisation of the microtubule network.

The second type of cytoskeletal polymer are the actin filaments which, possessing a persistence length of approximately 20 µm, are much less rigid than microtubules. Actin filaments are capable of forming cross-linked networks which are more rigid and able to exert and propagate stresses when compared with individual filaments. The organisation of the actin network is controlled by the regulation of polymerisation and cross-linking: actin can assemble in tightly polarised bundles which can support filopodia and form contractile stress fibres (Mattila & Lappalainen, 2008)(Pellegrin & Mellor, 2007), or be assembled into a branched network that is required for cell migration (e.g. lamellopodia) or phagocytosis (May & Machesky, 2001).

The final type of polymers are the intermediate filaments which are less rigid than actin and can be cross-linked together and interact with the actin and microtubule networks through plectins (Wiche, 1998). An example of an intermediate filament network has already been introduced in the form of the lamins that underlie the nuclear envelope.

The actin and microtubule networks are capable of bearing and propagating forces generated through the action of molecular motors, the direction of movement of which is established by the polarity of the microtubule and actin filaments. Motors specific to microtubules - from the dynein and kinesin family of proteins - are used to carry cargo around the cell as well as play an integral role in assembling the microtubule network. Motors specific to actin - from the myosin family of proteins - also play a critical role in the assembly of the actin cytoskeleton and, by acting on neighbouring actin filaments, create contractility in the cell. Myosin-generated tension exerts forces both on the extracellular environment and on intracellular structures,

for instance, to stabilise both cell-cell junctions and create mature focal adhesions (Cavey & Lecuit, 2009)(Oakes *et al.* , 2012).

1.4 Mechanotransduction

Mechanotransduction is the process of converting mechanical stimuli into signals that elicit a cellular response. In a majority of cases, forces are converted into biochemical signals, mediated by proteins that undergo structural rearrangement and a concomitant shift in function. To name just a few examples: pressure waves in the cochlea are transduced into electrical nerve impulses (Hudspeth, 2014); ion channels on the surface of the cell open in response to membrane tension (Martinac, 2004); and shear stress exerted by the blood on epithelial cells regulate arterial structure and atherogenesis (Hahn & Schwartz, 2009). While conversion of forces into biochemical signals is the most extensively studied mechanism of mechanotransduction, it has been postulated that forces may be propagated through the cytoskeleton to the nucleus where they would influence chromatin structure and transcription directly (Wang *et al.* , 2009). Figure 1.5 outlines the cellular components involved in this process:

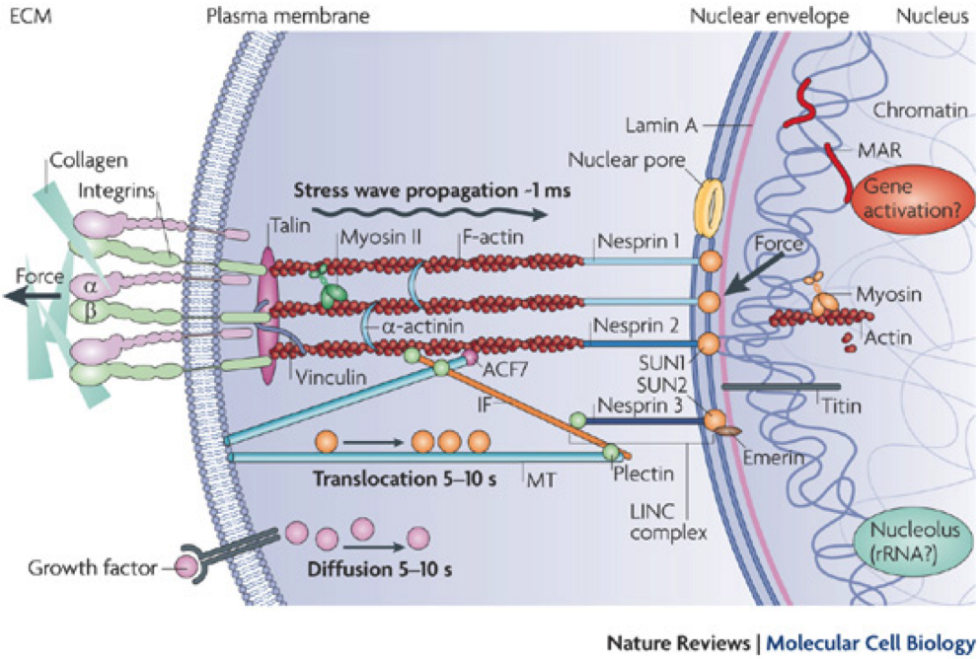

Figure 1.5: Propagation of forces to the nucleus. There is a direct physical link between the surface of the cell and the chromatin in the nucleus. Forces can be propagated through the cytoskeleton, when under tension, to the nucleus directly impacting the structure of chromatin. Figure taken from Wang *et al.* (2009).

There is a direct physical link from adherens junctions and focal adhesions on the surface of the cell to the chromatin in the nucleus: adherens junctions and focal adhesions that are attached, respectively, to neighbouring cells or the extracellular matrix are bound by their cytoplasmic domain to actin filaments which, in turn, bind a family of proteins called the nesprins. The nesprins localise to the outer nuclear membrane (ONM) where their KASH domain at the C-terminal end binds the luminal SUN domain of the inner nuclear membrane (INM) proteins SUN1 and SUN2, forming the LInker of Nucleoskeleton and Cytoskeleton (LINC) complex, that interacts with the nuclear lamina and chromatin. The nesprins are also capable of binding other components of the cytoskeleton, with four separate nesprin genes currently identified: the N-terminal domains of nesprins 1 and 2 bind actin; nesprin 3 binds plectin and by extension the intermediate filaments; and nesprin 4 binds to a subunit of the molecular motor kinesin-1 which interacts with the microtubule network (Rajgor & Shanahan, 2013). A physical connection is, by itself, not sufficient to transmit forces: by analogy with two

people pulling on opposite ends of a rope, if the rope is coiled and pulled by one party, the other will not experience a force until the rope has uncoiled and there is tension. Similarly, there must be tension in the cytoskeleton to transmit forces exerted on the adherens junctions (or generated internally) to the nucleus. This tension is, to a large extent, generated by the action of molecular motors, notably non-muscle myosin II, which pull on neighbouring actin filaments, in addition to the forces created by the polymerisation of actin.

The nuclear lamina plays an important role in mediating forces transmitted through the LINC complex. In Section 1.2 we discussed the finding that LMNA scales with tissue elasticity and that, in high strain environments, high levels of LMNA might protect the nucleus from deformation and DNA damage. The authors in Swift *et al.* (2013) show, specifically, that LMNA is mechanically regulated. The mechanism for this is as follows: when the nuclear lamina is put under tension from external forces, LMNA in the network changes its structural conformation and is no longer recognised by the kinase responsible for its phosphorylation, which leads to solubilisation from the nuclear lamina and degradation. While under tension and unfolded, the half-life of LMNA increases dramatically and the concentration of LMNA builds up in the nuclear lamina. When the concentration of LMNA is high enough, the tension per molecule drops and LMNA adopts its unstressed conformation where it is then targeted for phosphorylation and degradation. The concentration of LMNA in the nuclear envelope is tuned and scales with the magnitude of forces on the nucleus where it buffers the forces transmitted to the chromatin.

Mechanical stress that acts directly on chromatin has the potential to alter and facilitate transcriptional changes. Recent work by Le *et al.* (2016) has highlighted the importance of mechanical forces acting at the nuclear envelope by uncovering a mechanosensitive pathway in mouse epidermal stem cells that influences lineage commitment and tissue morphogenesis. The authors show that exposing epidermal stem cells to cyclic mechanical strain results in an accumulation of polymerised actin and non-muscle myosin IIA at the nuclear envelope and the redistribution of emerin from the inner nuclear envelope to the outer nuclear envelope. Emerin depletion at the inner nuclear membrane led to a loss of H3K9me2/3 and a re-arrangement of chromatin at the nuclear envelope (H3K9me2/3 is required for LAD/nuclear lamina tethering). The loss of H3K9me2/3 was compensated for by an increase in H3K27me3, which maintained transcriptional repression of heterochromatin.

Force driven enrichment of H3K27me3 at lineage specific genes resulted in a block in lineage specification, which was abrogated by small molecule inhibition of non-muscle myosin IIA.

In addition, a recent study by Tajik *et al.* (2016) has provided further evidence for the importance of forces acting on chromatin in the regulation of transcription. The authors used ferromagnetic beads attached to the surface of epithelial (CHO) cells via focal adhesion complexes to apply cyclic stresses to the cells. Chromatin was visualised with enhanced green fluorescent proteins (EGFP) targeted to evenly spaced sites within BAC constructs stably integrated into the CHO cell genome, the relative movement of which provided a read-out of chromatin deformation. The authors found that the distance between neighbouring EGFP spots was found to be a function of the cyclic stress and that, when a stress of constant amplitude was applied, all EGFP spots moved in the same direction synchronously but with a phase lag. Gene expression of the transgene inserted in the BAC constructs (dihydrofolate reductase - *DHFR*) was found to increase when cyclic strain was applied to the cells (by RNA fluorescence *in-situ* hybridisation). Additionally, quantification of RNA Polymerase II binding near GFP spots showed an increase five seconds after the application of stress. This provides strong evidence to suggest that the transcriptional machinery is poised to assemble and initiate transcription as the chromatin is unfolded and made accessible by forces acting directly on it. Finally, the authors showed that targeting actomyosin contractility or disrupting actin filaments with small molecule inhibitors led to a downregulation in *DHFR* expression, while increasing contractility led to an upregulation.

Taken together these studies highlight the importance of forces, propagated through the cytoskeleton when under tension, acting directly on chromatin in the mechanical regulation of transcription and cell fate decisions.

Chapter 2

Materials and methods

A list of kits and reagents used can be found in Appendix A.6. All other chemicals were obtained from Sigma-Aldrich or Thermo Fisher Scientific.

2.1 Cloning

Plasmids were constructed using either the Invitrogen™ Gateway™ cloning system or by In-Fusion® (Clontech®). Inserts were created by PCR amplification with Q5 Hot Start High-Fidelity DNA Polymerase using either mouse embryonic fibroblast (MEF) cDNA or the relevant plasmid as a template. The inserts were run on a 1% agarose gel and purified using a QIAquick Gel Extraction Kit (Qiagen). Plasmids were transformed into E. cloni 10G Chemically Competent DUOs, extracted using either a Plasmid Mini or Maxi Kit (Qaigen) and submitted for verification by Sanger sequencing.

A list of the oligonucleotides and plasmids can be found in Appendix A.1. Plasmids listed as Gateway cloned were created by cloning the desired insert into pDONR221 and sequencing, followed by moving into pPB-TAP IRI.

2.2 Routine cell culture

ES cells were restricted to the naive pluripotent state by culturing in N2B27 medium supplemented with inhibitors of mitogen-activated protein kinase signalling (PD03) and glycogen synthase kinase-3 (Chiron), in addition to the self-renewal cytokine leukaemia inhibitory factor (LIF), referred to as 2i/LIF. The recipe is detailed in Appendix A.2. Media was kept for up to one week in the fridge and warmed to room temperature before use.

Cells were passaged every three days and the media replaced after two days. Accutase was used to dislodge and separate the cells and removed by dilution with DMEM and centrifugation at 300 g for 3 minutes. For routine culture the cells were split using a dilution between 1/10 and 1/20 (judged by eye) dependent on the density. When accuracy was required, cells were counted using a Vi-CELL Cell Viability Analyser (Beckman Coulter).

2.3 Cell lines

The E14 Tg2a mouse ES cell line was used to generate the following stable lines:

- LMNA inducible overexpression (Tet-On)
- LBR inducible overexpression (Tet-On)
- mRFP-KASH inducible overexpression (Tet-On)
- mRFP-KASHΔL inducible overexpression (Tet-On)
- mRFP-SR-KASH (Tet-On)
- tagRFP-LMNB1
- tagRFP-LMNB1 LifeAct-GFP

The H2B-tomato ES cell line, a kind gift from J.Nichols (Morgani *et al.* , 2013), was used to generate the H2B-tomato LifeAct-GFP cell line. Plasmids were transfected using Lipofectamine 2000 Transfection Reagent and selected for using the appropriate antibiotic(s) with final concentrations of:

- Zeocin 100 µg/ml
- Hygromycin B 150 µg/ml
- Puromycin 1 µg/ml
- Geneticin (G418) 200 µg/ml

The LMNA and LBR lines were subcloned by passaging 1000 cells from the polyclonal line into a 10 cm dish. The cells were allowed to grow for a week and then picked in a laminar flow hood into a 96-well plate and expanded. Early expansions from a 96-well plate up until a 24-well plate were done using accutase without centrifugation in order to minimise cell loss; the

accutase was added to the cells and then diluted directly with culture media and transferred to a new well. Clonal lines were analysed by qPCR for the levels of overexpression and several pluripotency factors (Nanog/Klf4) in 2i/LIF and selected based on a comparison with the parental E14 tg2a cell line.

2.3.1 Proliferation rates

To measure proliferation rates, 4×10^4 cells were plated into (each of) 6 wells of a 12 well plate in 2i/LIF, per condition. The cells were harvested at 20 hours intervals and counted while suspended in 1ml accutase in order to avoid any loses in centrifuging and resuspension - this was not found to affect cell viability in the short term. All cell counts were obtained by using a Vi-CELL Cell Viability Analyser (Beckman Coulter). Cell counts were then plotted on a log scale against time and the doubling time extracted from the gradient.

2.4 Immunofluorescence

Immunofluorescence (IF) was performed using the following modified protocol from Cell Signalling Technologies[1]:

Blocking Buffer: 1X PBS, 0.3% Triton X-100, 5% normal serum.

Antibody Dilution Buffer: 1X PBS, 0.1% Triton X-100, 1% BSA.

1. Fix cells in 4% Paraformaldehyde for 10 min. Wash x3 with PBS.
2. Block for 1 hr at room temperature.
3. Remove blocking buffer and incubate with primary antibody overnight at 4°C or for 2 hr at room temperature. Wash 3x with PBS.
4. Incubate with secondary antibody for 1 hr at room temperature. Wash 2x with PBS.
5. Wash for 10 min with Hoechst staining solution (1 µg/ml) twice. Wash 2x with PBS.

Samples were imaged in PBS. Antibodies and their working dilutions are listed in Appendix A.3.

[1] "https://www.cellsignal.com/contents/resources-protocols/immunofluorescence-general-protocol/if" accessed Sept.2016

2.5 Fluorescence recovery after photobleaching

H2B-eGFP ES cells were passaged onto ibidi dishes at a density of 1×10^4 cells/cm^2 in 2i/LIF, or directly into N2B27 when required. FRAP was performed using an Andor Revolution XD spinning disk confocal with a Yokogawa CSU-X1 head using a 63x NA 1.4 OIL immersion objective. An environmental chamber was used to keep the cells at 37°C and supplied with 7% CO_2. A region of interest (ROI) was selected within the nucleus and two images taken before bleaching the ROI with 100% laser power. Post-bleach images were taken every second for the first 60 seconds and then at 20 second intervals for the next 180 seconds.

Image analysis was performed using ImageJ and MATLAB. FRAP series were imported into ImageJ and the bleaching frames discarded. The StackReg plugin was run to correct for cell rotation or translation. The FRAP Norm plugin was used to calculate the FRAP intensity using a double normalisation procedure outlined by Phair *et al.* (2004). This required manually selecting the following regions: 'FRAP Region' (Intensity I_t) - bleached region of the nucleus, 'Background' (Intensity B_t) - an area outside the cell and 'Whole cell' (Intensity N_t) - region encompassing the nucleus. These regions were selected from the first post-bleach image and the image series checked to ensure that they remained correct for the rest. The normalization procedure was as follows: for every post-bleach image the average whole cell intensity was divided by its pre-bleach value (N_t/N_0). This corrected for acquisition bleaching. This factor was then multiplied by intensity of the bleached region of the cell, normalised to its pre-bleach value (I_t/I_0). Before both of these operations, the relevant reference intensities were subtracted, giving the final 'double normalized' FRAP intensity as:

$$I_{t-Norm} = \frac{N_0 - B_0}{N_t - B_t} \times \frac{I_t - B_0}{I_0 - B_0} \tag{2.1}$$

The data sets were then imported into MATLAB.

2.6 Quantitative real-time PCR

RNA was extracted using a RNeasy Mini Kit (Qiagen) with the optional on-column DNase digestion steps included. cDNA was made using a SuperScript III First-Strand Synthesis Kit (Invitrogen) in 20 µl reactions with the amount of template RNA kept constant across the experiment - the lowest RNA concentration obtained was used to determine the total amount used,

anywhere between 100 ng and 1 µg. The cDNA was then amplified in 12 µl reactions (in triplicate) with TaqMan probes using GAPDH as an internal control. The choice of GAPDH as an internal control was verified through RNA-Seq data (not shown). A list of TaqMan probes used can be found in Appendix A.5.

The data was analysed by using the cycle threshold (C_T) values to calculate the fold-difference between the gene of interest and the internal GAPDH control for each reaction as follows:

$$Fold\ of\ GAPDH = 2^{-(C_T(Target) - C_T(GAPDH))} \tag{2.2}$$

The mean and standard deviation of the triplicate reactions was taken and normalised to the highest expression level of the control samples and then plotted on a bar graph.

2.7 siRNA knockdown

Knockdown was performed by transfecting E14 Tg2a cells using Lipofectamine RNAiMAX with siRNA at a concentration of 20 µmol. The Lipofectamine/siRNA mix was added to cells after passaging at a density of 3×10^4 cells/cm^2. The volumes for a well of a 24-well plate are listed in Appendix A.4. The ES cells were transfected in the evening and the lipofectamine was removed early the following morning to limit toxicity. siRNA knockdown efficiency was analysed using qPCR or by immunofluorescence when possible.

2.8 Nuclear shape changes

2.8.1 Cell culture and imaging

Nuclear shape experiments were performed on cells either in 2i/LIF or after 48 hrs in N2B27. For experiments in 2i/LIF, ES cells were passaged six hours before imaging onto laminin-coated ibidi dishes (overnight incubation at 10 µg/ml at 4°C) at high density ($\sim 3 \times 10^4$ cells/cm^2). For experiments conducted after culturing in N2B27 for 48hrs, cells were seeded into N2B27 on laminin coated ibidi dishes at a density of 1×10^4 cells/cm^2. Live imaging was performed using either a Leica SP5 confocal microscope or a Zeiss LSM 710 with a 63.0x NA 1.4 oil immersion objective. An environmental chamber was used to keep the samples at 37°C and supplied with 7% CO_2. Cell lines

that did not possess a fluorescent nuclear marker were incubated with 2 µM SiR-Hoechst for 45 min before washing to label the DNA. Images were acquired every 10 seconds for either 5 or 10 minutes using as low a laser power as possible to limit phototoxicity. Samples were imaged for a maximum of one hour.

2.8.2 Small molecule inhibitors

The H2B-Tomato and E14 Tg2a cell lines were used for the small molecule inhibitor experiments. Just prior to imaging the media was exchanged with media contain the inhibitors at the following concentrations: Blebbistatin at 10 µM, Y27632 at 10 µM, Jasplakinolide at 150 ng/ml and Nocodazole at 500 ng/ml.

2.8.3 Analysis - shape change magnitude

The data was analysed using a combination of ImageJ, CellProfiler and MATLAB. For experiments in 2i/LIF where the cells were all separated, videos of individual nuclei were extracted manually in ImageJ and the StackReg plugin was run to correct for any translation or rotation of the nucleus over the time-course. For experiments in N2B27, where nuclei were more dense, CellProfiler was first used to identify and track the nuclei using Otsu thresholding. The images were then exported into ImageJ where individual nuclei could be extracted and StackReg corrected. The videos were imported into MATLAB and analysed using the methods introduced and discussed in Chapter 4.

2.9 Differentiation rescue - kinetics of exit from naive pluripotency

Embryonic stem cells were passaged into N2B27 from 2i/LIF and plated onto laminin coated 24-well plates at a density of 1×10^4 cells/cm^2. The plates were coated with laminin the day before at a concentration of 10 µg/ml and left at 4°C overnight. Before seeding, the plates were warmed up in the incubator and the laminin replaced with N2B27 and returned to the incubator to equilibrate. One plate was used for each timepoint at 48 hours and 72 hours, with a control plated into 2i/LIF. At each timepoint, the cells were unstuck with accutase, re-suspended in 2i/LIF and counted using the Vi-CELL. The cells were then serial diluted until 400 cells could

be accurately obtained and then seeded onto laminin coated 24-well plates (created as above) in 2i/LIF in triplicate. The plates were left for 5-7 days, until colonies had grown, and then fixed in 4% PFA for 10 minutes. The plates were then stained with an alkaline phosphatase staining kit, per the manufacturer's instructions, and left to air dry. The plates were then scanned using an Olympus IX51 microscope and the colonies that stained positive for alkaline phosphatase counted manually in ImageJ.

2.10 Neural lineage specification

Embryonic stem cells were passaged into N2B27 from 2i/LIF and plated onto laminin coated 24-well plates at a density of 1×10^4 cells/cm^2. The plates were coated with laminin the day before at a concentration of 10 µg/ml and left at 4°C overnight. Before seeding, the plates were warmed up in the incubator and the laminin replaced with N2B27 and returned to the incubator to equilibrate. One plate was made for each timepoint at 24 hours, 48 hours, Day 3 and Day 4 with every perturbation containing a control and a treated well in duplicate.

Doxycycline was added at a concentration of 1 µg/ml to induce the over-expressions of LMNA, LBR, mRFP-KASH, mRFP-KASHΔL and mRFP-SR-KASH. Blebbistatin was used at a concentration of 2 µg/ml. siRNA knockdown was performed as detailed in Section 2.7. All perturbations were introduced when 2i/LIF was withdrawn. The cells at each timepoint were fixed using 4% PFA for 10 min and stored at 4°C. When all plates were collected the cells were stained for Sox1 (see Section 2.4).

The cells were imaged using wide-field fluorescence microscopy with exposure, gain and intensity selected to maximise dynamic range using a control sample at Day 4. The imaging settings were kept constant throughout the experiment. One set of samples was stained for Sox1 (CST) and the second set, for LMNA and LBR overexpression, was stained for Sox1 (R&D Systems) with, respectively, Lamin A (SC-20680) or Anti-Lamin B Receptor (Abcam).

Images were analysed using CellProfiler: the nuclei were identified and segmented using global Otsu thresholding and their outlines used to extract the mean intensities of Sox1 and any other relevant channels. Shape descriptors were extracted from the nuclei. The data was imported into MATLAB and plotted as a histogram, normalised as a probability distribution.

2.11 Statistical methods

All statistical analysis was conducted using MATLAB with hypothesis testing done at the 5% level. Data sets were first checked for normality using the Lilliefors test. Where data was normally distributed, the appropriate ANOVA was performed. If significant differences were detected, then a post-hoc multiple comparison test (Tukey's HSD) was used. Where data was not normally distributed the non-parametric Kruskal-Wallis test was performed and, if significant differences were detected, followed by a post-hoc multiple comparison test (Bonferroni). In figure captions, where appropriate, the following are reported; P values, the number of measurements/samples in each experiment (n), and the total number of times the experiment was conducted (N).

Chapter 3

Chromatin mobility in embryonic stem cells

At the beginning of this project, I was interested in exploring chromatin mobility: a study by Meshorer *et al.* (2006) had highlighted the highly dynamic nature of chromatin in pluripotent ES cells when compared with lineage committed (but undifferentiated) cells. The authors' hypothesis is that the highly dynamic nature of chromatin in ES cells contributes to their 'plasticity' which allows them to enact the global transcriptional and epigenetic changes that accompany differentiation. I wished to expand upon this study and apply it to our cell culture system to ask whether chromatin dynamics change in the early stages of differentiation - before, and during, the exit from naive pluripotency.

The cell culture system I am using confers major advantages over the previous study in which ES cells were cultured in serum/LIF: cells cultured in 2i/LIF are more transcriptionally homogeneous which means that the population exits naive pluripotency in a more synchronous fashion when the inhibitors are removed. In addition, culturing with serum is artificial: serum presents the cells with a myriad of factors and signals that are uncharacterised and not encountered in the embryo. Differentiation from serum/LIF is asynchronous and proceeds towards both endoderm and mesoderm lineages, in contrast to cells exiting from 2i/LIF which, without additional factors, commit solely to the neural lineage.

3.1 Fluorescence recovery after photobleaching

The technique used to look at ES cell chromatin dynamics was fluorescence recovery after photobleaching (FRAP). The methodology behind FRAP is to tag a protein of interest with a fluorescent marker and then to destroy (bleach) all fluorescent molecules in a targeted region with a high intensity burst from a laser. The cell is then imaged over time and the rate at which fluorescence intensity recovers in the bleached region provides a quantitative measure of the kinetics of the tagged protein. An example of the process is shown below in Figure 3.1, where histone 2B (H2B) has been tagged with an enhanced green fluorescent protein (eGFP).

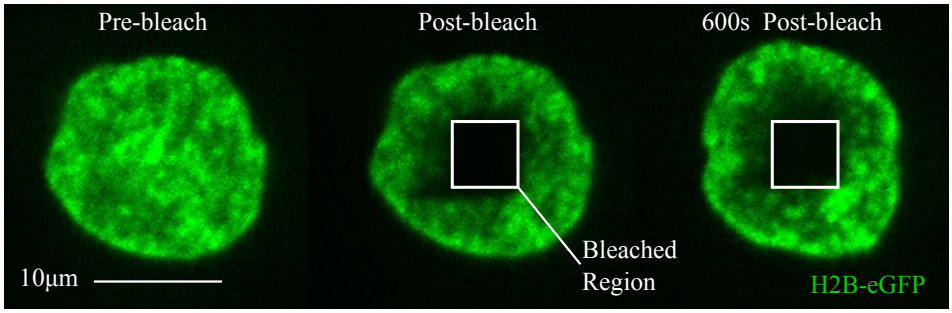

Figure 3.1: Example of FRAP timecourse. Nuclear H2B-eGFP intensity distribution imaged at various stages in a FRAP experiment. Images taken using an Andor Revolution XD spinning disk confocal. From left to right: pre-beached cell, cell immediately after bleaching and cell after 600 seconds of recovery.

The H2A/H2B dimers display recovery kinetics on multiple time scales, shown in Figure 3.2 where the recovery of H2B-eGFP was measured in mES cells cultured in 2i/LIF and 2 hrs, 24 hrs and 48 hrs post 2i/LIF withdrawal.

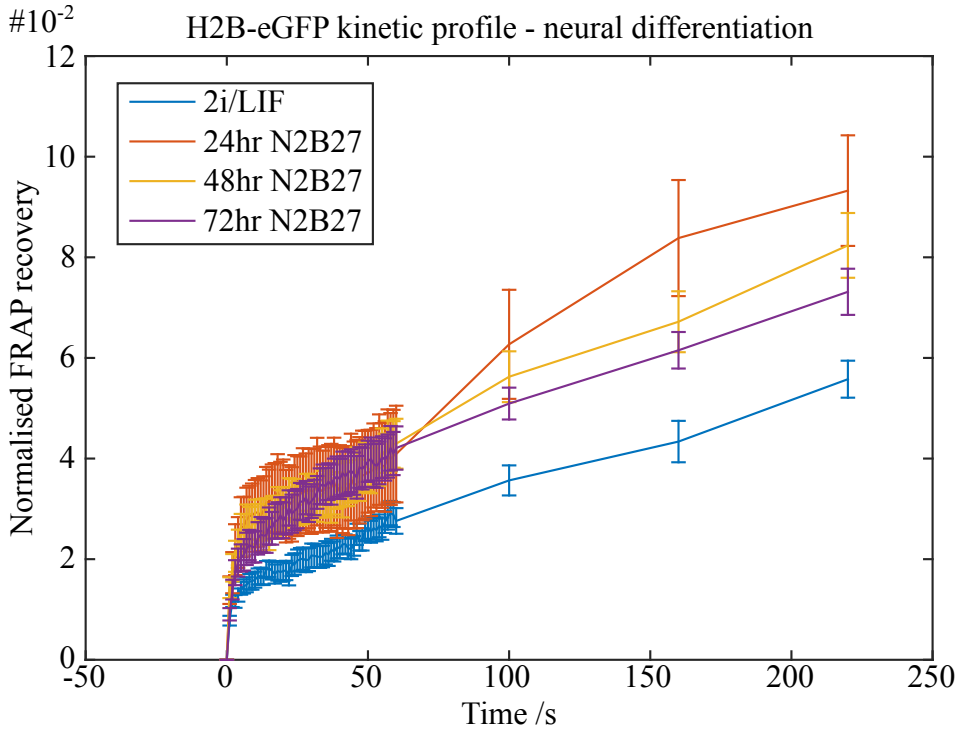

Figure 3.2: Kinetics of H2B-eGFP during ES cell differentiation, measured by FRAP. Normalised FRAP recovery of H2B-eGFP in mESC - comparing cells cultured in 2i/LIF with cells allowed to differentiate in N2B27 at 2, 24 and 48 hour time points. Post-bleach images were taken every second for the first sixty seconds to capture the recovery dynamics of the fast diffusing H2B-eGFP fraction. Error bars give the standard error of the mean. The data was acquired using an Andor Revolution XD spinning disk confocal microscope. N=2 for 2i/L, 24hr and 48hr timepoints. N=1 for the 2hr timepoint.

Immediately after bleaching there is a rapid recovery in intensity in the bleached region, after which recovery slows down. The intensity finally asymptotes to a value below the (normalised) pre-bleach level (not shown). The varied recovery kinetics have been attributed by Meshorer *et al.* (2006) to different pools of fluorophores as follows: initial recovery occurs due to freely diffusing molecules; slow recovery takes place as transiently binding H2A/H2B, postulated as occurring in euchromatin, moves into the bleached region; and a final asymptote is reached as there is an immobile pool fluorophores bound in heterochromatin that cannot be replaced. This contrasts with the recovery kinetics of H3 and H4 which, owing to a higher affinity for DNA when compared with H2A/H2B, exhibit bimodal kinetics; there is a freely diffusing pool and an immobile pool, the former of which van-

ishes upon DNA synthesis as the histones are absorbed into creating new nucleosomes (Meshorer *et al.* , 2006).

The data in Figure 3.2 were split into two groups to separate the dynamics; sub 15 seconds was treated as free diffusion and fit using an exponential model while post 15 seconds was fit to a linear model. The 15 second cut-off was chosen as it represents time taken for complete recovery of H3/H4-eGFP due to free diffusion (Meshorer *et al.* , 2006). The time constants for the fast and slow dynamics were extracted from the models and are shown in Figure 3.3.

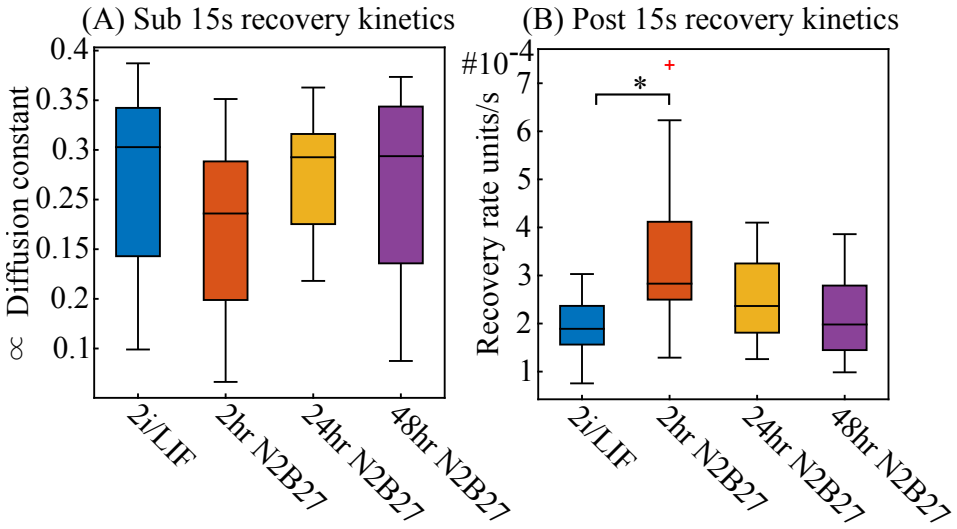

Figure 3.3: Diffusion rates of H2B-eGFP during ES cell differentiation. (A) Under 15 second H2B-eGFP recovery dynamics in mouse embryonic stem cells - dominated by free diffusion. Values given are the averages of the time constants for single exponential fits to the data. (B) Analysis of the slow dynamics (post 15 seconds) - representative of transient H2B-eGFP nucleosome binding in euchromatin. Values given are the averages of the gradients from individual FRAP measurements. (A) $p = 0.38$ (B) $p = 0.0087$ (Kruskal-Wallis with post hoc Tukey's HSD test).

The slow recovery kinetics of ES cells 2 hours after 2i/LIF withdrawal show a significant increase when compared with ES cells in 2i/LIF (Figure 3.3B). This suggests an opening of the chromatin structure which may be instrumental in facilitating global chromatin remodelling as cells exit naive pluripotency and transit to the formative phase prior to lineage commitment. The fast dynamics of H2B-eGFP recovery show no statistically significant difference across the timecourse (Figure 3.3A). This is consistent with the

hypothesis that it represents a freely diffusing pool of H2B-eGFP which would have the same kinetic profile regardless of cell state. This assumption might be questionable in genomes that are heavily dominated with heterochromatin, where free diffusion would be more sterically hindered; however, chromatin is much more open in ES cells when compared with somatic cells.

3.2 Hypotheses and goals

One of the major challenges encountered during the FRAP experiments described in Section 3.1 was that the shape of the bleached region would deform, which would render a large fraction of the data unusable. An example is shown in Figure 3.4 which compares the nucleus just after bleaching and 600 seconds later. It was obvious that some of the nuclei were undergoing significant changes in shape as a results of dynamic forces acting on the nucleus and that this was resulting in chromatin flowing in the nucleus.

- The first goal of this project was to understand how forces are generated and transmitted to the nucleus. We decided that the best approach was to characterise and quantify nuclear shape changes, which act as a proxy for the forces acting on the nucleus. We were interested in exploring whether nuclear shape changes are random, or possess defined periods of oscillation, and to examine the relationship between movements in the nuclear envelope and local changes in the cytoskeleton.

- The second goal was to find ways of perturbing the forces that are transmitted through the cytoskeleton and nuclear envelope and acting directly on chromatin. We hoped to achieve this by targeting components in both the cytoskeleton and the nuclear envelope. We wished to explore the role that forces acting on the nuclear envelope might be playing in modulating the interactions between peripheral heterochromatin and the nuclear lamina - in particular, to see whether the distributions of the repressive histone modifications H3K9me2 and H3K27me3, required for tethering chromatin to the nuclear envelope, are mechanosensitive.

- The final goal was to determine whether altering forces propagated to chromatin have an impact on the ability of ES cells to exit the

naive pluripotent state and to differentiate. We hypothesised that by either reducing the forces experienced by chromatin at the nuclear envelope (reducing nuclear shape changes) or increasing the strength of tethering between heterochromatin and the nuclear lamina, we would impair the ability of ES cells to access lineage specific genes enriched at the nuclear periphery and consequently reduce the efficiency of, or block, differentiation.

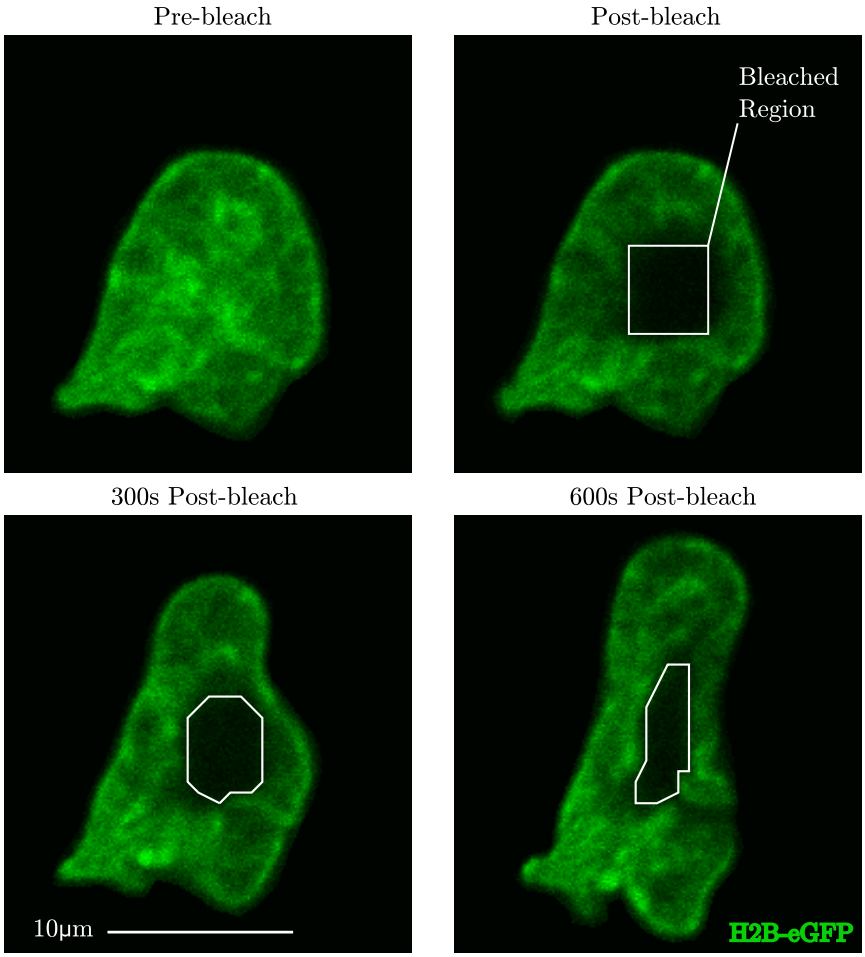

Figure 3.4: Nuclear shape changes deform chromatin. FRAP of H2B-eGFP. Panels outline FRAP series with pre-bleach, post bleach, 300 and 600 seconds post bleach. The bleached region is highlighted in white and deforms during the timecourse as the nucleus changes shape.

Chapter 4

Actomyosin drives nuclear shape changes

In this Chapter I outline the work that we have done to characterise nuclear shape changes in mouse ES cells and to determine how they are driven. Before the experiments that were conducted are introduced and discussed I explain the methodology behind our analysis of quantifying the amplitude of nuclear shape changes.

4.1 Quantification of magnitude of nuclear shape changes

There are a number of ways that shape changes can be quantified, all of which have their advantages and disadvantages. I have, primarily, chosen two methods to calculate the magnitude of the shape changes. The first method looks at the absolute area differences between images as a function of their frame separation, n. The method is highlighted below in Figure 4.1.

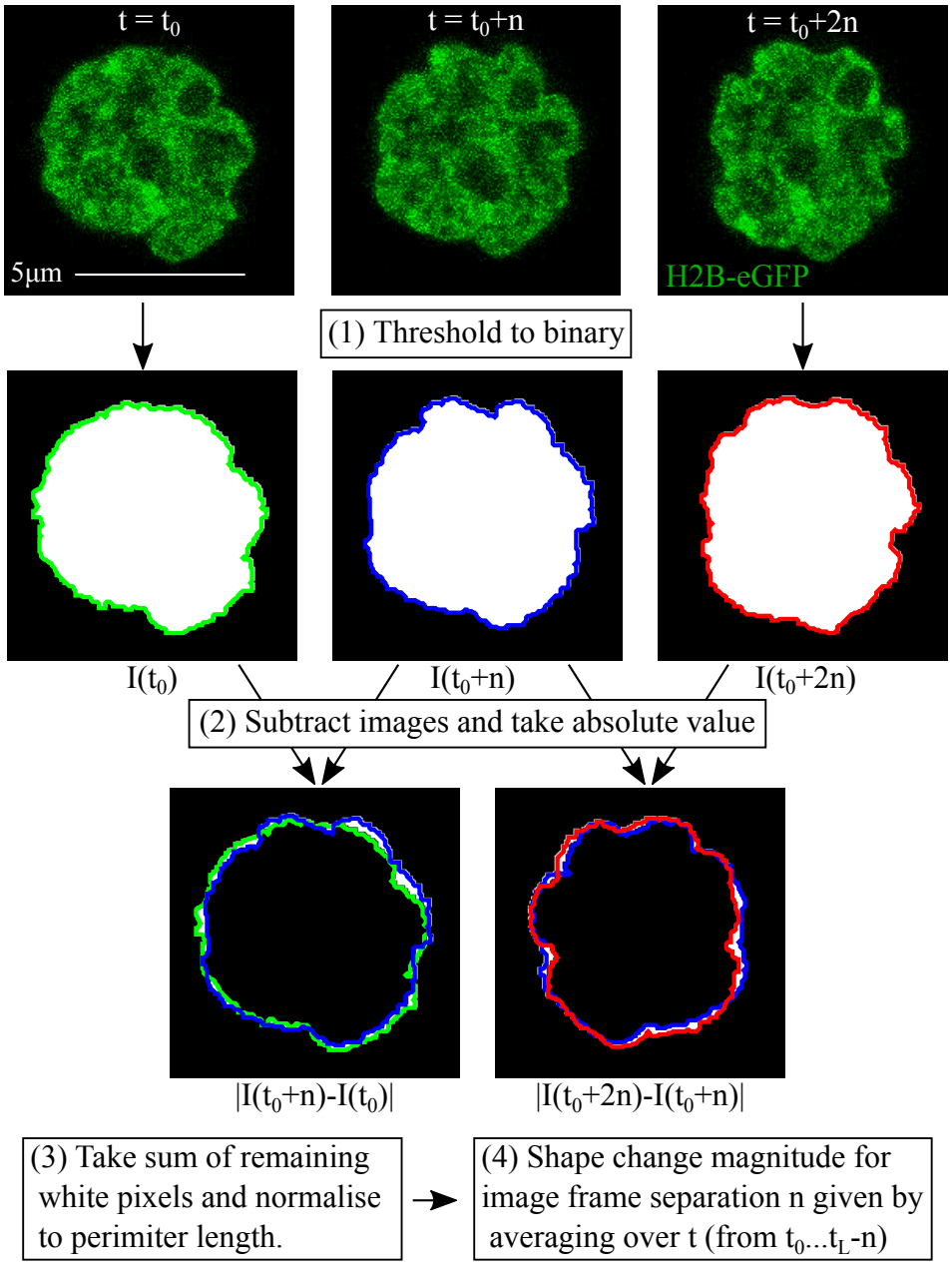

Figure 4.1: Method A of nuclear shape change quantification. Method A relies on taking the absolute difference, in pixels, between images of ES cell nuclei as a function of image/frame separation. The resulting shape change magnitude provides information of global shape changes at all timescales, but cannot provide any information of fluctuations in the nuclear boundary.

The first step is to threshold the video of the nucleus to create binary images. The absolute difference between images separated by n frames is

then calculated - the sum of the remaining non-zero pixels - and normalised by the length of the nuclear perimeter. These values are then averaged over time, from $t = 0$ to $L - n$, where L is the total number of images, to give the nuclear shape change magnitude as a function of n - summarised in equation 4.1.

$$Magnitude_n = \frac{\sum_{t=0}^{L-n} \left(\frac{abs(Image_t - Image_{t+n})}{Perimeter_t} \right)}{L - n} \tag{4.1}$$

The advantages of this method are that it can deal with a nucleus of any shape and that it gives a measure of how the shape changes over both short (low n) and long (high n) timescales. The downside of this method is that, by using a global approach, it cannot provide any information about local fluctuations in the nuclear envelope.

The second method, which looks at the fluctuations in the radial position of the nuclear boundary, is summarised below in Figure 4.2.

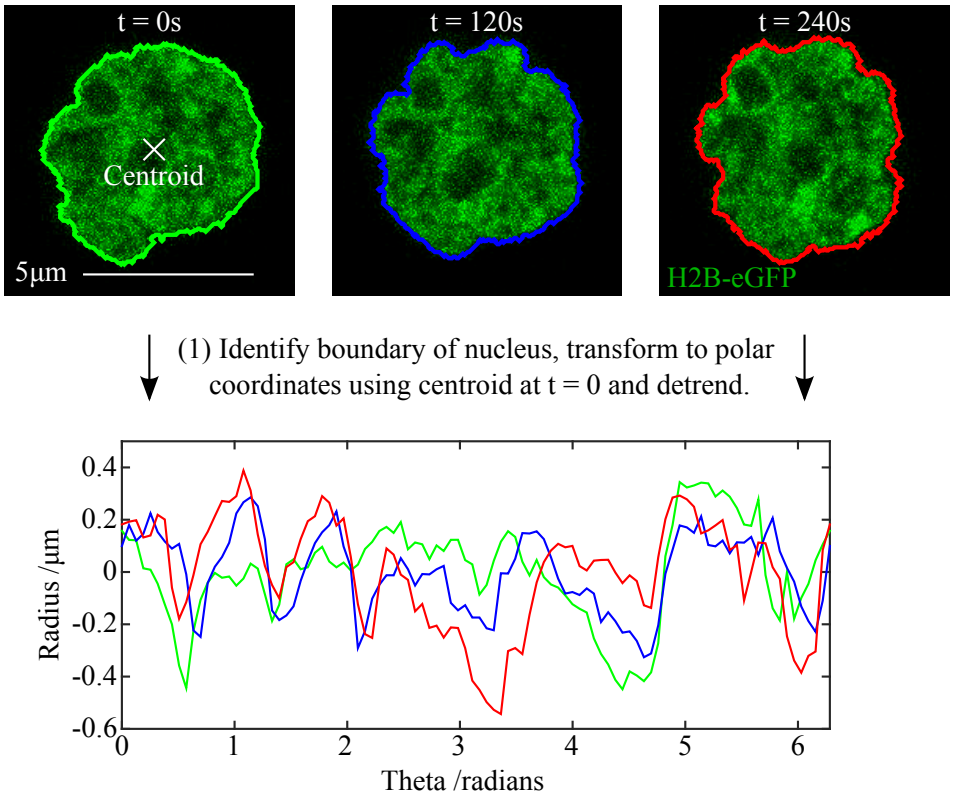

Figure 4.2: Method B of nuclear shape change quantification. Method B looks at the fluctuations in the radial position of the nuclear boundary. Nuclear shape change magnitude is given by taking the standard deviation of the radial nuclear boundary coordinate at angle *theta*, averaged over all angles. This method gives information about the size of fluctuations in the nuclear boundary, but it not robust to analysing nuclei with odd shapes.

First, using the centroid of the first image as the centre of the new coordinate system, the coordinates of the nuclear boundary are converted from Cartesian coordinates into polar coordinates using linear interpolation. Second, the boundary coordinates, now plotted as radius (R) vs. angular coordinate (θ), are detrended so that the average radial value is zero - this normalises for any differences in the size of the nucleus and also controls for any small fluctuations of the focal plane in the z-axis. The magnitude of the shape changes is then given as follows in equation 4.2, where L is the total number of images and N is the total number of θ values in each image:

$$Magnitude = \frac{\sum_{\theta=0}^{2\pi} \left(\sqrt{\sum_{t=1}^{L} \left(R_{t,\theta}\right)^2 / L} \right)}{N} \tag{4.2}$$

This analysis has the advantages that it provides a single value that represents the magnitude of the nuclear shape changes, controls for nuclear size and focal plane drift, and provides the basis for more complicated analyses of the fluctuations in the nuclear envelope (to be discussed in further detail later). It cannot, however, be used to analyse nuclei which have odd shapes where the position of the nuclear envelope in polar coordinates can become multivalued (i.e. the centroid of a bean-shaped nucleus can lie outside of the nucleus).

4.2 The cytoskeleton and nuclear shape changes

Shape changes necessitates motion and motion necessitates forces. In Section 1.4 I discussed how tension is necessary for the propagation of forces through the cytoplasm to the nucleus and that this tension is largely generated by the action of molecular motors, notably non-muscle myosin II, and the polymerisation of actin. In order to explore this we chose to use small molecules to inhibit the action of non-muscle myosin II (Blebbistatin and Y27632) and to promote polymerisation and stabilisation of actin (Jasplakinolide) in E14 Tg2a mouse ES cells cultured in 2i/LIF, which we hypothesised would reduce the magnitude of the nuclear shape changes. The inhibitor, Nocodazole, which targets microtubule polymerisation was also included as microtubule polymerisation forces have been implicated in driving nuclear fluctuations in the literature (Hampoelz *et al.* , 2011)(Schreiner *et al.* , 2015). The results are shown in Figure 4.3 where the magnitude of nuclear shape changes, quantified using the first method (A) and second method (B) outlined in Section 4.1 respectively, are significantly reduced when treated with Blebbistatin, Y27632 and Jasplakinolide. Figure 4.3A indicates that treatment with Nocodazole may increase nuclear shape changes, although the experiment lacks the statistical power to detect any significant difference in the means between control and Nocodazole treatment in Figure 4.3B.

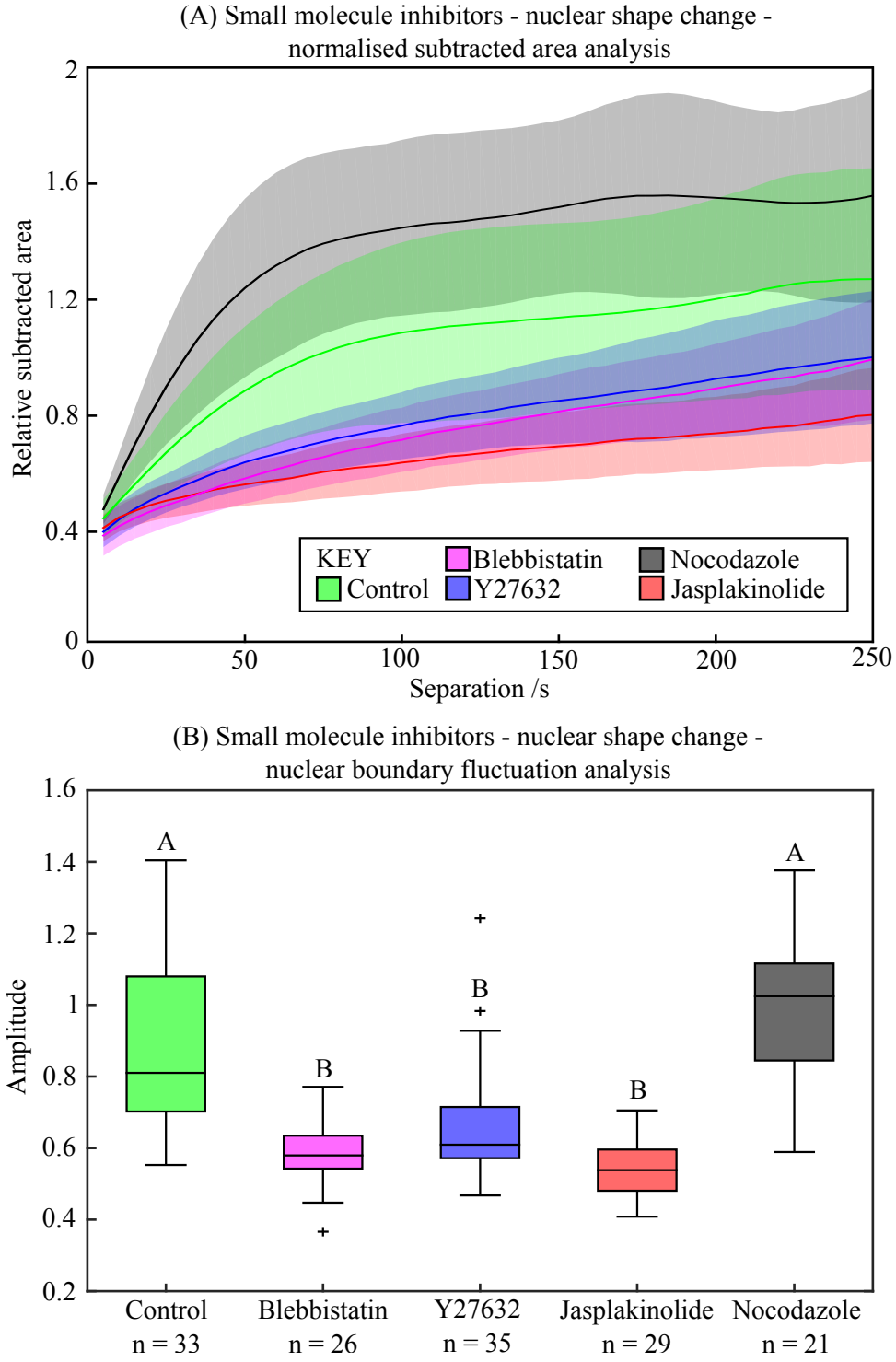

Figure 4.3: Perturbation of nuclear shape change with small molecule inhibitors. Caption continued on following page.

Figure 4.3: E14 Tg2a ES cells in 2i/LIF treated with 10 µM Blebbistatin, 10 µM Y27632, 150 ng/ml Jasplakinolide and 500 ng/ml Nocodazole. Nuclei visualised after 45 min incubation with 2 µM SiR-Hoechst. (A) Magnitude of nuclear fluctuations calculated with equation 4.2. Solid line and shaded area represent the mean and standard deviation, respectively. Blocking the action of non-muscle myosin IIA with Y27632 and Blebbistatin, or stabilising the polymerisation of actin with Jasplakinolide suppresses nuclear shape changes. De-polymerising the microtubule network with Nocodazole enhances nuclear shape changes. (B) Subtracted nuclear area as a function of incremental frame separation, calculated using equation 4.1. Analysis of nuclear boundary fluctuations shows significantly reduced nuclear shape changes when inhibiting non-muscle myosin IIA and stabilising actin polymerisation. Statistical analysis was performed in MATLAB using a one-way ANOVA followed by a multi-comparison test. Samples with different letters show significant differences at the five percent confidence level, whereas those with the same letter do not.

4.3 Fluctuations in cortical actin intensity and the nuclear envelope

The data in the previous section confirms that actin and myosin are required for propagating forces to the nucleus and driving nuclear shape changes. To take this further we wished to investigate the relationship between the polymerisation of actin and the dynamics of the nuclear envelope in more detail. To achieve this, we used the H2B-eGFP mouse ES cell line and stably transfected it with LifeAct-RFP. LifeAct is a small peptide (17 amino acids) that binds selectively to filamentous (F-) actin, dissociates when F-actin is disassembled into monomeric form, and does not interfere with polymerisation dynamics (Riedl *et al.* , 2010), and has been fused to a red fluorescent protein. Figure 4.4A depicts a thin optical slice through the nucleus of a H2B-eGFP LifeAct-RFP ES cell. Strikingly, the F-actin is primarily localised in a thin band that underlies the cell membrane known as the cortex.

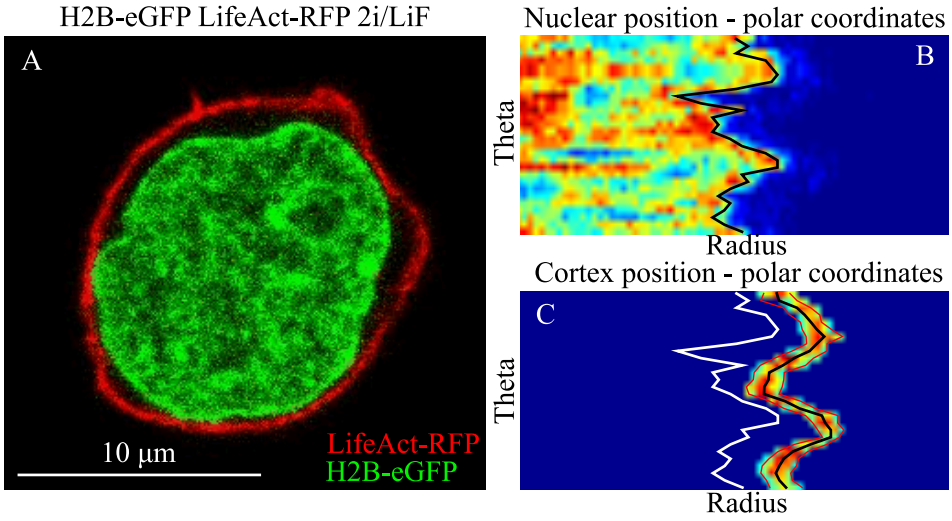

Figure 4.4: Localisation of the nuclear boundary and cortical actin. (A) Optical slice through the centre of an H2B-eGFP LifeAct-RFP mouse ES cell, taken with an Andor Revolution XD spinning disk confocal with a 63x 1.4NA objective. Actin, predominately localised to the cortex, in red and the nucleus in green. (B) Custom MATLAB script to extract the position of the nuclear boundary in polar coordinates ($R_N(\theta, t)$). (C) Custom MATLAB script to extract cortex position ($R_C(\theta, t)$) and intensity ($I_C(\theta, t)$), with the position of the nuclear boundary shown in white for reference.

Using an Andor Revolution XD spinning disk confocal with a 63x 1.4 NA objective we took live images through the centre of the nucleus of H2B-eGFP LifeAct-RFP cells cultured in 2i/LIF. Thirty images were captured with an eight second interval and laser intensity was kept as low as possible to avoid phototoxicity and to minimise bleaching. In order to analyse the data, the images were first imported into ImageJ and split into separate channels (nucleus and cortex) where the multistackreg plugin was used to remove any translation or rotation of the nucleus during the timecourse. The same transformations were then applied to the images of the cortex. Videos of individual nuclei and cortical actin were then loaded into MATLAB and analysed using a custom script: using the centroid of the nucleus from the first frame of the time series as a reference, the images of the nucleus and cortex were transformed into polar coordinates. The coordinates of the nuclear boundary, shown in Figure 4.4B in black, were then identified and extracted. The analysis of the cortex, shown in Figure 4.4C, was more complicated: cortical position and width were measured by fitting a Gaussian in every angular bin. The centre of the Gaussians were used as the radial coordinates of the cortex, shown in black, and cortical thickness

was taken as plus and minus one standard deviation (red lines). The angular cortical intensity was calculated as the mean pixel value of the top five highest intensity pixels contained within the red lines. The position of the nuclear boundary is shown in white for reference.

To start with, we employed Fourier analysis to determine whether there were any dominant frequencies of oscillation in both cortical actin intensity and nuclear envelope position. The analysis was conducted on H2B-eGFP cells cultured in 2i/LIF. We also chose to supplement the cells with 5 µM Blebbistatin in order to reduce the forces propagated to the nucleus and determine what effect this had on the frequencies of oscillation. Local cortical intensity and nuclear boundary positions were first detrended over time (with a constant), multiplied with a Hanning window[1] and then zero padded[2]. The Fourier transforms were then averaged over all θ and then over all cells. The results in Figure 4.5 show that both the nuclear boundary and cortical actin intensity possess a dominant low frequency oscillation, centred on 0.0045 Hz, which corresponds to a period of just over 200 seconds. Treatment with 5 µM Blebbistatin results in a drop in the amplitude of nuclear boundary fluctuations as expected; however, as the dominant low frequency mode is still present, it is likely that the cytoskeleton and nucleus are not completely decoupled.

[1]The Hanning window is a window function designed to tackle the finite nature of the sampling in the time domain. Multiplication by the Hanning window ensures that there is no discontinuity when the beginning and end of the signal are joined together due to the circular topology of the Fourier transform. If the discontinuity were present, the Fourier transform would be corrupted by both high and low (aliased) frequency components.

[2]Zero padding is the process of artificially increasing the length of the time domain signal by adding zeros to the end of signal before taking the Fourier transform. This increases the number of frequency bins which aids in localising isolated frequencies, but does not alter the resolution.

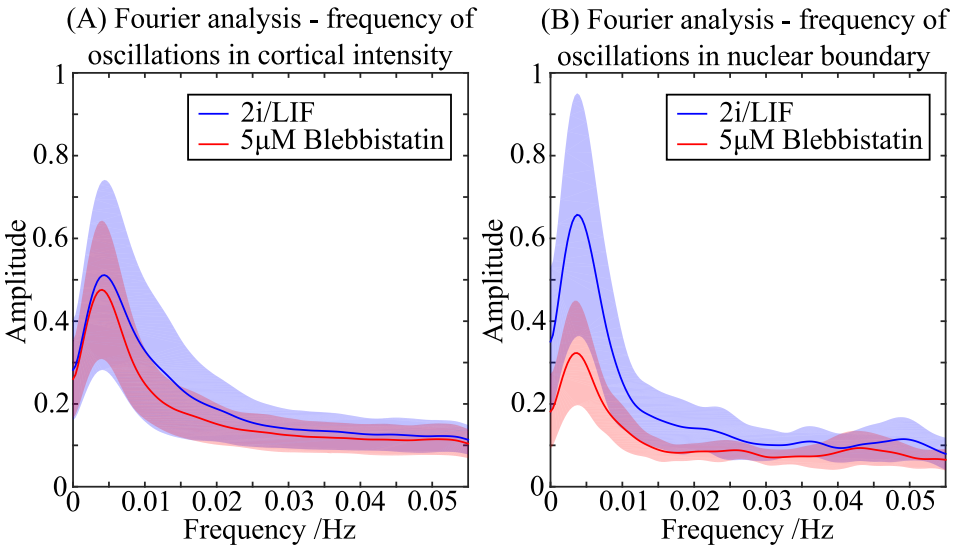

Figure 4.5: Fourier analysis of cortical actin intensity and nuclear boundary fluctuations. Frequency spectrum of cortical actin intensity (A) and radial nuclear boundary position (B) in H2B-eGFP mouse ES cells cultured 2i/LIF. Fourier analysis conducted using a Hanning window and detrended (constant value) data. Solid line and shaded area represent the mean and standard deviation, respectively. A dominant low frequency oscillation is present - centred on 0.0045 Hz in both plots. Treatment with 5 μM Blebbistatin significantly dampens the magnitude of nuclear boundary fluctuations but does not remove the dominant frequency of oscillation.

To take this one step further and see whether there is a relationship between local fluctuations in cortical actin intensity and the movement of the nuclear boundary directly radially inward, we took cross-correlations of the intensity of actin in the cortex with both the position of the nuclear boundary and the separation between the nuclear boundary and the cortex. A schematic of the variables involved is shown below in Figure 4.6.

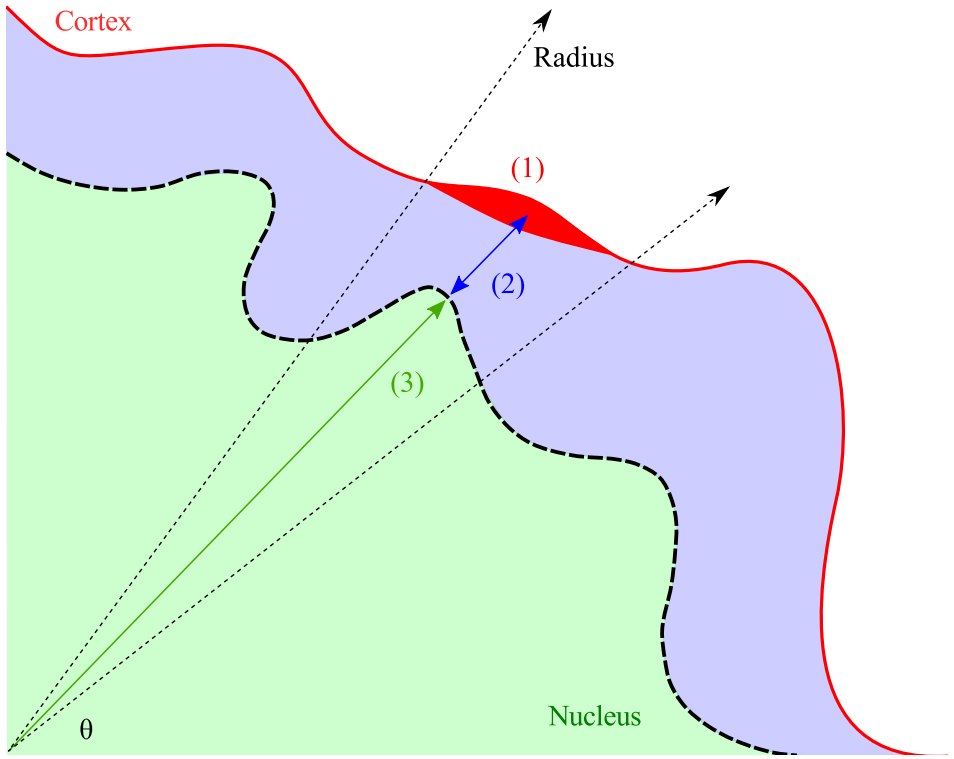

Figure 4.6: Schematic of variables in the cross correlation analysis of cortical actin and nuclear boundary. The variables are: cortical actin intensity (1) $I_C(\theta, t)$, separation of cortex and nuclear boundary (2) $S_{NC}(\theta, t) = R_C(\theta, t) - R_N(\theta, t)$ and nuclear boundary position (3) $R_N(\theta, t)$.

The results are shown in Figures 4.7A and 4.7B for H2B-eGFP LifeAct-RFP cells cultured in 2i/LIF and in Figures 4.7C and 4.7D for H2B-eGFP LifeAct-RFP cells cultured in 2i/LIF supplemented with 5 µM Blebbistatin. In both cases, we chose to separate the data set and distinguish between cells that were blebbing ((B) and (D)), and those that weren't ((A) and (C)), the reasons for which will be explained later below. The cross-correlations all possess a dominant oscillatory frequency; this is expected as we have already shown that both cortical actin intensity and the position of nuclear boundary fluctuate with similar periods (Figure 4.5). The key result, however, is that the local fluctuations in cortical actin intensity and the position of the nuclear boundary underneath are out of phase by π radians - Figure 4.7A, in green. By comparing the cross-correlations of the cortex with the position of the nuclear boundary and the cortex with the separation of the cortex and nuclear boundary it is possible to discern how the positions of the nucleus and cortex are changing with respect to one another. The separation, shown above as variable (2) in Figure 4.6, is defined as the position of the nucleus

boundary subtracted from the position of the cortex. If the cortex remains static, the separation is the negative of the nuclear boundary which, when comparing cross-correlations of both variables with the intensity of actin in the cortex, would result in the cross-correlations being the reflection of one another in the y-axis at zero offset. This is what is seen in Figures 4.7(C) and 4.7(D) where the cells have been treated with Blebbistatin. We can therefore infer that suppressing the action of non-muscle myosin II does not alter the frequency of oscillations in cortical actin intensity but does significantly reduce any movement of the cortex to an amplitude below that of the fluctuations in the nuclear boundary. Figures 4.7A and 4.7B show the opposite trend: the cross-correlations (blue vs. green) are remarkably similar to one another. This implies that the fluctuations in the local positions of the cortex and the nuclear boundary with respect to the centre of the nucleus are in phase with one another, with movements in the cortex being greater in amplitude. Support for these inferences is given in Figure 4.8A by checking that the cross-correlations of cortical and nuclear positions are in phase in 2i/LIF conditions and out of phase when treated with 5 µM Blebbistatin.

Blebbing represents a significant source of bias in this analysis. Blebbs are thought to arise from hydrostatic pressure created by actomyosin contractility in the cell. A local weakening in the cortex results in the uncoupling of the cortex from the cell membrane and a reduction in hydrostatic pressure as cytoplasm flows in to create the blebb. Blebb expansion stops when membrane tension in the blebb balances out the hydrostatic pressure. The cortex is then reassembled under the plasma membrane in the blebb and actomyosin contractility subsequently leads to its collapse. With regards to the analysis above, a blebb represents a significant increase in the local nuclear boundary/cortex separation, followed by an increase in actin intensity. This effect dominates the cross-correlation between cortical actin intensity and the separation of the nuclear boundary and the cortex, shown in Figure 4.7B - where separation between cortex and nuclear boundary leads the oscillations $\pi/2$ out of phase with cortical actin intensity. The data sets were therefore separated into blebbing and non-blebbing populations to try to minimise this effect and prevent it from biasing the analysis.

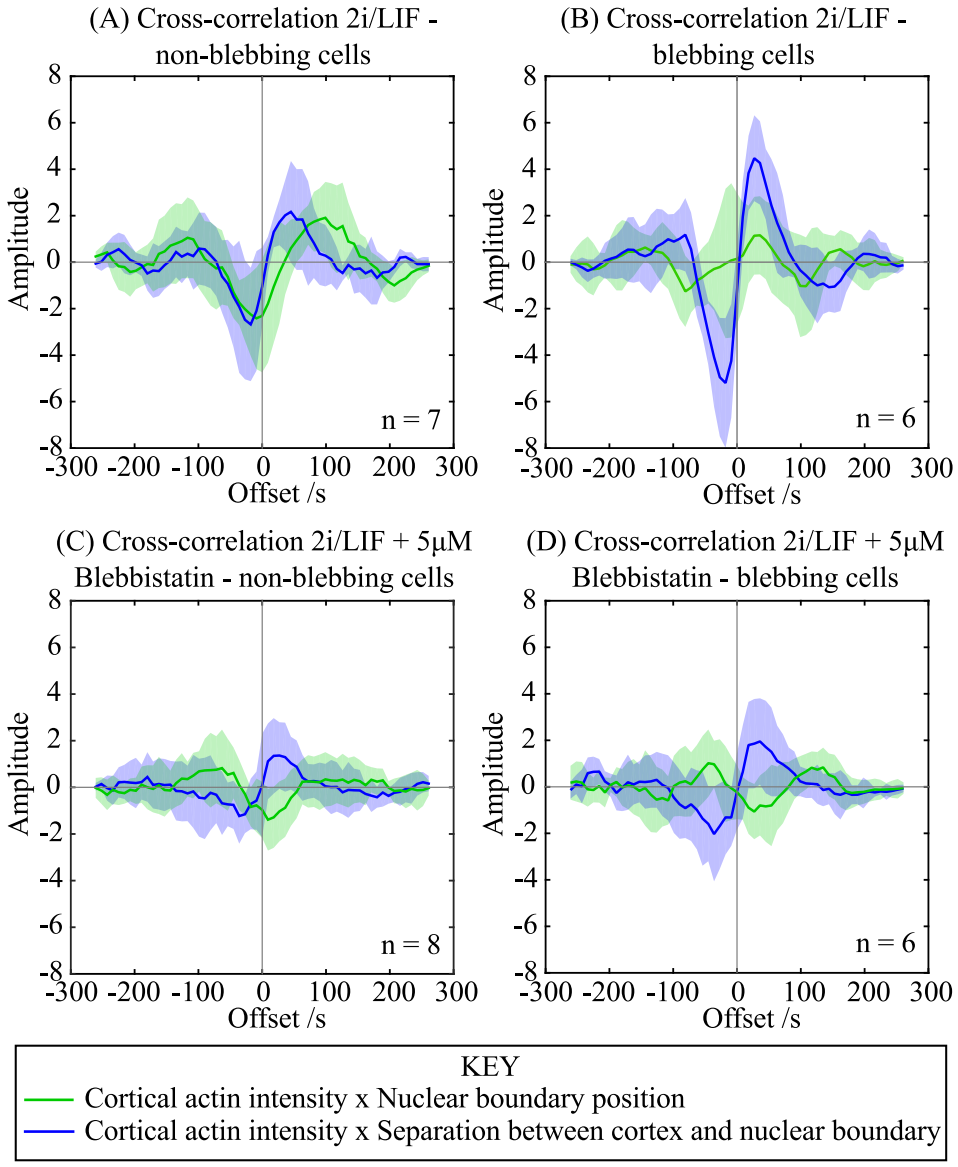

Figure 4.7: Cross-correlations between local position and intensity of cortical actin and the position of the nuclear boundary radially inwards. Each plot contains the cross-correlation between cortical actin intensity and the separation of the nucleus and cortex (blue) and between cortical actin intensity and position of the nuclear boundary (green) in H2B-eGFP LifeAct-RFP mouse ES cells cultured in 2i/LIF. The cross-correlations are first calculated in angular sections and averaged to give a trace for each cell. Solid line and shaded area represent the mean and standard deviation, respectively, between cells. (A) Cross-correlations in non-blebbing cells show cortical actin intensity fluctuates *pi* out of phase with the position of the nuclear boundary. (B) Cross-correlation in blebbing cells shows large magnitude (blue) indicating analysis sensitive to blebbs. (C) Cross-correlations in non-blebbing Blebbistatin treated cells. (D) Cross-correlations in blebbing Blebbistatin treated cells.

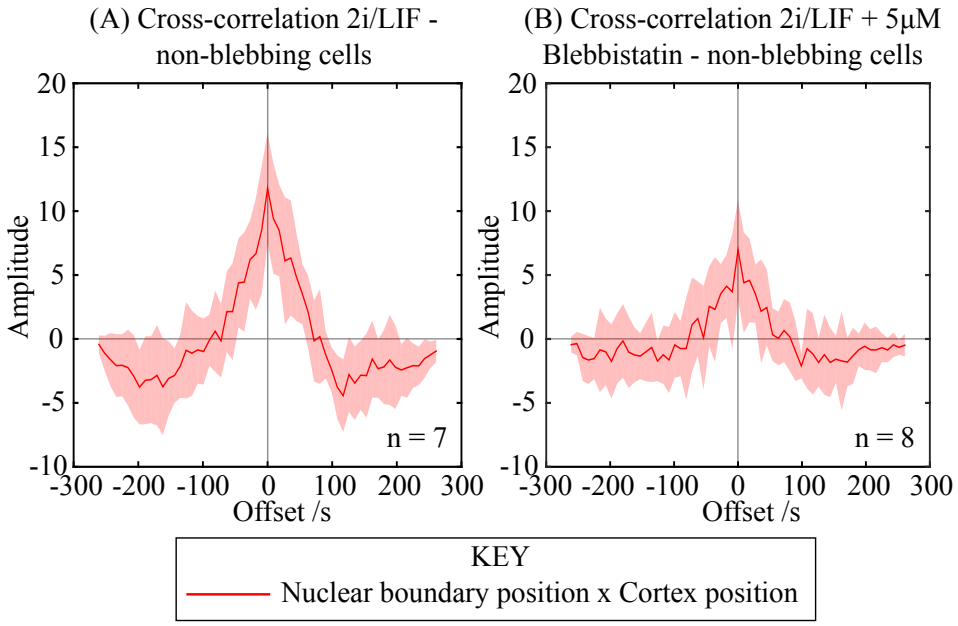

Figure 4.8: Cross-correlation between the local position of cortical actin and the position of the nuclear boundary radially inwards. Analysis conducted in H2B-eGFP LifeAct-RFP mouse ES cells cultured in 2i/LIF. The cross-correlation is calculated at each angular section and then averaged to give a trace for each cell. Solid line and shaded area represent the mean and standard deviation, respectively, between cells. (A) Cross-correlation in non-blebbing cells. (B) Cross-correlation in non-blebbing cells treated with 5 μM Blebbistatin. The correlations show that the radial positions of the nuclear boundary and the cortex move in phase with one another.

4.4 Discussion

We have shown in Figure 4.3 that components of the actomyosin cytoskeleton are involved in driving nuclear shape change. Inhibiting the action of non-muscle myosin II or promoting the polymerisation of actin both lead to a significant reduction in the amplitude of nuclear shape changes. We also found inhibition of microtubule polymerisation led to a possible, but not statistically significant, increase in the amplitude of nuclear shape changes. Our findings agree with a prior study, which compared nuclear area fluctuations in mouse ES cells with primary mouse embryonic fibroblasts (PMEFs) - a differentiated cell type (Talwar *et al.* , 2013). The authors found that microtubule dynamics had no impact on nuclear area fluctuations in ES cells (Nocodazole treatment) and that depolymerising actin stress fibres in PMEFs increased nuclear area fluctuations to an amplitude comparable with

ES cells. The authors concluded that the presence of an actin stress fibre network in PMEFs, lacking in ES cells where F-actin is constrained to the cortex (Figure 4.4), was stabilising the nucleus against fluctuations. The study did not, however, explore the origin of the driving forces of ES cell nuclear fluctuations, which we have sought to address in this study.

There are a couple of possible mechanisms that explain our results. Firstly, inhibition of non-muscle myosin II would result in a loss of cytoskeletal tension and the inability to transmit forces through the cytoskeleton and the LINC complex to the nucleus. Additionally, the magnitude of the forces generated within the cytoskeleton by actomyosin contractility would be significantly reduced. If the polymerisation of actin is promoted and the filaments stabilised, while the cells would be capable of generating and transmitting forces through their cytoskeleton to the nucleus, the distribution of these forces are likely to be much less dynamic. Both scenarios would lead to a sharp reduction in nuclear shape changes.

As second explanation is that actomyosin contractility is generating a fluid flow in the cytoplasm that exerts dynamic pressure on the nucleus. In a study by Kumar *et al.* (2014), the authors found that a hydrodynamic approach could be used to describe observed rotations in the nuclei of fibroblast cells (NIH3T3). They found that nuclear rotation correlated with a hydrodynamic flow of actin around the nucleus and that the speed and coherence of the rotations were significantly reduced by lowering actomyosin contractility with blebbistatin treatment. Stabilising the polymerisation of actin filaments and lowering cytoskeletal stress through inhibition of non-muscle myosin II could therefore dampen nuclear shape changes by reducing this flow of fluid.

The observation that treatment with the microtubule depolymerising drug Nocodazole may result in an increase in nuclear shape changes when compared with controls (Figure 4.3A) is consistent with the fact that disassembly of the microtubule network is known to increase actomyosin contractility (Danowski, 1989) - this process is mediated through activation of RhoA GTPase and subsequent increase in the assembly of actin-myosin contractile filaments (Chang *et al.* , 2008). It is worth noting that, while microtubule dynamics do not drive nuclear shape changes in mouse ES cells, studies performed in the early *Drosophila* embryo have identified microtubule dynamics as the driving force of nuclear envelope fluctuations (Hampoelz *et al.* , 2011).

The fluctuations in the nuclear envelope are not random - they have a well-defined period of approximately 200 seconds which coincides with the

timescale of oscillations in the intensity of cortical actin (Figure 4.5). A similar period of fluctuation, centred on 140 seconds, has also been observed in fluctuations of ES cell nuclear area (Talwar *et al.* , 2013). Our result, in conjunction with the correlations between the local intensity of cortical actin and the position of the nuclear boundary radially inward (Figure 4.7), provides strong evidence that cortical actin and the nucleus are mechanically coupled. The observation that the intensity of cortical actin fluctuates π radians out of phase with, and ahead of, the nuclear boundary could be explained by hysteresis in the system: the build-up and dissipation of non-muscle myosin II may follow, but lag, the fluctuations in cortical actin. This could explain why the forces on the nucleus are out of phase with the intensity of cortical actin.

Chapter 5

Nuclear envelope proteins influence nuclear shape, dynamics and chromatin structure

In this Chapter I introduce the perturbations of our *in vitro* mouse embryonic stem cell system and outline what we hoped to achieve with them. I then present the data and the results of our analysis into their characterisation.

5.1 Perturbing the forces on chromatin and the regulation of peripheral heterochromatin

Our goal is to explore whether forces acting on the nucleus are important for facilitating changes in gene expression during the exit from naive pluripotency and linage specification in mouse ES cells. Our hypothesis is that forces acting on the nuclear envelope may facilitate transitions between transcriptional states during differentiation through the bulk movement of chromatin in the nucleus as a result of global nuclear shape changes, or the re-organisation of nuclear lamina/LAD contacts driven by local fluctuations in the nuclear envelope. To test whether this is the case, we set out to accomplish the following with our perturbations:

1. To modulate the magnitude of the forces that are transmitted directly to chromatin.

2. To modulate the strength of the tethering between peripheral heterochromatin and the nuclear envelope.

The first perturbation targets force generation in the cytoskeleton through treatment with the small molecular inhibitor Blebbistatin, which acts as a highly selective inhibitor of non-muscle myosin II. We have demonstrated, in Chapter 4, that the magnitude of nuclear shape changes can be significantly reduced by treatment with 10 µM Blebbistatin, indicative of a reduction in the forces transmitted to the nucleus. We believe this is a result of not only inhibiting force generation in the cytoskeleton, but also removing the ability to propagate any forces to the nucleus due to lack of cytoskeletal tension - as discussed in Section 1.4.

The other perturbations modify the structure of the nuclear envelope and nuclear lamina through overexpression and, where appropriate, knockdown of key structural proteins designed to either modulate forces transmitted to chromatin, or alter the strength of heterochromatin tethering at the nuclear envelope.

The second perturbation is the overexpression of LMNA. LMNA has been shown to stiffen and buffer the nucleus against external forces (Pajerowski *et al.* , 2007) and act as an anchor for tethering peripheral heterochromatin to the nuclear lamina (Solovei *et al.* , 2013). LMNA is not thought to be expressed in ES cells (Constantinescu *et al.* , 2006) although this fact has been disputed by Eckersley-Maslin *et al.* (2013) who have found LMNA expressed at low levels. We hoped that stiffening the nucleus and increasing heterochromatin binding at the nuclear envelope would act in a synergistic way to reduce the movement of chromatin at the nuclear envelope and restrict access to genes bound there.

The third perturbation is the overexpression and knockdown of lamin B receptor (LBR). LBR has been identified as acting as the primary heterochromatin tether in ES cells, which lack the LMNA tether (Solovei *et al.* , 2013). We hoped that overexpressing LBR would increase the strength of peripheral heterochromatin tethering and restrict access to any genes bound there, resulting in a decrease in plasticity, while knockdown of LBR would have the opposite effect.

The final, fourth, set of perturbations are the overexpressions of truncated KASH domain proteins, shown below in Figure 5.1. The vectors used were a kind gift from the lab of G.W. Gant Luxton (Luxton *et al.* , 2011). The truncated KASH domain proteins, mRFP-KASH and mRFP-

SR-KASH, when overexpressed, act as dominant negatives for the endogenous Nesprins - outcompeting them for binding to the SUN proteins. The result is that the LINC complex is broken and the nucleus and cytoskeleton become decoupled at the outer nuclear membrane, while any unwanted perturbations to chromatin interactions with the nuclear lamina at the inner nuclear membrane are minimised. The protein mRFP-KASHΔL possesses a truncated KASH domain and therefore, as it cannot bind to the SUN proteins, acts as a negative control.

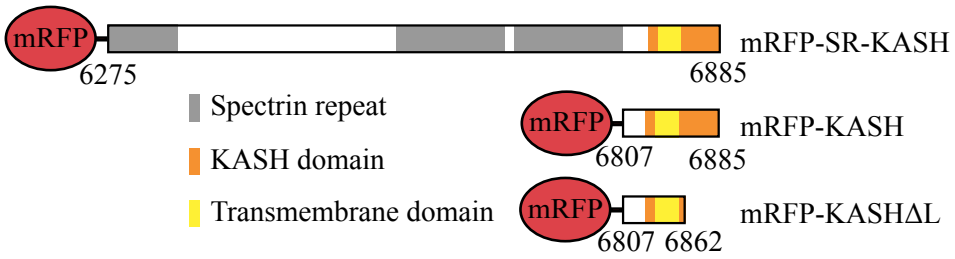

Figure 5.1: Constructs to decouple the nucleus and the cytoskeleton. Truncated human Nesprin-2 (SYNE-2) KASH domain containing proteins which, when overexpressed, are designed to outcompete endogenous Nesprin binding to the inner nuclear membrane bound SUN proteins and decouple the nucleus from the cytoskeleton at the outer nuclear membrane. mRFP-SR-KASH and mRFP-KASH act as dominant negatives to SYNE-2. mRFP-KASHΔL, which possesses a truncated KASH domain and is unable to bind the SUN proteins, acts as the control. The proteins are based on human SYNE-2. Figure from G.W. Gant Luxton.

The proteins in Figure 5.1 are truncated forms of human Nesprin-2 (SYNE-2). The KASH domain amino acid sequence in humans, however, is almost identical to the sequence in mice with one amino acid substituted from glutamate to aspartate. There should therefore not be a problem with specificity as aspartic and glutamic acid are almost identical chemically. Unfortunately, due to time constraints, the KASH construct overexpressing ES cells have not been fully characterised and the results obtained from them will therefore be discussed separately in the final Chapter.

5.2 Inducible overexpression with the tetracycline-controlled transcriptional activation system

To overexpress our LMNA, LBR and KASH constructs in an inducible fashion we decided to use the tetracycline-controlled transcriptional activation

system, specifically, the derivative in which transcription is activated in the presence of a tetracycline - referred to as the Tet-On system. A schematic of the Tet-On system, which is based upon the interaction between two complementary control circuits, is shown in Figure 5.2 below:

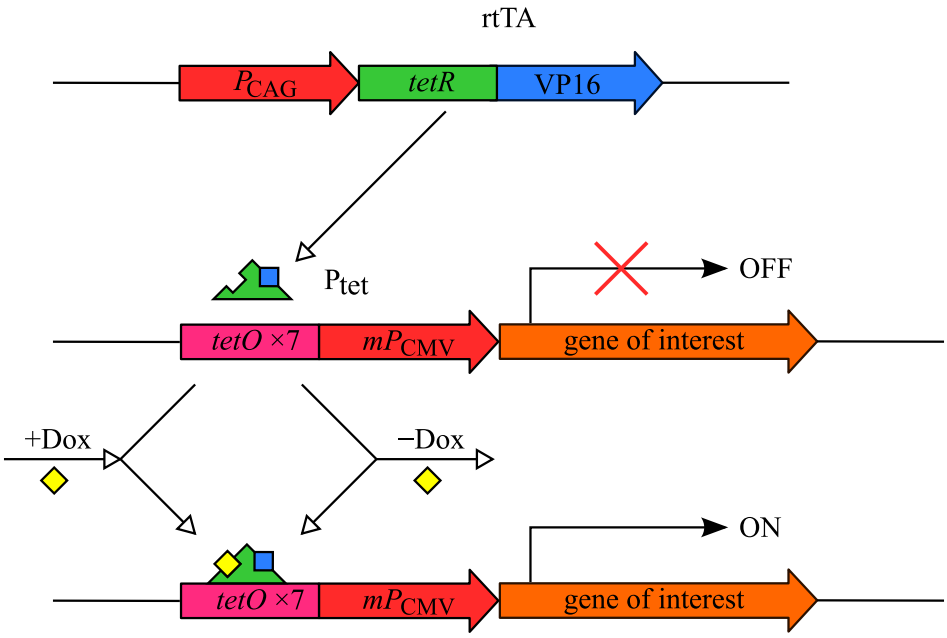

Figure 5.2: Schematic of the tetracycline-controlled transcriptional activation system (Tet-On). In the presence of doxycycline (+Dox) the transcription factor rtTA can bind to the *tetO* elements in the synthetic promotor P_{tet} and activate transcription of the gene of interest. When doxycycline is removed, the rtTA dissociates from the promotor region and transcription of the gene of interest is halted.

The Tet-On system requires the stable integration of two plasmids into the genome. The first plasmid encodes for, and constitutively expresses, the transcription factor rtTA. The second plasmid contains a synthetic promotor (P_{tet}) that responds to the binding of rtTA and the gene of interest. P_{tet} is formed of seven *tetO* sequences followed by a minimal CMV promotor. In the absence of rtTA binding, transcription of the gene of interest is silenced. For rtTA to bind to the *tetO* sequences, it must be bound by a tetracycline; addition of the tetracycline derivative doxycycline (+Dox) initiates transcription, mediated by rtTA promotor binding. Subsequent removal of doxycycline leads to rtTA dissociating from the promotor region and gene silencing. The vector that contains the Tet-On system used for this study - PB-TAP IRI - was a kind gift of the Silva lab (Dos Santos *et al.* , 2014) and

was cloned into using the Invitrogen™ Gateway™ cloning system.

5.3 Validation of the perturbations

The first perturbation is treatment with the small molecule inhibitor of myosin II activity - Blebbistatin - which causes embryonic stem cell colonies, that possess tight cell-cell junctions when cultured in 2i/LIF, to break apart where they then favour attachment to the (2D) substrate. Figure 5.3, shows an example of this. In (A) the cells are bound tightly to one another and individual cells cannot be identified from the bright field image. At the boundary of the colony the nuclei are elongated under tension and compression from non-muscle myosin II driven contractility in the cortex. After treating the cells with 20 µM Blebbistatin for 10 minutes, shown in (B), the cells have lost their strong adhesion to one another and can readily be individually identified in the brightfield image. This is indicative of loss of cortical tension which is known be required for stabilisation of cell-cell junctions (Miyake *et al.* , 2006). Loss of actomyosin contractility and the release of intracellular tension leads to the cell and nucleus relaxing into a spherical shape - an example of which is highlighted in green.

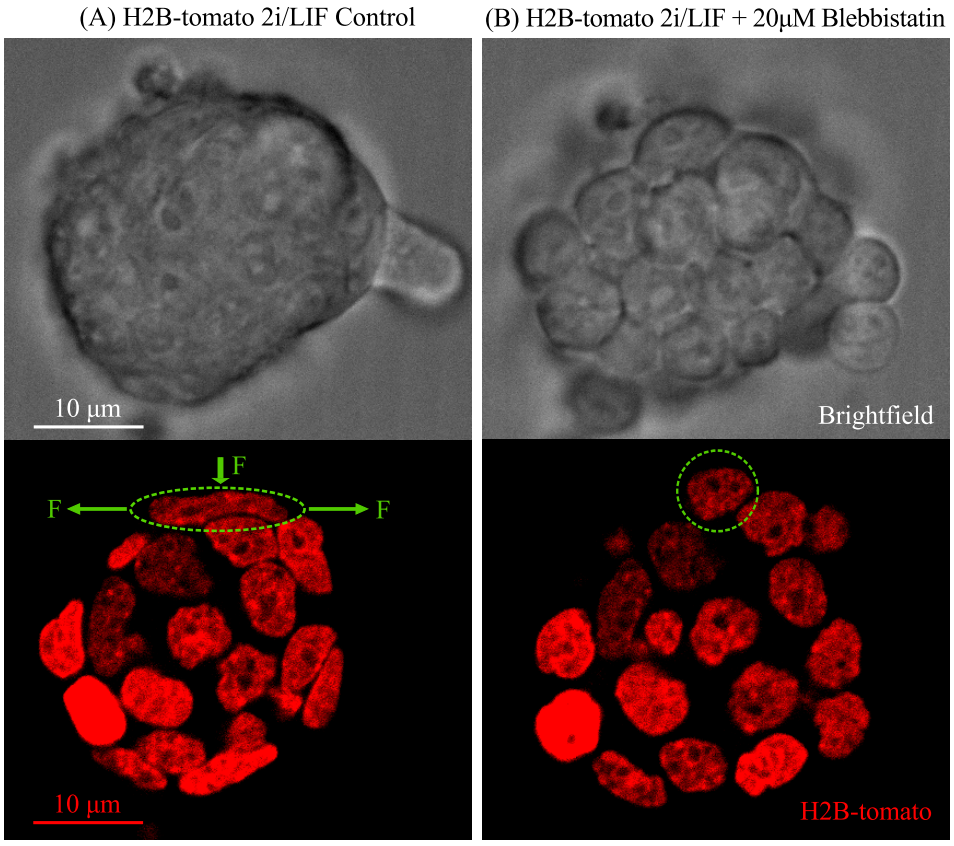

Figure 5.3: Reducing cytoskeletal tension breaks cell-cell junctions and alters nuclear morphology.(A) H2B-tomato mouse ES cell cultured in 2i/LIF. (B) H2B-tomato mouse ES cell cultured in 2i/LIF 10 minutes after the addition of 20 μM Blebbistatin. The nuclear channel highlights the forces on nuclei at the periphery of the colony, compressing and elongating them. Inhibition of actomyosin contractility causes cell-cell junctions to break and increases nuclear circularity.

The second perturbation is the inducible overexpression of the full transcript encoding mouse Lamin A. Figure 5.4A shows an immunofluorescence (IF) stain of an ES cell colony stained for LMNA and LMNB1 in the induced (+Dox) LMNA overexpression polyclonal line in 2i/LIF. First, because the line is polyclonal, there is a large range in expression levels of LMNA and not all the cells express it at detectable levels by IF. This was addressed by subcloning the population and picking clones, one of which was used for all future experiments. The clone was chosen based upon possessing the following characteristics: exhibiting the correct morphology in 2i/LIF (compact colonies), overexpressing LMNA at a reasonable level when induced, and not

expressing low quantities of LMNA (leaking) when not induced. Secondly, as expected, LMNA localises to the nuclear envelope where it forms a ring - Figure 5.4B shows an expanded view of the nuclear envelope where DNA has been counterstained for using Hoechst33342. Interestingly LMNA and LMNB1 are not homogeneously distributed, but rather juxtapositioned in the network forming the nuclear lamina - an observation that is consistent with the literature (Swift *et al.* , 2013).

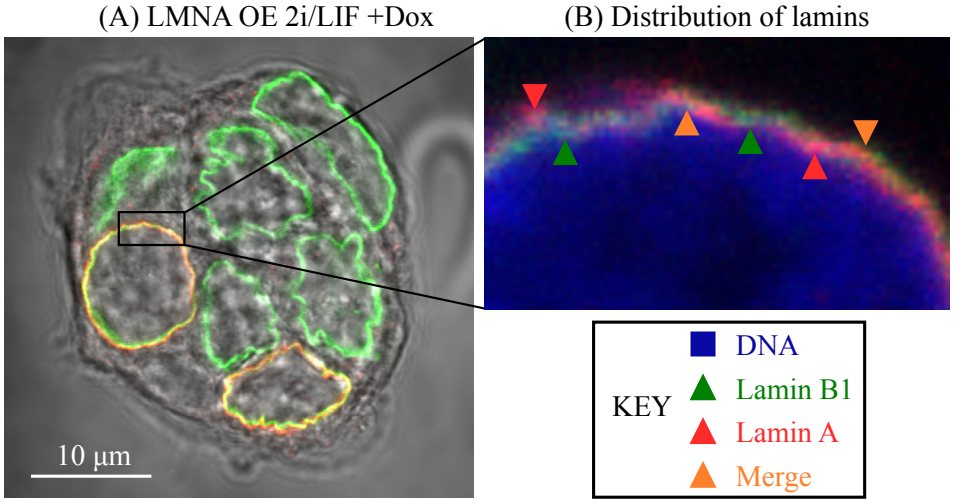

Figure 5.4: LMNA correctly localises to the nuclear periphery. (A) Immunofluorescence of induced (+Dox) polyclonal LMNA overexpressing mouse ES cells, cultured in 2i/LIF and stained for LMNA (red) and LMNB1 (green). (B) Highlights the juxtapositioning of LMNA and LMNB1 at the nuclear envelope. Images taken using a Leica SP5 confocal microscope with a 63x 1.4 NA oil immersion objective.

The third perturbation is the inducible overexpression of LBR. Upon induction with doxycycline we expected to find an enrichment of LBR at the nuclear lamina; instead we found that nuclear architecture was significantly altered. Figure 5.5 shows the clonal LBR ϵ line after 24 hours in N2B27. The doxycycline treated cells exhibit aberrant nuclear shapes, when compared with controls, with LBR distributed throughout the nucleus where it forms lamina like structures. The organisation of heterochromatin was also affected with a shift in organisation from distinct foci to filaments. The filaments of heterochromatin, stained with Hoechst 33342, that are most clearly shown in Figure 5.5C overlap precisely with the distribution of LBR, shown in Figure 5.5D.

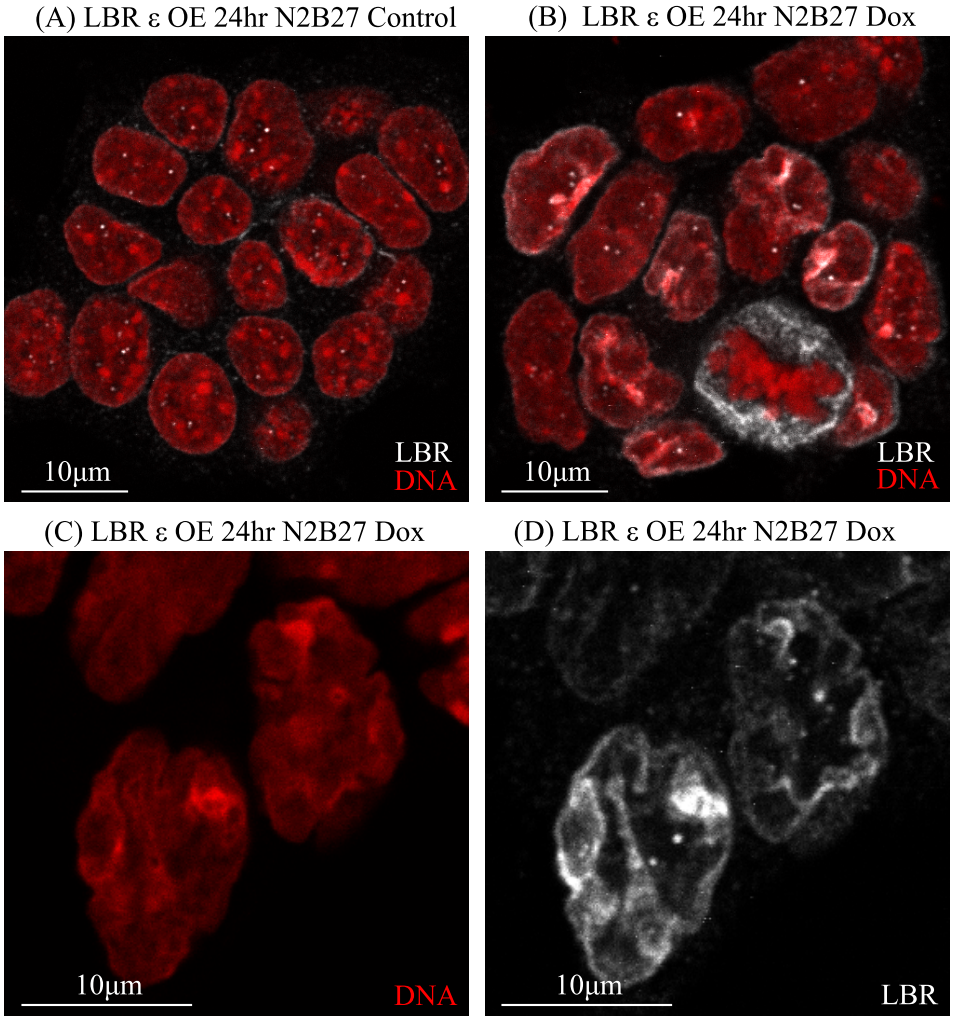

Figure 5.5: LBR overexpression significantly perturbs nuclear structure and the organisation of heterochromatin. (A) Immunofluorescence of LBR in LBR ϵ overexpressing cells cultured for 48 hours in N2B27 without doxycycline (Control). (B) Immunofluorescence of LBR in LBR ϵ overexpressing cells cultured for 48 hours in N2B27 with doxycycline. (C) Expanded image of (B) which shows filamentous heterochromatin upon induction of LBR. (D) Image (C), but only the LBR channel. Overexpression of LBR reorganises the distribution of chromatin from punctate foci into filamentous structures which strongly correlate with the distribution of LBR. A strong possibility is that, upon overexpression, high/excess levels of LBR interact with heterochromatin in the nuclear interior driving assembly of nuclear lamina like structures which perturb heterochromatin organisation.

To take this a step further we checked to see whether any proteins that are known to interact with LBR showed a similar phenotype. The obvious candidate was LMNB1 which, strikingly - shown by immunofluorescence in

Figure 5.6 in LBR ϵ overexpressing cells cultured in N2B27 for 48 hours - also forms filamentous structures within the nucleus upon overexpression of LBR. The distribution of the filaments of heterochromatin and LMNB1 shown in Figures 5.6C and 5.6D shows a similar degree of overlap to that of heterochromatin and LBR (Figures 5.5C and 5.5D). This strongly suggests that the overexpression of LBR is sequestering LMNB1 from the nuclear envelope to the nuclear interior where they interact with and alter the organisation of heterochromatin.

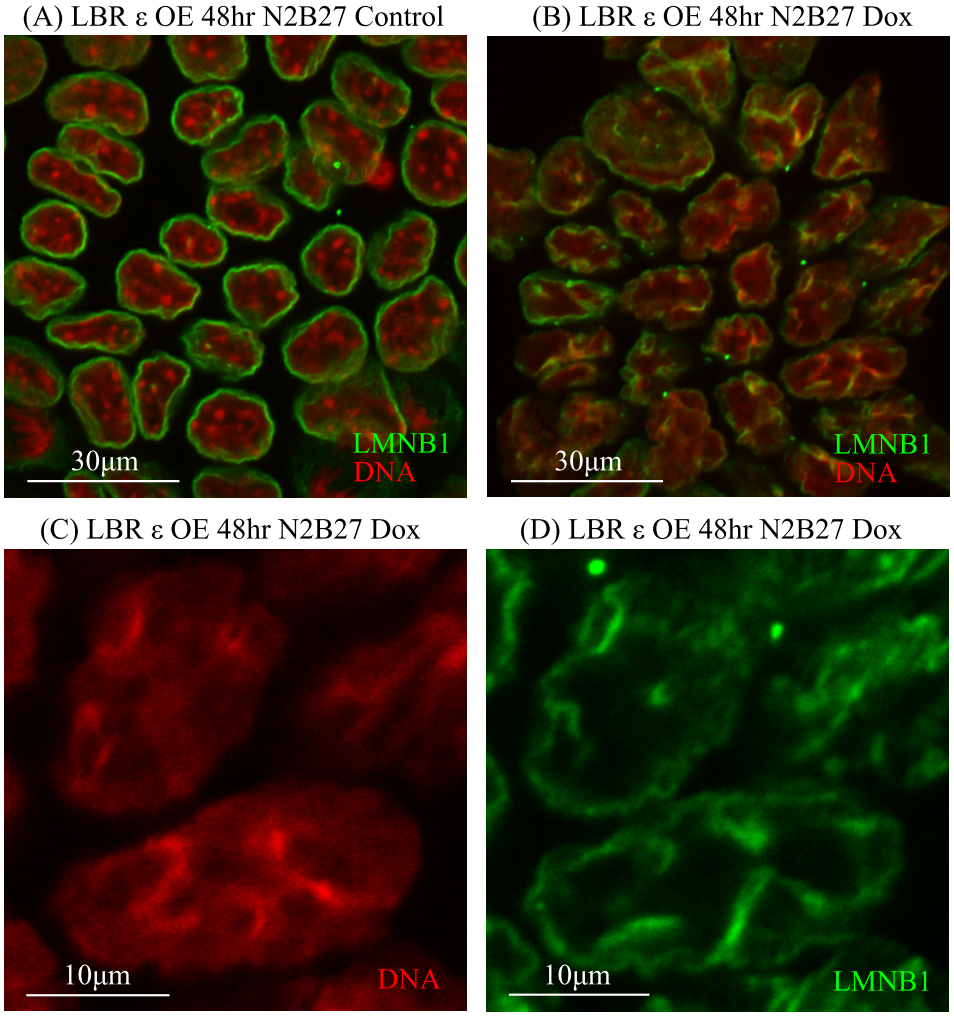

Figure 5.6: LBR overexpression alters the distribution of LMNB1. (A) Immunofluorescence of LMNB1 in LBR ϵ overexpressing cells cultured for 48 hours in N2B27. (B) Immunofluorescence of LMNB1 in LBR ϵ overexpressing cells cultured for 48 hours in N2B27 with doxycycline. (C) Expanded version of (B), highlighting the presence of filaments of heterochromatin in doxycycline treated LBR ϵ overexpressing ES cells. (D) Image (C) but showing the distribution of LMNB1. LBR overexpression causes a shift in the distribution of LMNB1, moving it away from the nuclear envelope into the nuclear interior where its distribution shows strong overlap with filaments of heterochromatin.

Before moving on to examine the effects of the perturbations on nuclear shape and dynamics, because the perturbations target both force generation and the structure of the nuclear envelope - the former which is required for cell division and the latter which must be broken down during it - we measured the proliferation rates in ES cells overexpressing LMNA and LBR and

treated with different concentrations of Blebbisatin - shown below in Figure 5.7. The results show that: while treatment with 5 µM Blebbistatin and above completely blocks cell division; 2 µM has no significant effect, overexpression of LBR in the clonal ϵ line increases the rate of cellular division by 20% (Figures 5.7B and 5.7D); and the overexpression of LMNA in the clonal γ line has no significant effect (Figures 5.7C and 5.7D).

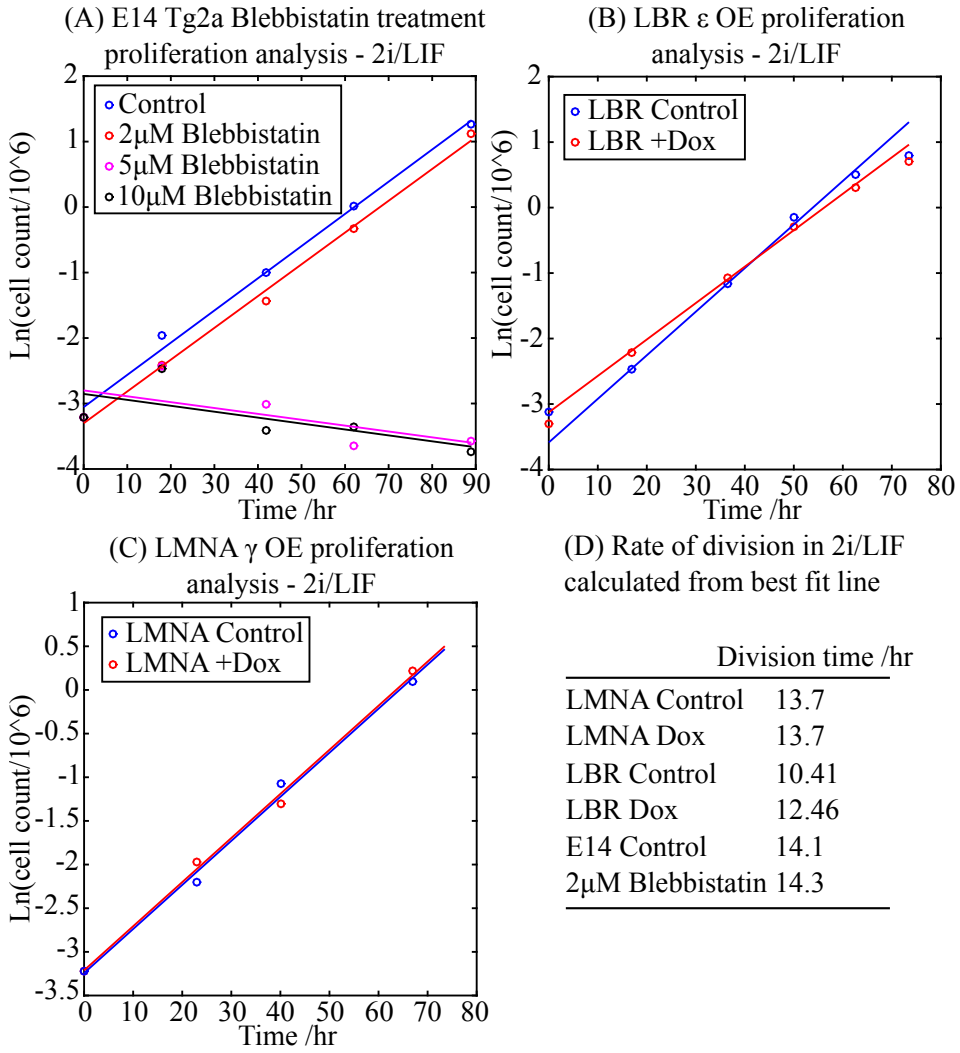

	Division time /hr
LMNA Control	13.7
LMNA Dox	13.7
LBR Control	10.41
LBR Dox	12.46
E14 Control	14.1
2μM Blebbistatin	14.3

Figure 5.7: LBR overexpression decreases proliferation rate by 20%. Overexpression of LMNA or treatment with 2 μM Blebbistatin has no significant effect. Assay of proliferation rates in (A) E14 Tg2a + Blebbistatin treatment, (B) LBR ϵ OE and (C) LMNA γ OE mouse ES cells in 2i/LIF. Division rates - calculated from the gradient of the best fit lines in (A), (B) and (C) and listed in (D) - show that, while LBR overexpression slows down division by 20%, LMNA overexpression and treatment with 2 μM Blebbistatin has no significant effect. Treatment with 5 μM and 10 μM Blebbistatin blocks proliferation and causes significant cell death.

5.4 Cellular and nuclear morphology

In this Section I examine the effect of the perturbations introduced in this Chapter on nuclear morphology. The morphology of the nucleus is important to characterise because it is intimately connected to, and acts as an indirect

read-out of, the forces acting on and propagated within the cell.

To characterise the shape of the nucleus we have chosen to use the shape descriptors defined below:

$$Eccentricity = \frac{Foci\ Separation}{Major\ Axis} \tag{5.1}$$

An eccentricity of 0 is a circle, a value of 1 is a line segment.

$$Circularity = 4\pi * \frac{Area}{Perimeter^2} \tag{5.2}$$

A circularity of 1 is a circle, a value of 0 is a line segment.

$$Solidity = \frac{Area}{Convex\ Area} \tag{5.3}$$

Eccentricity and circularity give complementary measurements of how elliptical the nucleus is; however, because circularity uses the perimeter of the nucleus, the measurement is sensitive to undulations in the nuclear envelope that would otherwise be missed by eccentricity. Solidity is included to give a measure of how much the shape of the nucleus deviates from elliptical. Lastly, we have included projected area, which gives a measure of how spread the nuclei are. Representative images of the effect of LMNA overexpression, LBR overexpression and LBR knockdown on nuclear shape are shown below in Figure 5.8. Quantification of nuclear shape using the shape descriptors discussed above are presented in Figure 5.9 and the results summarised as follows:

- LMNA overexpression: reduces eccentricity but does not alter circularity, and has no effect on solidity or area.
- LBR overexpression: increases eccentricity, reduces circularity and solidity, and does not alter area.
- LBR knockdown: reduces eccentricity, increases circularity and solidity, and reduces area.
- Treatment with 2 µM Blebbistatin: has no effect on eccentricity, increases circularity and solidity, and has no effect on area.

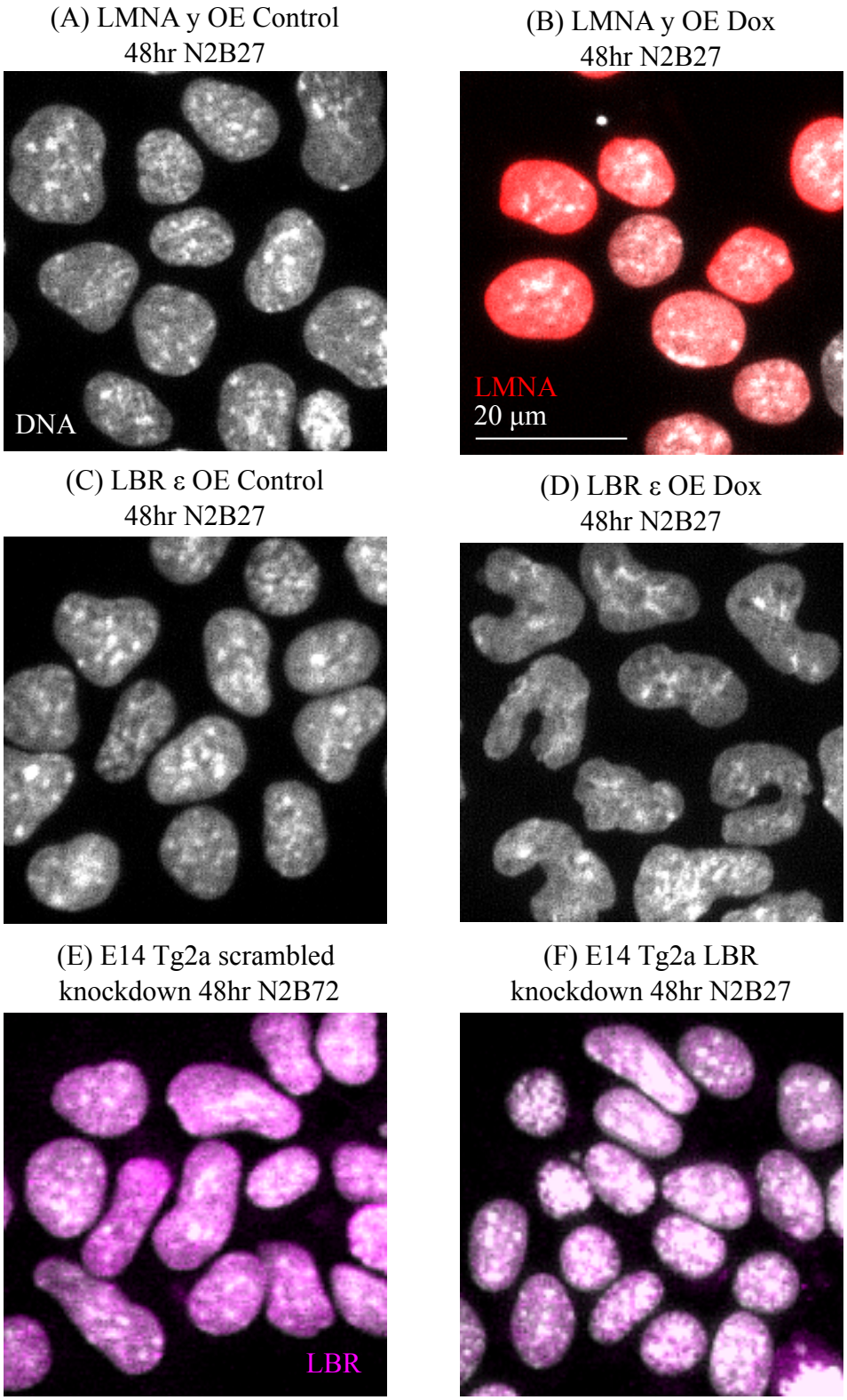

Figure 5.8: Comparison of nuclear morphology. Nuclear morphology after 48 hours in N2B27, analysed quantitatively in Figure 5.9. (A)/(B) LMNA overexpression, (C)/(D) LBR overexpression and (E)/(F) LBR knockdown (siRNA).

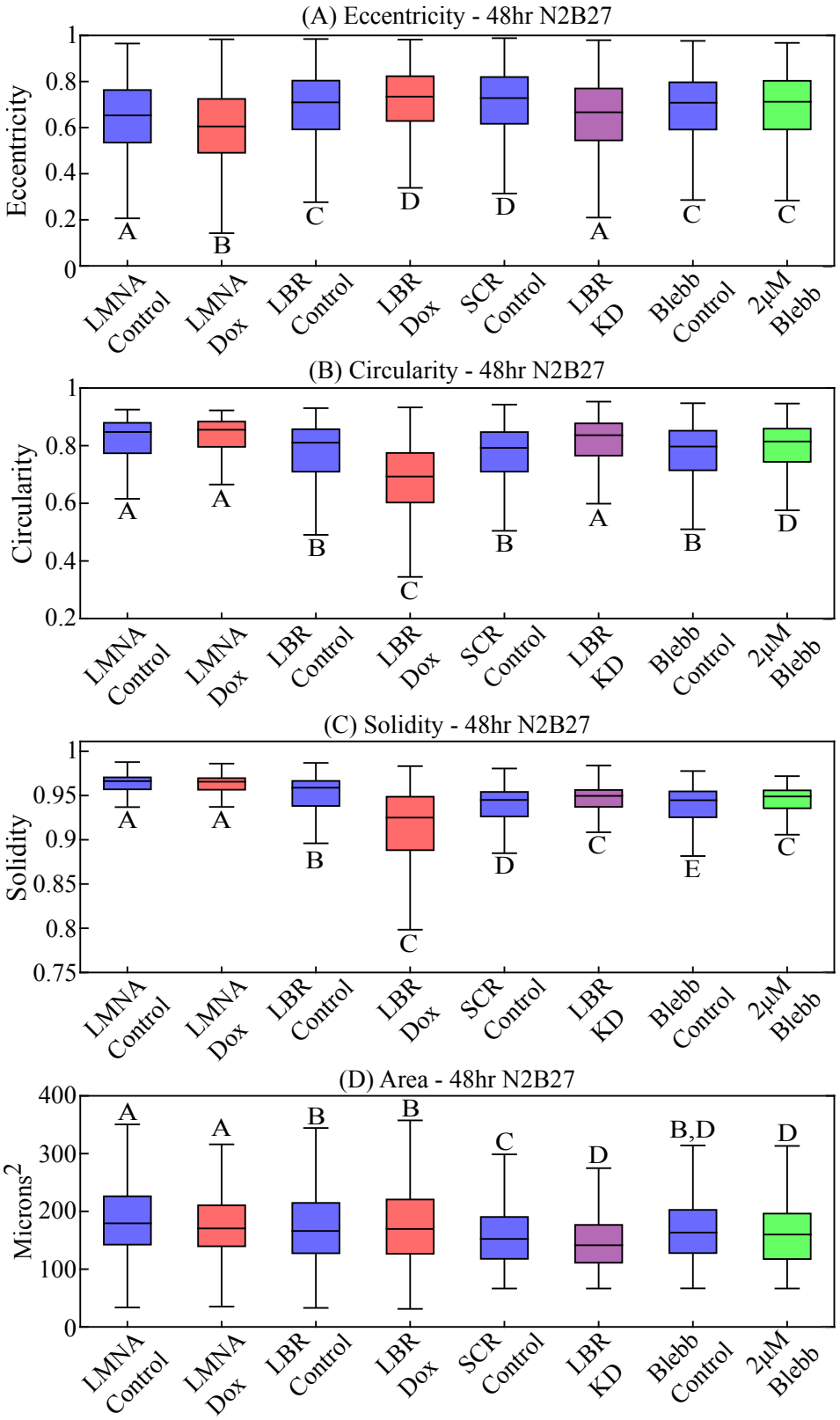

Figure 5.9: Quantification of nuclear shape. Caption on following page.

Figure 5.9: Shape descriptors of mouse ES cell nuclei. Cells were cultured on laminin coated (10 µg/ml) 24-well plates in N2B27 for 48 hours with the following perturbations: overexpression of LMNA, overexpression of LBR, LBR knockdown and treatment with 2 µM Blebbistatin. (A) Comparison of nuclear eccentricity - equation 5.1. (B) Comparison of nuclear circularity - equation 5.2. (C) Comparison of nuclear solidity - equation 5.3. (D) Comparison of nuclear projected area. Statistical analysis was performed in MATLAB using a Kruskal-Wallis test and a multi-comparison test. Samples with different letters show significant differences at the five percent confidence level, whereas those with the same letter do not. LMNA overexpression reduces nuclear eccentricity. LBR overexpression results in elongated and aberrantly shaped nuclei, while LBR knockdown has the opposite effect, giving smaller, and more circular, nuclei. Reduction in actomyosin tension through non-muscle myosin II inhibition (Blebbistatin treatment) also leads to an increase in nuclear circularity. N = 3, with n > 1000 for each cell type.

5.5 Nuclear shape change dynamics

After exploring the effect of the perturbations on static nuclear morphology, we turned our attention to looking at the dynamics of the nuclear envelope. Using the nuclear shape change characterisation methods discussed in Chapter 4 - equations 4.1 and 4.2 - we analysed the amplitude of nuclear shape changes in LMNA-overexpressing, LBR-overexpressing and Blebbistatin-treated mouse ES cells cultured in N2B27 for 48 hours. We chose to use a low concentration of Blebbistatin - 2 µM - as this was found by titration to be the highest dose before the rate of cellular proliferation was significantly increased (Chapter 6 - Figure 5.7). The results of the analysis of the magnitude of nuclear shape change are shown in Figure 5.10: treatment with 2 µM Blebbistatin has no significant effect - (A)/(D), LMNA overexpression reduces shape change - (C)/(D), and LBR overexpression increases shape change (B). It was not possible to perform the shape change analysis that looks at fluctuations in the nuclear boundary, shown in Figure 5.10D, in LBR-overexpressing cells because a significant fraction of the cells yielded radial nuclear boundary coordinates (as a function of angle) that were multivalued due to aberrant nuclear shape.

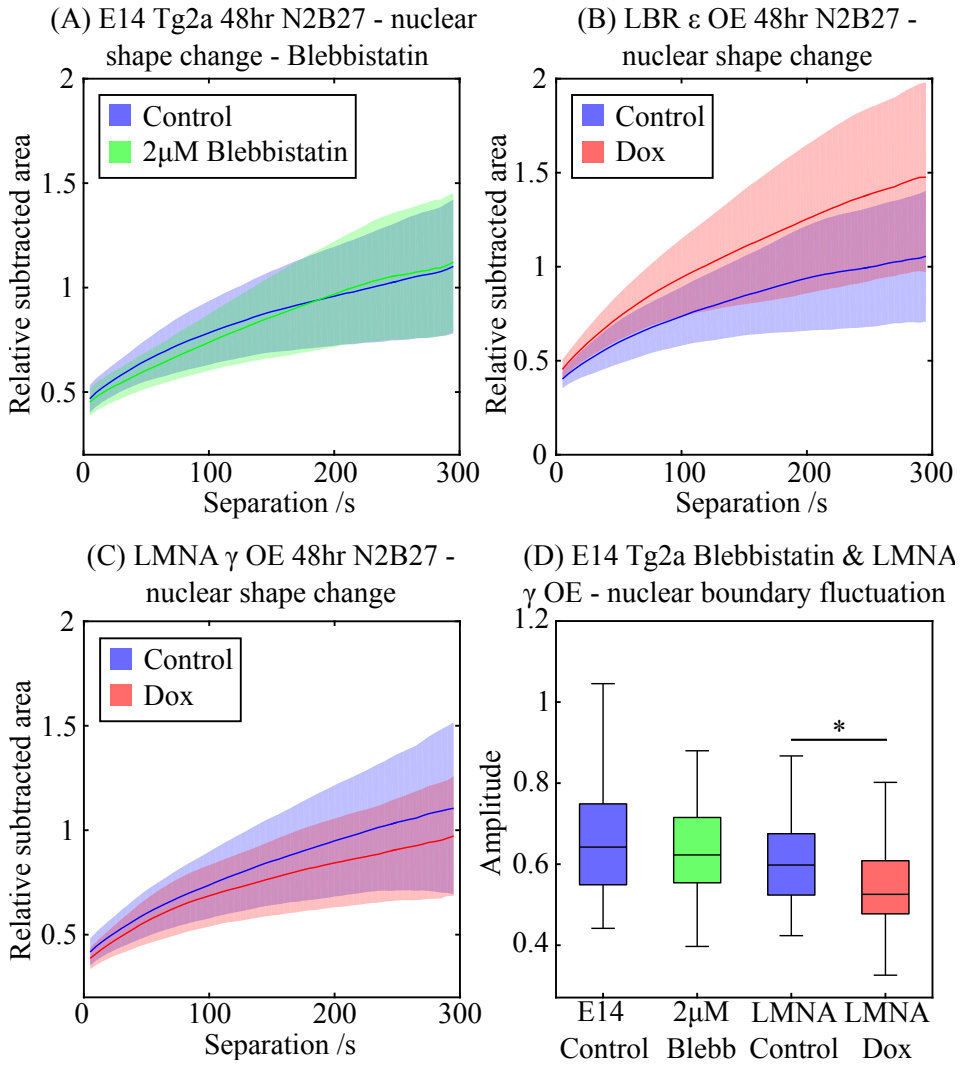

Figure 5.10: LMNA overexpression reduces nuclear shape change, LBR overexpression increases it. Analysis of dynamics of nuclear shape change of LBR & LMNA overexpression and treatment with 2 μM Blebbistatin in E14 Tg2a ES cells after 48 hrs in N2B27, using equation 4.1 in figures (A-C) and equation 4.2 in figure (D). (A-C) - solid line and shaded area represent the mean and standard deviation, respectively. E14 Tg2a Control: n = 84, E14 Tg2a + 2 μM Blebbistatin: n = 74, LBR ϵ Control: n = 75, LBR ϵ +Dox: n = 77, LMNA γ Control: n = 118, LMNA γ +Dox: n = 89. Statistical analysis performed in MATLAB using a Kruskal-Wallis test, followed by a multi-comparison test. (D) $p < 0.05$ shown by asterisk.

The next stage of the project was to characterise the frequency spectrum of the fluctuations in the nuclear boundary with the perturbations. In order to increase the throughput in our experiments we lowered the magnification in our imaging compared with experiments referenced in Chapter 4, switch-

ing from a 63x 1.4 NA to a 40x 1.2 NA oil immersion objective. While this allowed us to image significantly more cells and increase our population sampling rate, it exacerbated the problem of the discrete nature of the images. This is summarised in Figure 5.11: Figure 5.11B illustrates an example of the fluctuation in the radial position, in pixels, of a point on the boundary of the nucleus over time. When using a thresholding method for detecting the nuclear envelope, depicted in blue, it results in significant high frequency fluctuations as the boundary oscillates between pixels. Correspondingly the resultant Fourier transform, shown in Figure 5.11A in blue, is corrupted by a broad range of frequencies that, while unable to mask the dominant low frequency oscillation, removes any high frequency information. In order to combat this, we took advantage of the fact that the pixels in the image are blurred by the point spread function (PSF) of the microscope, the form of which is known to be a Gaussian. By fitting a Gaussian to the radial intensity across the nuclear boundary (Figure 5.11D), we can obtain sub-pixel resolution of the localisation of the nuclear envelope, shown in Figure 5.11B in red. As a result the majority of the high frequency noise in the Fourier transform, Figure 5.11A - red, is removed.

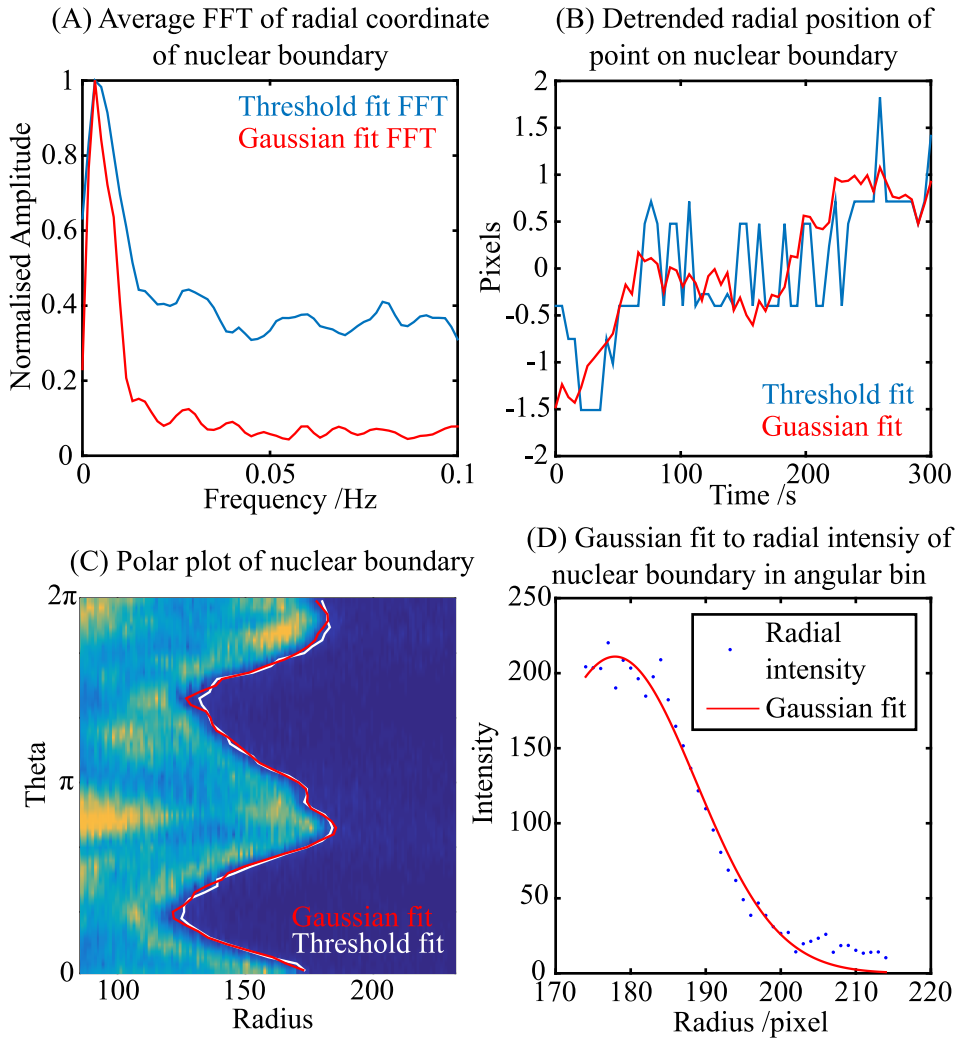

Figure 5.11: Obtaining sub-pixel localisation of the nuclear boundary improves Fourier analysis. (A) Using a Gaussian fit of the nuclear boundary significantly reduces high frequency corruption of the FFT that results from identifying nuclear boundary based on threshold value. (B) Sub pixel localisation of point on nuclear boundary obtained with Gaussian fit. (C) Polar plot of nuclear boundary fit with threshold method and Gaussian fit. (D) Example fit of Gaussian to radial pixel intensity across the nuclear boundary.

We applied the improvements to our Fourier analysis to look at the frequency spectrum of oscillations in the nuclear envelope in LMNA-overexpressing and Blebbistatin-treated E14 Tg2a mouse ES cells, cultured in N2B27 for 48 hours. The results, shown below in Figure 5.12, show a dominant period of oscillation centred on 0.0045 Hz with no significant difference when LMNA is overexpressed, or the cells are treated with 2 µM Blebbistatin.

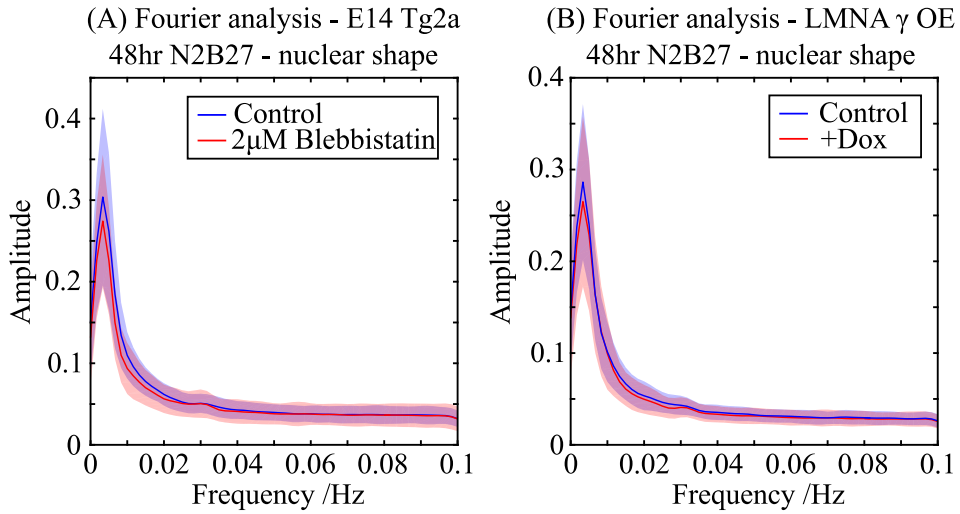

Figure 5.12: Overexpression of LMNA or treatment with 2 µM Blebbistatin does not alter the Fourier spectrum of nuclear shape change. Fourier analysis of nuclear shape change in E14 Tg2a supplemented with 2 µM Blebbistatin and LMNA γ overexpressing mouse ES cells, cultured for 48 hrs in N2B27. Fourier analysis conducted using a Hanning window and detrended (constant value) data on fluctuations in radial boundary co-ordinates, averaged over all angles and then over all cells. Solid line and shaded area represent the mean and standard deviation, respectively. E14 Tg2a Control: n = 84, E14 Tg2a + 2 µM Blebbistatin: n = 74, LMNA γ Control: n = 118, LMNA γ +Dox: n = 89.

This Chapter has focused, so far, on characterising the effect of the forces acting on the nucleus and introducing ways in which to perturb these forces. We have measured the impact on both nuclear morphology and nuclear shape change dynamics - magnitude and frequency. In the next part of the Chapter we explore to what extent the perturbations modulate the interactions between heterochromatin at the nuclear periphery and the nuclear envelope. As a read-out, we chose to look at the distributions of epigenetic modifications that are required for regulating these interactions, the specifics of which are discussed in the next section. In particular, we expected to find the overexpression of LMNA and LBR - both implicated as chromatin tethers (Solovei *et al.* , 2013) - would result in an enrichment of repressive histone modifications at the nuclear periphery during differentiation as, we hypothesised, the cells would struggle to release and access any lineage genes stuck there.

5.6 Distribution of repressive histone modifications

In this section I look at the distribution of repressive histone modifications in the pluripotent ground state and during differentiation. We chose to look at histone 3 lysine 9 di-methylation (H3K9me2) and histone 3 lysine 27 tri-methylation (H3K37me3) for two reasons. Firstly, these repressive histone modifications are implicated in the positioning of peripheral heterochromatin to the nuclear lamina (Towbin *et al.* , 2012) (Bian *et al.* , 2013) (Harr *et al.* , 2015). Secondly, the distributions of H3K9me2 and H3K27me3 have also been shown to be mechanosensitive, responding to forces acting on the nucleus (Le *et al.* , 2016).

We found that H3K9me2 was always enriched at the nuclear periphery regardless of cell state - Figures 5.13, 5.14, 5.16 and 5.17. Interestingly, we observed that H3K9me2 is strongly enriched at the periphery of nuclei that are on the outside of compact colonies of cells cultured in 2i/LIF, but away from cell-cell junctions - Figure 5.13A/C. Upon removal of 2i/LIF, however, after 24 hours H2K9me2 was much more uniformly distributed in a ring - Figure 5.13B/D. It is possible that this change in distribution at the nuclear periphery is an artefact of the staining protocol but, while hard to rule out completely, it is unlikely as the antibody against LMNA has no trouble penetrating to the nuclear periphery of cells inside the colony - Figure 5.13A/B. Important to note is that this observation is independent of LMNA expression - doxycycline LMNA γ OE ES cells stained for LMNA were shown in Figure 5.13 to demonstrate antibody penetration.

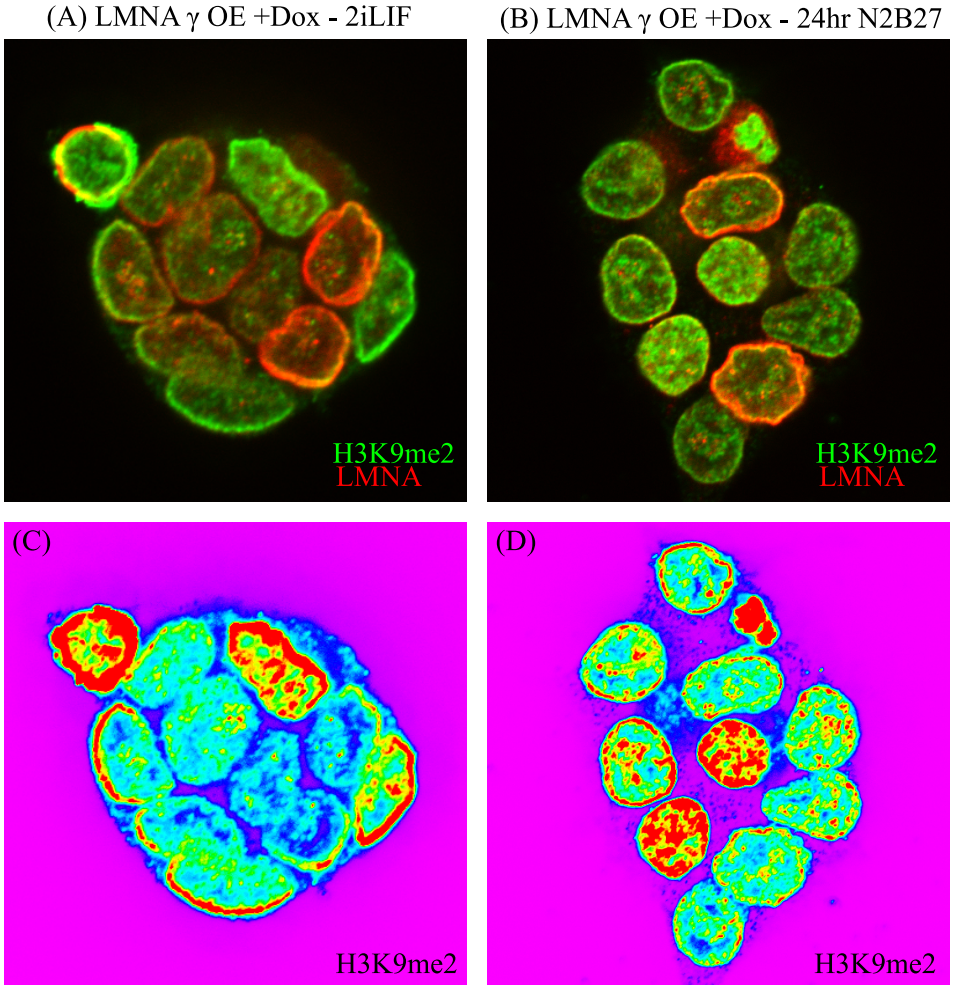

Figure 5.13: H3K9me2 localises to nuclear periphery away from cell-cell junctions. Immunofluorescence of H3K9me2 (green) and LMNA (red) in LMNA γ OE mouse ES cells cultured in 2i/LIF (A) and N2B27 for 24 hours (B). The distribution of H3K9me2 is shown more clearly in a heat map in (C) and (D): in compact colonies H3K9me2 is distributed towards the nuclear periphery of cells away from cell-cell contacts (C) - in more spread colonies (D) the H3K9me2 is distributed in a uniform ring. N = 3.

To determine if the release from the pluripotent state (2i/LIF withdrawal) was responsible for reorganising the distribution of H2K9me2, or whether the effect was a result of cell-matrix adhesion and spreading, we plated LMNA γ OE mouse ES cells in 2i/LIF on ibidi dishes coated in gelatin or 10 µg/ml laminin. The former results in compact colonies that favour cell-cell adhesion while the latter gives spread colonies that favour matrix attachment. The results, shown in Figure 5.14, suggest that it is cell spreading and matrix adhesion which is responsible for redistributing

H3K9me2 from a partial ring that is enriched away from cell-cell junctions, to a more uniform ring.

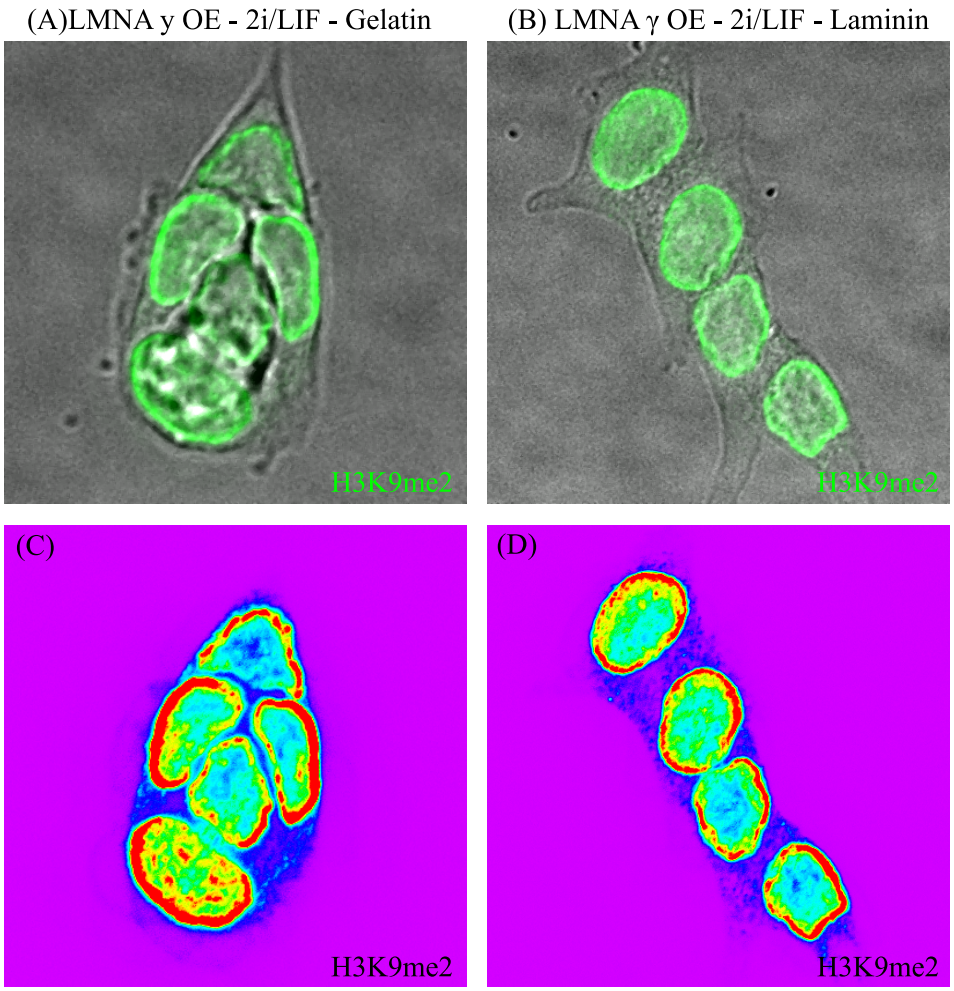

Figure 5.14: The distribution of H3K9me2 is a function of cell spreading. Immunofluorescence of H3K9me2 in LMNA γ OE mouse ES cells cultured in 2i/LIF on gelatin (A) and 10 µg/ml laminin (B). Culturing on gelatin results in compact colonies with cells favouring cell-cell contacts with H3K9me2 distributed to the nuclear periphery away from cell-cell junctions. Culturing on laminin results in spread colonies with a more uniform distribution of H3K9me2 in at the nuclear periphery. N = 1.

Next, we explored what effects the overexpression of LMNA and LBR had on distributions of H3K9me2 and H3K27me3 at the nuclear envelope during the differentiation process. Figures 5.16 and 5.17 show, respectively, representative immunofluorescence images of LMNA γ and LBR ϵ ES cells co-stained for H3K9me2 and H3K9me3 after 24 and 48 hours in N2B27.

Quantification of the enrichment of H3K9me2 and H3K27me3 at the nuclear periphery was calculated using CellProfiler. To begin with, all image channels were aligned and nuclei identified (IdentifyPrimaryObjects module), the mask of which was used as a template to obtain more accurate masks of H3K9me2, H3K27me3 and LMNA/LBR in their respective channels (IdentifySecondaryObjects module). Obtaining accurate masks of the edge of the nucleus was found to be critical to ensure that the distributions calculated below were comparable. To obtain the radial distributions of H3K9me2 and H3K27me3 we used the MeasureObjectRadialDistribution module, its function described as follows: nuclei were first segmented into five bands (scaling with nuclear size) at radius r, emanating from the centroid of each nucleus. The radial intensity in each band was then normalised by the total cell intensity (I_T) and then by area (A) as follows:

$$NI_r = \frac{I_r}{I_T} * \frac{A_T}{A_r} \tag{5.4}$$

An example of the results from calculating the radial distribution of H3K9me2 in LMNA γ OE ES cells after 24 hours in N2B27 (without doxycycline) is shown below in Figure 5.15A, with the 5th bin showing the relative enrichment at the nuclear periphery. We also calculated the intensity of LMNA at the nuclear periphery and, plotting a histogram of control vs. doxycycline treated cells, identified a cut-off value of LMNA intensity to exclude doxycycline treated LMNA γ OE ES cells that did not express LMNA above control values from the downstream analysis. This cut-off value was chosen by eye.

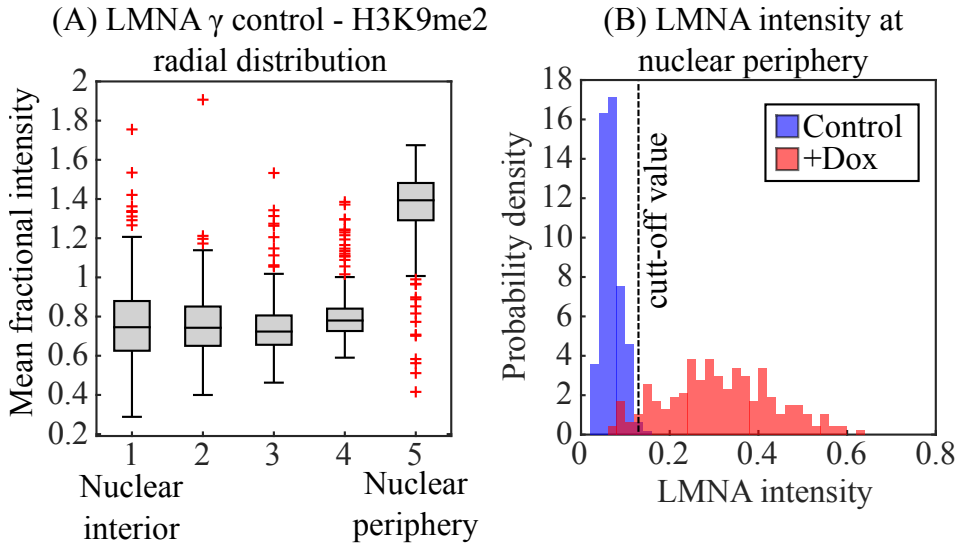

Figure 5.15: Analysing the radial distribution of histone modifications. (A) Example of output from CellProfiler analysis of the radial distribution of H3K9me2 in LMNA γ ES cells (without doxycycline) after 24 hours in N2B27. Radial distribution divided into 5 bins, with the 1st bin representing the nuclear interior and the 5th bin the nuclear periphery. Analysis shows strong enrichment of H3K9me2 at the nuclear periphery - as expected from representative images (Figures 5.13, 5.14, 5.16 and 5.17). (B) Histogram of LMNA intensity at nuclear periphery from CellProfiler analysis - used to determine a cut-off value, bye eye, for LMNA γ +Dox cells (example shows 24 hours in N2B27) that do not express levels of LMNA above control values for exclusion from downstream analysis.

The results of our analysis of the distributions of H3K9me2 and H3K27me3 with LMNA and LBR overexpression at 24 and 48 hours after 2i/LIF withdrawal are shown below in Figure 5.18. Overexpression of LMNA and LBR both result in a significant reduction in the relative fraction of H3K9me2 at the nuclear periphery, as does increasing time after 2i/LIF withdrawal. The distribution of H3K27me3 shows the opposite trend: LMNA overexpression results in an increase in the fraction at the nuclear periphery, as does increasing time after 2i/LIF withdrawal. LBR overexpression has no effect on the distribution of H3K27me3 at the nuclear periphery, however increasing time after 2i/LIF withdrawal also lead to an increase in the relative fraction.

We have also quantified the mean whole-cell immunofluorescence staining intensities of H3K9me2 and H3K27me3, given as a percentage value normalised to the intensity of the 24 hour N2B27 control population in Figures 5.16 and 5.17. The results show that the mean H3K9me2 intensity increases during differentiation, while the mean H3K27me3 intensity falls.

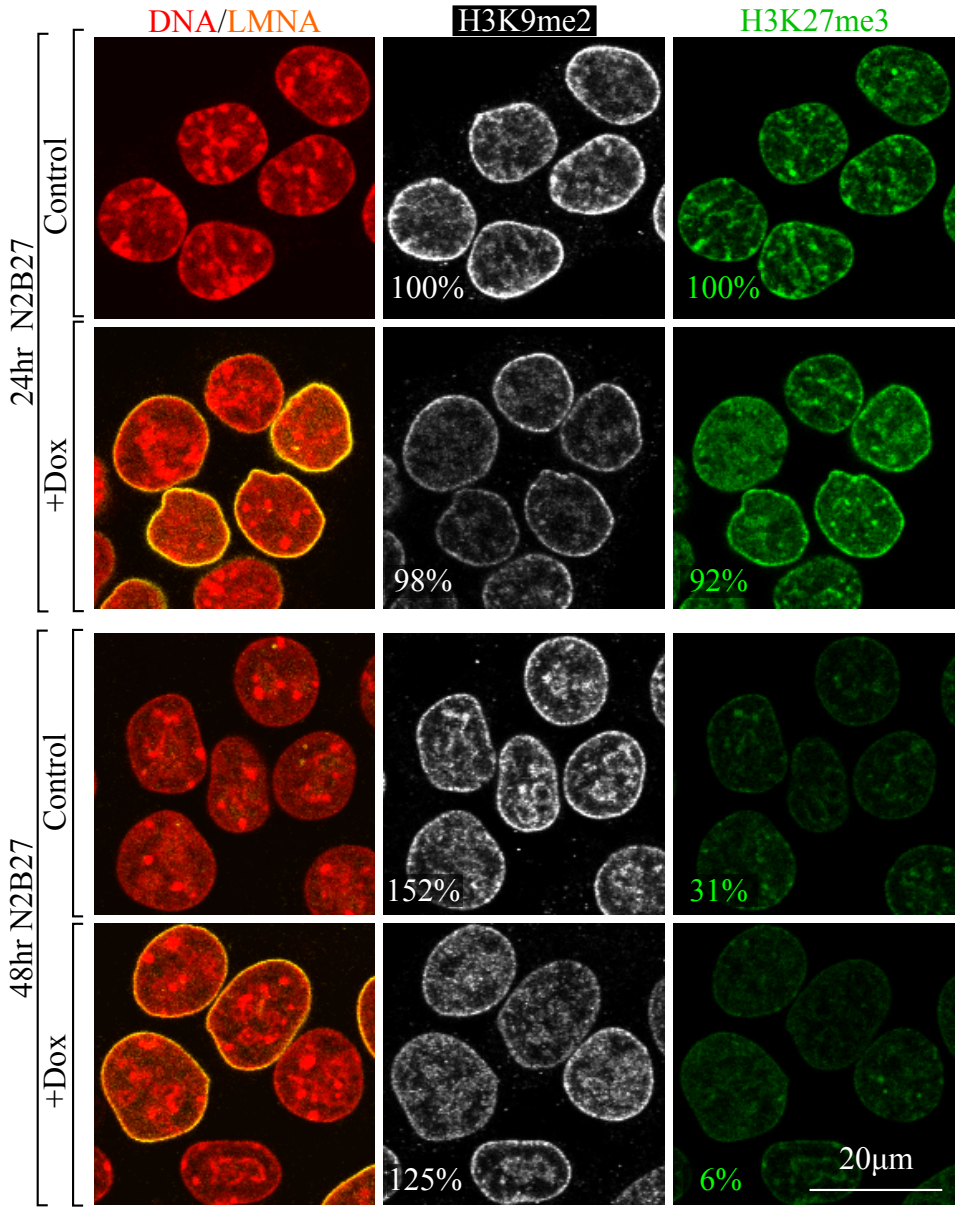

Figure 5.16: Representative images for radial distribution analysis of H3K9me3 and H3K27me3 with LMNA overexpression. Immunofluorescence co-stain for H3K9me2 and H3K27me3 in LMNA γ mES cells, cultured for 24 and 48 hours in N2B27 on laminin coated ibidi dishes (10 µg/ml), +/− Dox. H3K27me3 antibody was directly conjugated to Alexa 488 and was applied after the normal secondary antibody step. Percentages given in H3K9me2 and H3K27me3 images represent mean total cell intensities - normalised to 24hr N2B27 control value. Standard error of the mean is < 5 percent. Images show; the enrichment of H3K27me3 with LMNA overexpression (24hr N2B27), reduction in mean total cell intensity of H3K27me3 with differentiation and an increase in mean total cell intensity of H3K9me2 with differentiation.

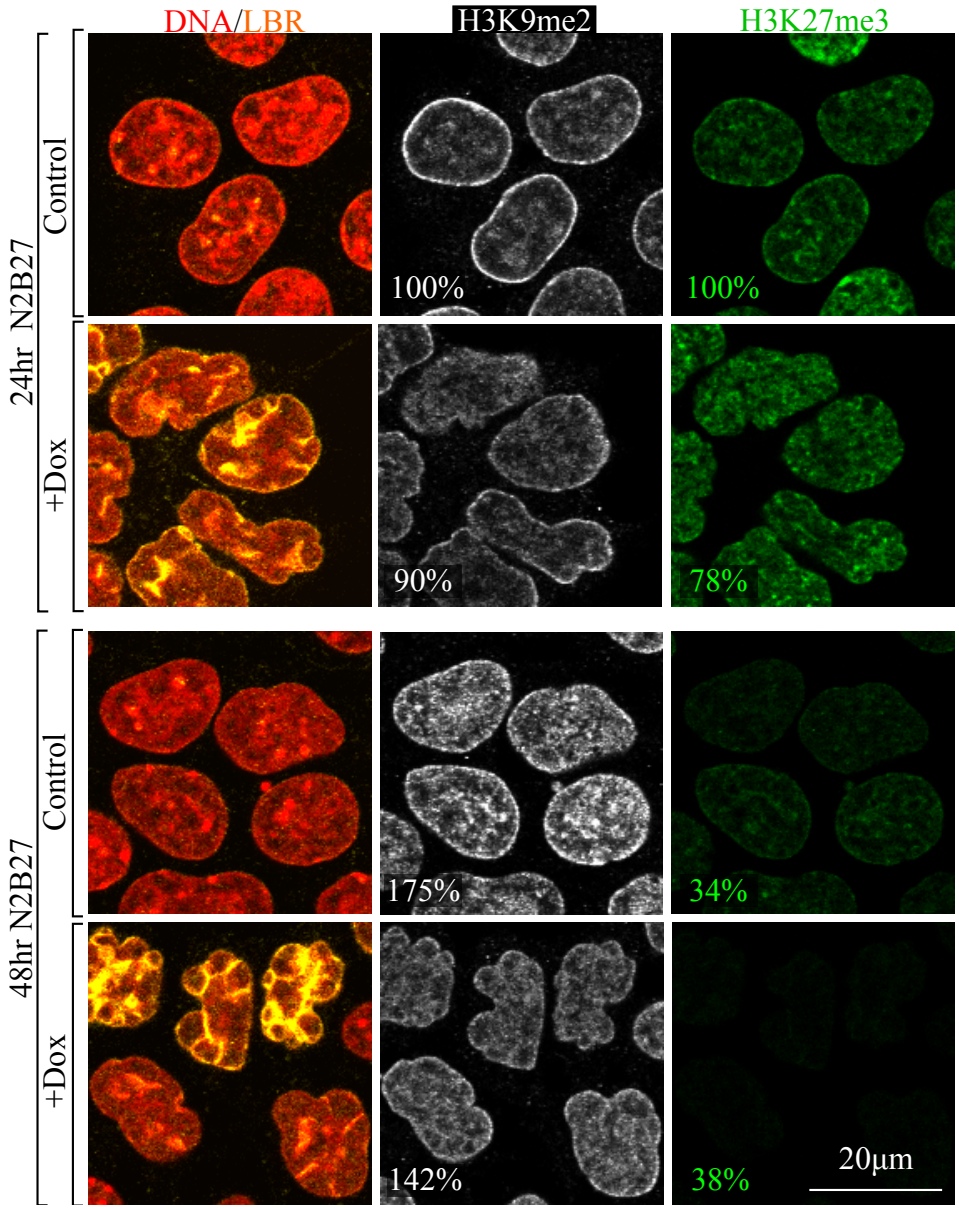

Figure 5.17: Representative images for radial distribution analysis of H3K9me3 and H3K27me3 with LBR overexpression. Immunofluoresence co-stain for H3K9me2 and H3K27me3 in LBR ϵ mES cells, cultured for 24 and 48 hours in N2B27 on laminin coated ibidi dishes (10 µg/ml), +/− Dox. H3K27me3 antibody was directly conjugated to Alexa 488 and was applied after the normal secondary antibody step. Percentages given in H3K9me2 and H3K27me3 images represent mean total cell intensities - normalised to 24hr N2B27 control value. Standard error of the mean is < 5 percent. Images show a reduction in mean total cell intensity of H3K27me3 with differentiation and an increase in mean total cell intensity of H3K9me2 with differentiation.

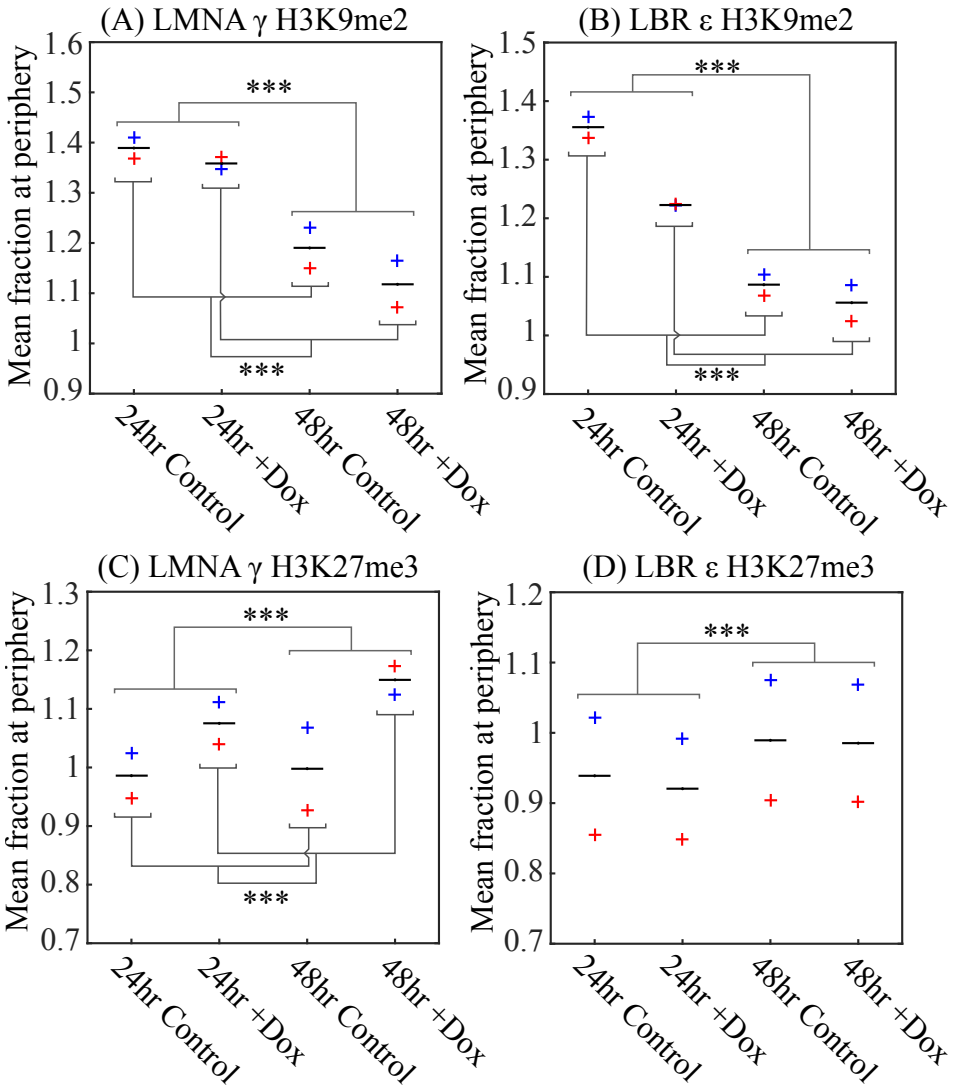

Figure 5.18: LMNA and LBR overexpression reduce the relative fraction of H3K9me2 at the nuclear periphery. LMNA overexpression also enriches the relative fraction of peripheral H3K27me3. (A)/(C) Comparison of (the mean of) the mean fraction of H3K9me2 and H3K27me3, respectively, in LMNA γ mES cells cultured in N2B27 for 24 and 48 hours. (B)/(D) Comparison of (the mean of) the mean fraction of H3K9me2 and H3K27me3, respectively, in LBR ϵ mES cells cultured in N2B27 for 24 and 48 hours. Independent of LBR and LMNA overexpression, increasing differentiation time (24 hours to 48 hours in N2B27) significantly reduces the relative proportion of H3K9me2 at the nuclear periphery and enriches the relative peripheral fraction of H3K27me3. Statistics performed using an N-Way ANOVA with the following groups - 24 hours vs. 48 hours, Control vs. Dox and Experiment 1 vs. Experiment 2. Three asterisks represent p value < 0.001. There is a significant difference between the two experiments, however the trends in both experiments are the same.

5.7 Discussion

This Chapter has introduced and characterised perturbations to the cytoskeleton and the nuclear envelope. Our goals were twofold: to reduce the forces acting at the nuclear envelope and transmitted to chromatin and to alter the binding between peripheral heterochromatin and the nuclear lamina. In order to reduce forces transmitted to chromatin we: targeted force generation in the cytoskeleton through small molecule inhibition of the molecular motor non-muscle myosin II, overexpressed LMNA to stiffen the nuclear envelope and decoupled the nuclear envelope from the cytoskeleton by breaking the LINC complex (data discussed and presented in Chapter 6). To alter the binding of peripheral heterochromatin to the nuclear lamina we overexpressed and knocked-down LBR, and overexpressed LMNA, both of which are known to be important tethering chromatin to the nuclear envelope (Solovei *et al.* , 2013).

Targeting of force generation in the cytoskeleton was achieved using the small molecule inhibitor Blebbistatin which significantly reduces nuclear shape change - Figure 4.3. We chose to measure nuclear morphology as a means of quantifying the effect of forces acting on both bulk chromatin and, we hoped, local fluctuations at the nuclear envelope. We found that short term treatment ($<$ 1 hour) with high concentrations of Blebbistatin (20 µM) had a rapid effect on cell morphology, causing compact ES colonies (2i/LIF) to be rapidly broken apart - Figure 5.3. This observations is in agreement with studies that have identified the importance of non-muscle myosin II activity for the formation and stabilisation of cell-cell junctions (Shewan, 2005)(Smutny *et al.* , 2010). Additionally, the nuclei also became rounder, indicative of a reduction in the magnitude of the forces acting on the nucleus. It is possible the forces that drive nuclear elongation at the edge of ES cell colonies are compressional from the direct contact of the nucleus with the cell boundary. This mechanism has been proposed as an explanation for the observation of increasing nuclear elongation with greater cell spreading in a recent study conducted on NIH3T3 fibroblasts (Li *et al.* , 2015). Treatment with high concentrations of Blebbistatin is not suitable for long term cell culture as it blocks cellular proliferation above 2 µM - Figure 5.7. At 2 µM, the effect of Blebbistatin is very small - we observed no significant reductions in nuclear shape changes - Figure 5.10A/D, or changes to the frequency spectrum of nuclear boundary fluctuations - Figure 5.12A. We did find an effect on nuclear morphology with an increase in circularity and solidity -

Figure 5.9 - indicative of a loss of tension on the nucleus.

The overexpression of LMNA was designed to stiffen the nucleus and to provide the nuclei with an addition mechanism of tethering chromatin to the nuclear envelope (Swift *et al.* , 2013)(Solovei *et al.* , 2013). We found that LMNA reduced the eccentricity of the nuclei - Figure 5.9 and reduced nuclear shape changes - Figure 5.10C/D. These findings are consistent with LMNA acting to stiffen the nucleus: a stiffer nuclear envelope would result in increased nuclear circularity, owing to an increase in energy cost to deform the nuclear envelope, in addition to reducing force-mediated chromatin deformation. We did not find any differences in the Fourier analysis of fluctuations in the nuclear boundary when LMNA was overexpressed - Figure 5.12B. This result is expected as the frequency of oscillation of a damped driven oscillator is determined solely by the frequency of oscillation of the driving force. In our system, the output is the position of the nuclear envelope; the driving force is periodic and generated in the cytoskeleton; and the nuclear envelope provides both elastic and viscous damping terms. LMNA confers the viscous component of the nuclear envelope, in contrast to LMNB1 which governs its elasticity (Shin *et al.* , 2013)(Swift *et al.* , 2013)(Harada *et al.* , 2014). Addition of LMNA into the nuclear lamina would increase the viscous damping, which would alter the amplitude and phase of nuclear envelope fluctuations (the latter with respect to the driving force), but not the frequency. It is worth noting that overexpression of LMNA may be producing competing effects: high levels of LMNA have been shown to increase actomyosin-generated contractility through the serum response factor (SRF) pathway (Swift *et al.* , 2013), which would act to increase forces on the nucleus. It is evident, however, that stiffening the nuclear envelope is the dominant effect.

The overexpression of LBR, designed to increase the tethering between heterochromatin and the nuclear envelope, had an unexpected and very large effect on nuclear morphology and the organisation of heterochromatin - shown in Figure 5.5. We believe that the overexpression of LBR is breaking down the nuclear lamina and reassembling it throughout the nucleus at sites of heterochromatin as evidenced by both the strong overlap of LBR and heterochromatin - Figure 5.5 - and the redistribution of LMNB1 away from the nuclear envelope and into the nucleus - Figure 5.6. These findings are contrary to previous studies which found overexpression of LBR resulted in increased heterochromatin density at the nuclear periphery (Solovei *et al.* , 2013)(Carvajal *et al.* , 2015). Breakdown of the nuclear lamina would result

in a softer nucleus that is more susceptible to forces. This is consistent with our observations of both nuclear morphology, where LBR overexpression causes significant drops in circularity and solidity - Figure 5.9, and nuclear shape changes, which are significantly increased - Figure 5.10B.

The overexpression of LMNA led to a reduction in the relative fraction of H3K9me2, and an increase in the relative fraction of H3K27me3, at the nuclear periphery during differentiation - Figure 5.18 A/C. A large reduction in the amount of H3K9me2 at the nuclear periphery was observed moving from 24 hours to 48 hours in N2B27, with this effect being greater than that from LMNA overexpression. The distribution of H3K27me3 showed the opposite trend; while moving from 24 hours to 48 hours in N2B27 gave a statistically significant increase in the amount of H3K27me3 at the nuclear periphery, the relative increase observed from LMNA overexpression was much greater. The overexpression of LBR also resulted in a significant drop in the relative enrichment of H3K9me2 at the nuclear periphery, but had no effect on the distribution of H3K27me3 - Figure 5.18 B/D. We also found identical trends in the distribution of H3K9me2 and H3K27me3 with differentiation time - moving from 24 hours to 48 hours in N2B27 resulted in a large drop in the relative amount of H3K9me2 at the nuclear periphery, while H3K27me3 showed increased enrichment. In addition, using the average staining intensities of H3K9me2 and H3K27me3 as a rough guide to the total amount in the nucleus, we found a significant increase in H3K9me2 and a significant reduction in H3K27me3 during differentiation - Figures 5.16 and 5.17.

The large drop in the relative amount of H3K9me2 at the nuclear periphery during differentiation is likely due to the deposition of new H3K9me2 marks within the nuclear interior. The increase in the relative fraction of H3K27me3 at the nuclear periphery during differentiation, coupled with a global reduction in staining intensity, implies that DNA enriched in H3K27me3 in proximity with the nuclear envelope may be preferentially protected from enzymatic modification. This may be important for ensuring genome stability as H3K27me3 is known to repress transposons, especially during the loss of DNA methylation which occurs during embryogenesis (Walter *et al.* , 2016). The increase in the relative amount of H3K27me3 at the nuclear periphery with LMNA overexpression is consistent with the role of LMNA and H3K27me3 in positioning DNA at the nuclear envelope (Harr *et al.* , 2015). The reduction in the relative peripheral enrichment of H3K9me2 with LMNA is, however, surprising as positioning of DNA proximal to the nuclear lamina has also shown to be dependent on H3K9me2/3 (Towbin

et al. , 2012)(Bian *et al.* , 2013)(Harr *et al.* , 2015). A possibility is that H3K9me2 and H3K27me3 possess redundant functions in their interactions with the nuclear lamina and increasing the amount of H3K27me3 at the envelope reduces the amount of H3K9me2 - the authors in Le *et al.* (2016) noted that a mechanically driven reduction in H3K9me2 at the nuclear periphery was compensated for by an upregulation in H3K27me3. Finally, we also observed that H3K9me2 is enriched at the nuclear lamina away from cell-cell contacts in tight colonies which shifts to a more uniform enrichment upon cell spreading - Figure 5.14. H3K9me2 has been shown to respond to mechanical forces in epidermal stem cells (Le *et al.* , 2016) and our results suggest that H3K9me2 may also be mechanically regulated in embryonic stem cells.

Chapter 6

Nuclear envelope structure influences lineage specification, but not the exit from naive pluripotency

This Chapter explores the effect of the perturbations, introduced in Chapter 5, that modify the strength of forces transmitted to chromatin and the strength of binding chromatin binding to the nuclear lamina on the capacity of mouse ES cells to both exit the naive pluripotent state, and to specify to the neural lineage.

6.1 Exit from naive pluripotency

To begin with, we asked whether reducing the forces transmitted to chromatin by overexpressing LMNA, or perturbing the interactions between chromatin and the nuclear lamina by overexpressing LMNA or LBR restricted the exit from naive pluripotency. To accomplish this, we performed a functional test. Chemical restriction of ES cells to the naive pluripotent state by culturing with 2i/LIF does not support any ES cells that have committed to differentiation. By differentiating ES cells towards the neural lineage for 48 and 72 hours in N2B27 and then replating each time point at clonal density back into 2i/LIF, any colonies that formed originated from a single cell that had not yet entered the formative phase - we can use this to compare the kinetics of exit from the naive pluripotent state. The results

of the differentiation rescue experiment for LBR and LMNA overexpression are depicted below in Figure 6.1, which show that overexpression of LBR (A) or LMNA (B) does not have an effect on the kinetics of the exit from the naive pluripotent state.

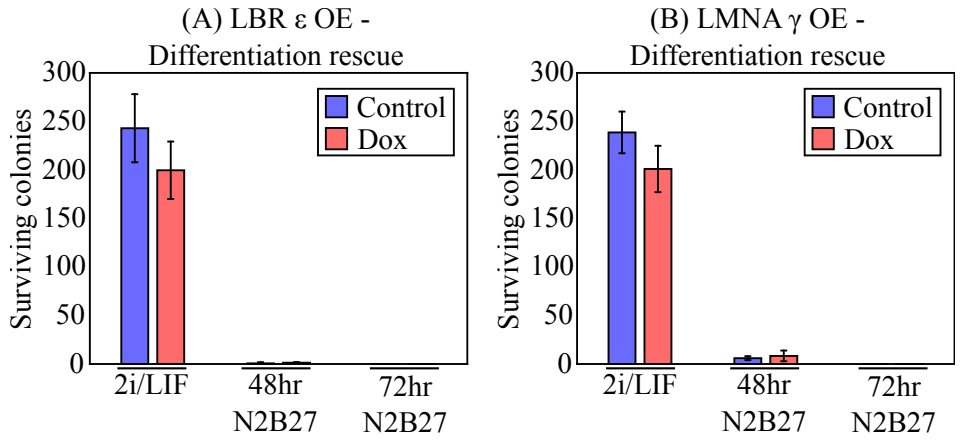

Figure 6.1: LMNA and LBR overexpression do not alter the kinetics of exit from the naive pluripotent state. LMNA γ and LBR ϵ ES cells cultured in 2i/LIF and N2B27 for 48 and 72 hours and replated into 2i/LIF at clonal density (400 cells total). There is no significant difference in the number of cells capable of proliferating in 2i/LIF after culturing in N2B27 for 48 or 72 hours. Error bars display standard deviation. N = 2.

In order to solidify this result, we conducted qPCR analysis of the pluripotency factors Nanog and Oct4 during neural differentiation - shown below in Figure 6.2 - with LBR overexpression (B), LMNA overexpression (A) and treatment with 2 µM Blebbistatin (C), none of which show significant differences. Figure 6.2 also shows the rise and fall of an intermediate, transition phase, transcription factor Pou3f1 and the upregulation of the neuroectoderm marker Sox1. While we did not see any striking differences in the qPCR results, there is a lower amount of Sox1 expressed at Day 4 in N2B27 in LMNA-overexpressing mouse ES cells and a lower amount of Pou3f1 in LBR-overexpressing ES cells after 48 hours in N2B27.

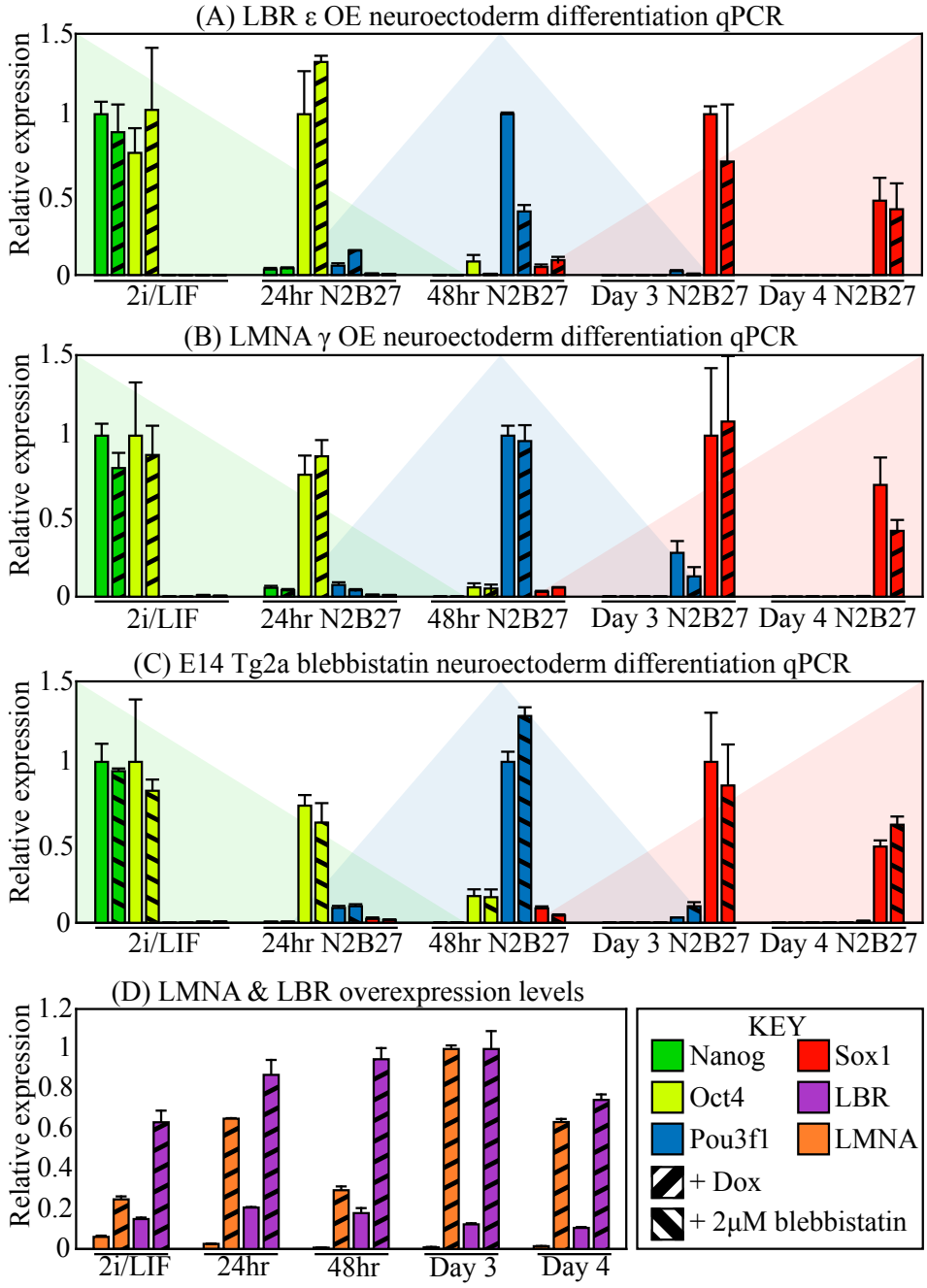

Figure 6.2: qPCR timecourse of neural differentiation in ES cells overexpressing LBR, LMNA and treated with 2 μM Blebbistatin. Caption on following page.

Figure 6.2: qPCR timecourse of neural differentiation in: (A)/(D) LBR ϵ overexpressing, (B)/(D) LMNA γ overexpressing and (C) E14 Tg2a + 2 µM Blebbistatin mouse ES cells, released from 2i/LIF and cultured in N2B27 for four days. Solid colours represent controls. Striped colours represent overexpression or Blebbistatin treatment. The coloured triangles represent: green - loss of naive pluripotency (downregulation of Nanog/Oct4), blue - a transition state (upregulation and downregulation of Pou3f1), red - neural lineage specification (upregulation of Sox1). (D) shows the levels of overexpression of LBR and LMNA throughout the timecourse. The results show the perturbations have no effect on downregulation of pluripotency factors, but show a reduction in the levels of Sox1 with LMNA overexpression - indicative of a possible defect in neural lineage specification. Error bars display standard deviation. N = 2.

6.2 Neural lineage specification capacity

The qPCR results above hint that the overexpression of LBR and LMNA may be altering the kinetics or ability of mouse ES cells to commit to the neural lineage. However, it is not possible to say more because the expression levels in the qPCR experiment are population averages. In order to examine the distribution of Sox1 expression within the population, we conducted immunofluorescence stains of Sox1. The staining intensity provided a quantitative measure of the amount of Sox1 protein on an individual cell-by-cell basis. The details of the experimental setup are presented in Chapter 2. Where appropriate, we also stained for LBR and LMNA which allowed us to correlate the intensity levels of the LBR and LMNA perturbations with Sox1, the data which is presented and discussed later below. Histograms of the intensity of Sox1 - normalised by area - after two, three and four days in N2B27 in mouse ES cells, are shown below in Figure 6.3 with: LBR overexpression (A), LMNA overexpression (B) and treatment with 2 µM Blebbistatin (C). The results show that overexpression of LBR (A) and LMNA (B) exhibit similar phenotypes: both create a bimodal response where a significant fraction of the population does not express Sox1 after four days in N2B27 (+Dox) while the cells that have not been induced (control) express Sox1 and are either entirely (A), or almost entirely (B) specified to the neural lineage. Treatment with 2 µM Blebbistatin (C) results in a delay in Sox1 upregulation that effects the whole population. We then asked whether knockdown of LBR or the double knockdown of inner nuclear envelope proteins SUN1 and SUN2 by transient transfection with

siRNA had a phenotype in Sox1 expression, with siRNA introduced at the same time the 2i/LIF inhibitors were withdrawn. SUN1 and SUN2 form part of the LINC complex, binding the KASH domain of the nesprins in the space between the inner and outer nuclear membranes, with Sun1 expressed tenfold higher than Sun2 in ES cells (RNA-Seq data - not shown). The results of the LBR and SUN1/2 double knockdown on intensity of Sox1 after culturing in N2B27 for 48 and 72 hours are shown in Figure 6.4A, neither of which show a phenotype. Knockdown of LBR was verified at the protein level by immunostaining - Figure 6.4C/D, and at the transcript level by qPCR - Figure 6.4E. The results show that LBR was successfully knocked down at the protein level 48 hours after transfection with 10% of the transcript remaining; however, after 72 hours in N2B27 the protein had returned to control levels and the transcript to 30% of control. Unfortunately, while we were able to obtain a reliable antibody for SUN2, we could not find an antibody for SUN1 which meant that we were unable to verify knockdown of SUN1 at the protein level. The effectiveness of SUN1/2 double knockdown was therefore assessed at the transcript level with qPCR - Figure 6.4E - which showed that Sun1 was reduced to 35% of control levels after 48 hours and had returned to 70% of control by 72 hours. Sun2 was knocked down to 20% of control levels after 48 hours and had risen to 40% of control 24 hours later. It is therefore unlikely, comparing expression levels of Sun1 with those of Lbr, that knockdown at the protein level was likely to have been successful.

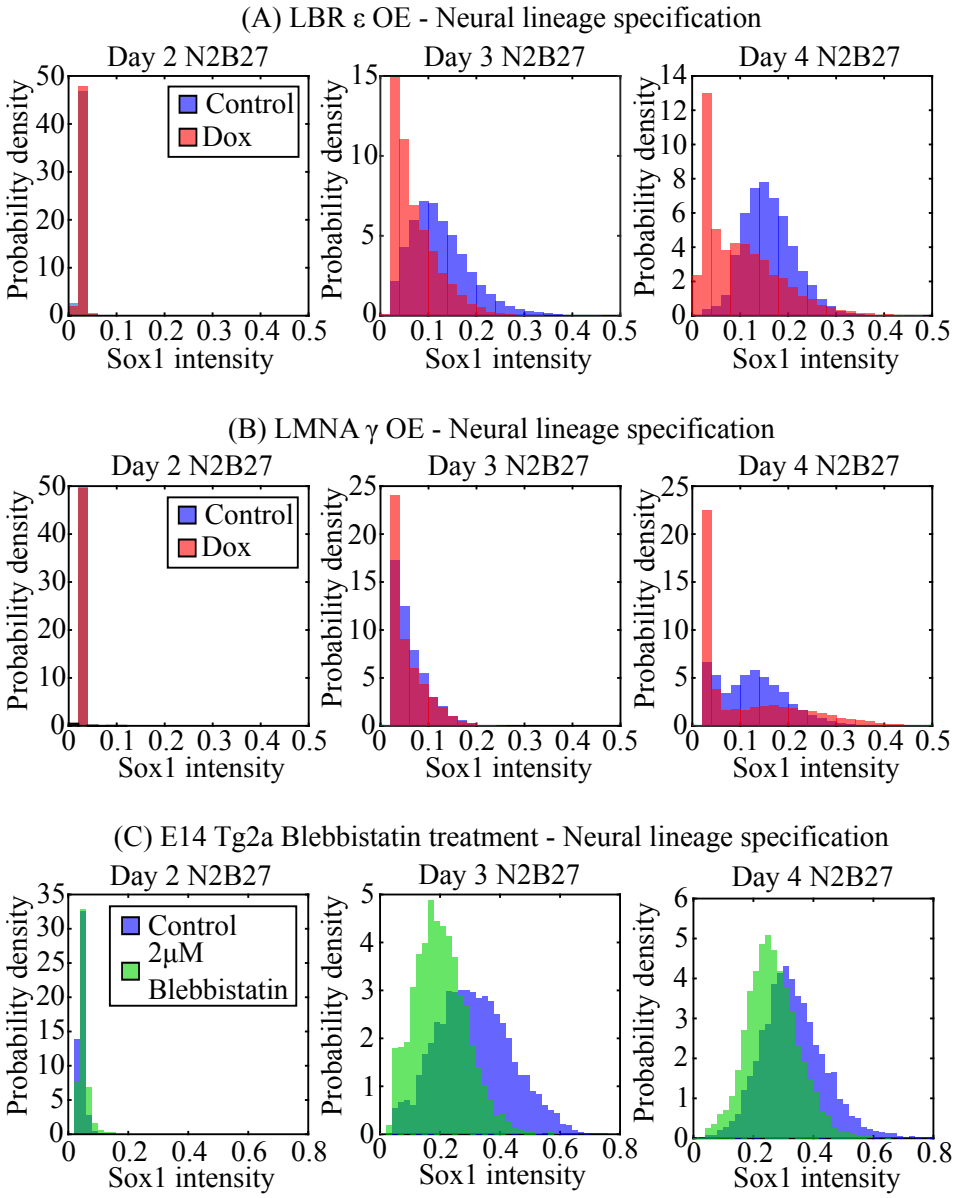

Figure 6.3: LMNA and LBR overexpression blocks neural lineage specification in a bimodal fashion - treatment with 2 µM Blebbistatin delays it. Sox1 immunofluorescence in (A) LBR ϵ overexpressing, (B) LMNA γ overexpressing and (C) E14 Tg2a + 2 µM Blebbistatin mouse ES cells differentiated towards neuroectoderm. Histograms for Sox1 intensity are shown at Day 2, Day 3 and Day 4 after 2i/LIF withdrawal, normalised so their total area is one. N = 3.

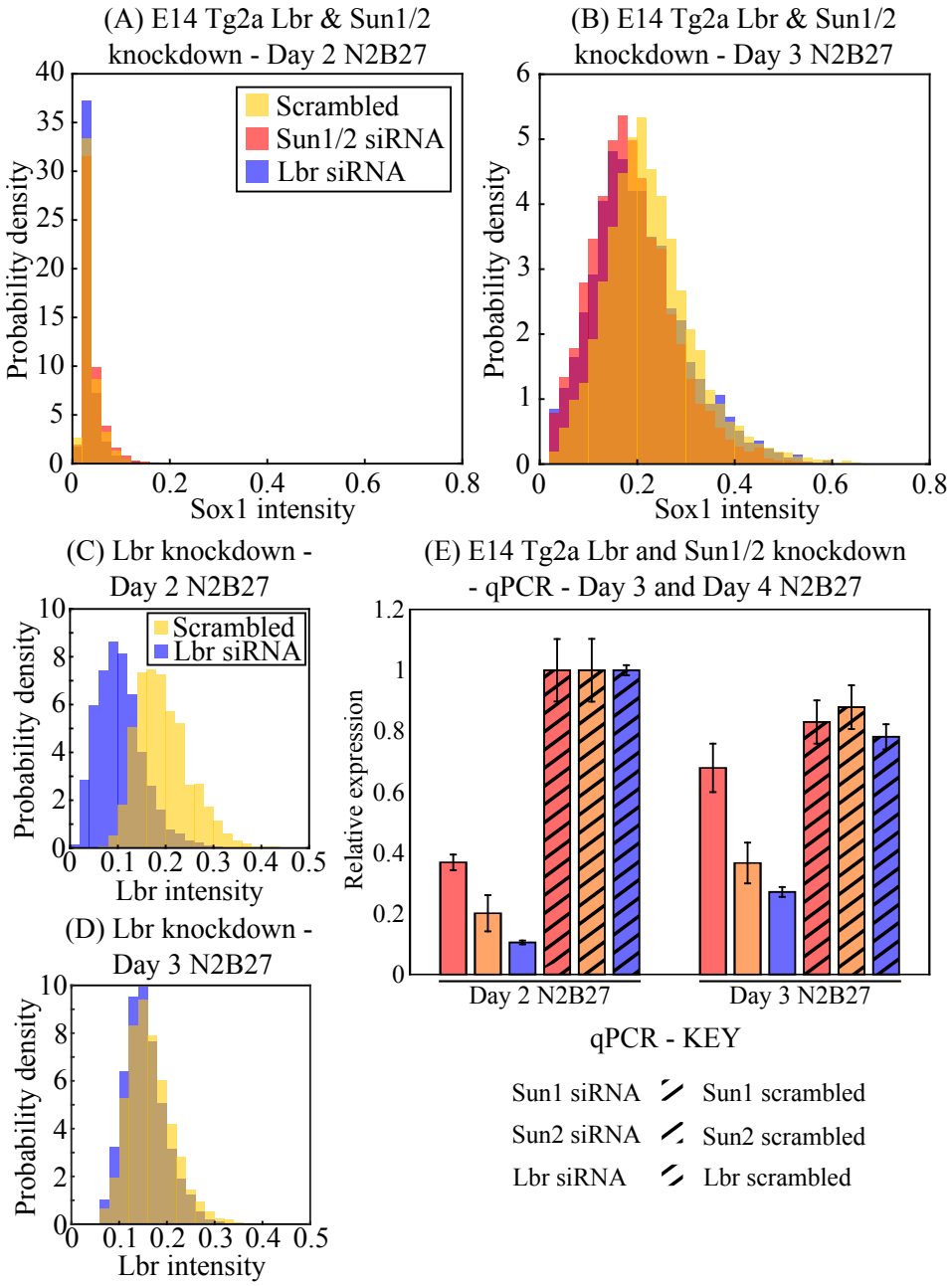

Figure 6.4: Knockdown of LBR has no effect on the kinetics of neural lineage specification. (A)/(B) Immunofluorescence of Sox1 after 48 and 72 hours in N2B27, respectively, in E14 Tg2a mouse ES cells treated with scrambled siRNA, Sun1&2 siRNA and Lbr siRNA. Results show no significant differences in the intensity distributions of Sox1. (C)/(D) Knockdown of LBR verified by immunofluorescence - LBR intensity was successfully reduced on day 2 but returned to control levels by day 3. (E) Knockdown of LBR and SUN1&2 assessed by qPCR. Error bars represent the standard error of the mean. Sun1 expression levels, with siRNA treatment, do not indicate that knockdown was likely to have been successful. N = 2.

6.3 Correlating the intensity of Sox1 with LMNA and LBR overexpression

The next step was to determine whether there were any correlations between the levels of overexpression of LMNA and LBR and the amount of Sox1, as determined by immunofluorescence. Figure 6.5 shows the scatter plot of LMNA intensity vs. Sox1 intensity (A) and of LBR intensity vs. Sox1 intensity (B) after 72 hours in N2B27, using the data from Figure 6.3A and 6.3B. The results show a strong negative correlation between the intensity of LMNA and Sox1: the vast majority of LMNA-overexpressing cells do not express Sox1 at all. The correlation between the intensity of LBR and Sox1 is more complicated: the control population of non-induced LBR-overexpressing ES cells is positively correlated with the intensity of LBR which means that more analysis is necessary to determine what the effect LBR overexpression is having on the intensity of Sox1.

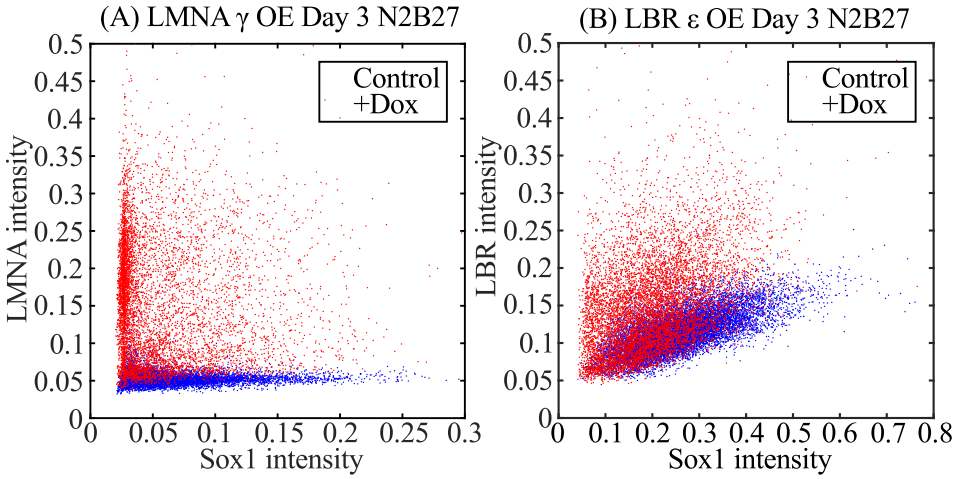

Figure 6.5: Intensity correlations between LMNA/LBR and Sox1 in LMNA γ/LBR ϵ overexpressing mouse ES cells. (A) Scatter plot of Sox1 intensity vs. LMNA intensity by immunofluorescence in LMNA γ overexpressing mouse ES cells cultured in N2B27 for 72 hours. (B) Scatter plot of Sox1 intensity vs. LBR intensity by immunofluorescence in LBR ϵ overexpressing mouse ES cells cultured in N2B27 for 72 hours. The intensity of LMNA shows a strong negative correlation with the intensity of Sox1. The intensity of endogenous LBR (control) shows a positive correlation with Sox1 intensity which complicates effect of LBR overexpression and necessitates a more detailed analysis.

In order to investigate the correlation between Sox1 and LBR, we first divided up the populations of doxycycline treated and control LBR over-

expressing mouse ES cells into quartiles based on their intensity of LBR - Figure 6.6A. As expected, because the overexpression of LBR is not uniform when induced, the bottom quartile of LBR overexpressing cells have the same intensity of LBR when comparing control vs. doxycycline treated whereas, in the upper quartile, the doxycycline treated cells have significantly higher intensities of LBR when compared with controls. We noticed that the density of cells changed throughout the dish - Figure 6.6B - and that the density of cells was greater in regions that expressed high levels of LBR - Figure 6.6C. We then took the cells in the upper and lower quartiles of LBR intensity and separated them again into quartiles of high and low density, before making boxplots of their Sox1 intensity - Figure 6.6D. The results show that, in both high and low density regions in cells expressing high levels of LBR the cells treated with doxycycline express significantly lower levels of Sox1 when compared with controls. In spite of the positive correlation between Sox1 and LBR intensity, shown in Figure 6.5B, when the effects of density are taken into account overexpression of LBR negatively correlates with Sox1.

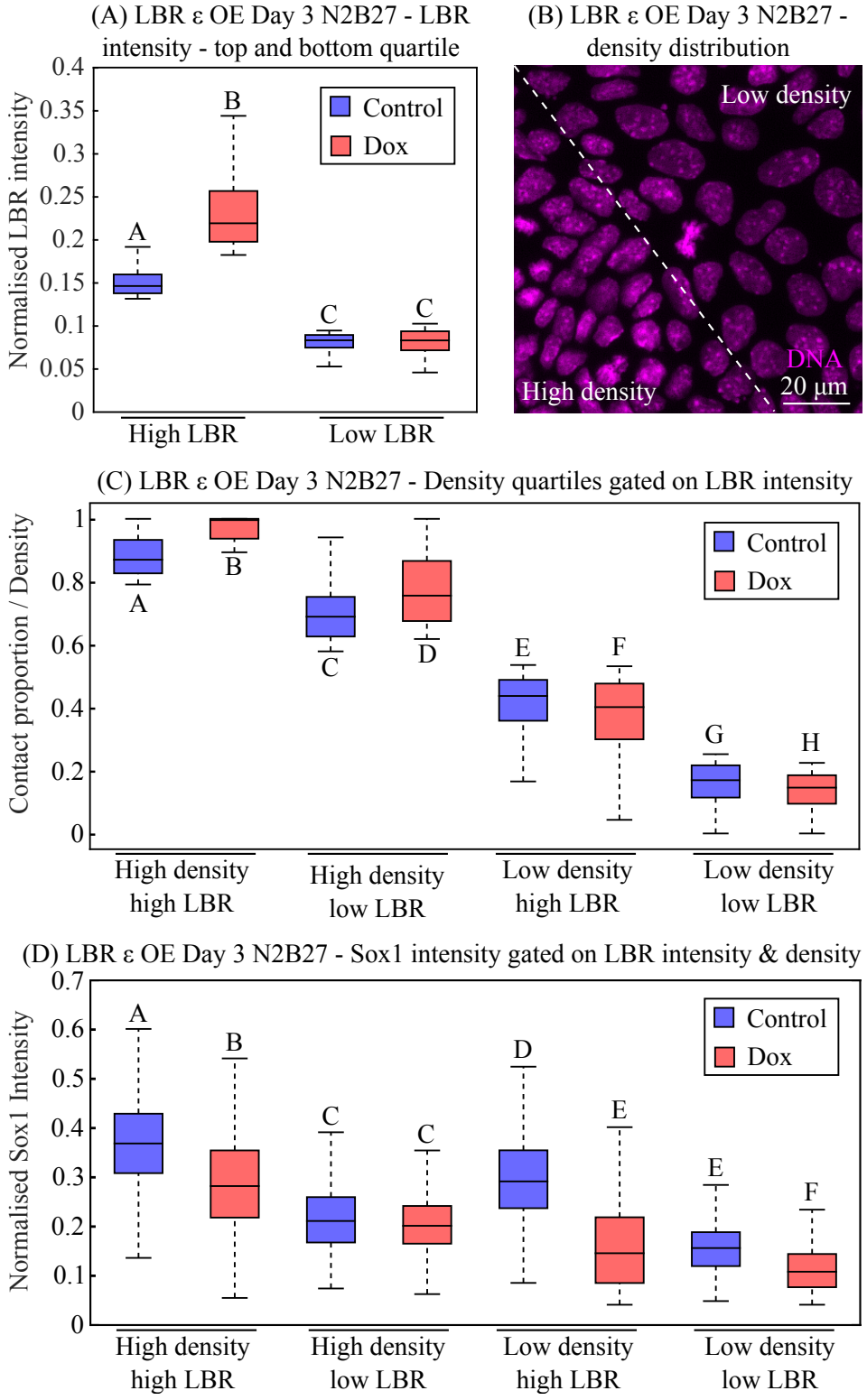

Figure 6.6: LBR intensity negatively correlates with Sox1 intensity. Caption on following page.

Figure 6.6: Immunofluorescence of Sox1 and LBR in LBR ϵ overexpressing mouse ES cells, cultured in N2B27 for 72 hours. (A) Boxplots of upper and lower quartiles of LBR intensity. Doxycycline treatment gives a wide range of LBR intensities - high LBR levels are significantly higher with Dox treatment when compared with controls. (B) DNA stain (Hoechst 33342) showing changes in cell density. (C) Boxplots of upper and lower quartiles of cell density/proportion of cell in contact with neighbours, gated on LBR intensity using data in (A). (D) Normalised Sox1 intensity - gated on LBR intensity and cell density - data from (C). LBR negatively correlates with Sox1 intensity when the data is gated on both LBR expression and density effects are taken into effect - in the high LBR intensity quartile, irrespective of density, Sox1 expression is lower in Dox treated cells. Statistical analysis performed in MATLAB using a Kruskal-Wallis test, followed by a multi-comparison test. Boxplots with separate letters indicate that theirs means are significantly different at the 5% level.

6.4 Discussion

This Chapter has explored the effect of both reducing forces transmitted to chromatin, through inhibition of non-muscle myosin II and stiffening of the nuclear envelope with LMNA, and altering the binding of peripheral heterochromatin to the nuclear lamina, through overexpression of LMNA and LBR, on the ability of embryonic stem cells to exit the naive pluripotent state and specify to the neural lineage. Our hypothesis is that forces acting at the nuclear envelope are required to facilitate access to lineage specific genes that are sequestered there in the pluripotent state and required during the differentiation process - where global changes in transcription occur. We have shown that the overexpression of LMNA or LBR does not affect the ability of ES cells to exit the naive pluripotent state - Figure 6.1. These results indicate that, while the nuclear envelope may play an active role in the silencing of nearby genes (Finlan *et al.* , 2008) (Reddy *et al.* , 2008) (Zullo *et al.* , 2012), close proximity to the nuclear lamina is unlikely to be a requirement for transcriptional repression.

The next step was to look at the effect our perturbations have on the ability of mouse ES cells to differentiate towards the neural lineage, the evidence of which is given by the expression of the neuroectoderm marker Sox1. While we did not find significant changes in Sox1 expression with LBR overexpression and 2 µM Blebbistatin treatment, we found a downregulation of Sox1 at Day 4 after 2i/LIF withdrawal with LMNA overexpression - Figure 6.2. Inhibition of non-muscle myosin II in both human and mouse embry-

onic stem cells has been shown to enhance the self-renewal factors Nanog and Oct4 (Walker *et al.* , 2010). We did not see this effect in the qPCR data, however, it is important to note we were using a much lower dose of Blebbistatin at 2 µM, compared with the 10 µM required in the previous study to see significant enhancements in Nanog and Oct4 expression.

To look at the distribution of Sox1 expression within the population we stained for Sox1 using immunofluorescence. We found that LBR and LMNA overexpression created a bimodal distribution of Sox1 where a significant fraction of the population did not express Sox1 at all, while treatment with 2 µM Blebbistatin delayed Sox1 expression in the whole population - Figure 6.3A, 6.3B and 6.3C, respectively. When looking at the correlations between LMNA intensity and the intensity of Sox1 it is clear that overexpression of LMNA above a threshold blocks Sox1 expression - Figure 6.5A. We did not find any significant differences in the rate of proliferation upon LMNA overexpression - Figure 5.7C, which indicates that the LMNA phenotype is likely a result of either decreasing forces propagated to chromatin through the nuclear envelope, or altering the interactions of chromatin with nuclear lamina - or a combination of the two. If the block on Sox1 expression upon overexpression of LMNA was a result of reducing the forces transmitted to chromatin, we would expect that reducing the forces on the nucleus by other means, such as targeting force generation in the cytoskeleton with Blebbistatin, would have a similar phenotype. In order to avoid blocking cell division we had to use a low concentration of Blebbistatin (2 µM) - Figure 5.7A - such that the forces on the nucleus were not significantly reduced - Figure 5.10A and 5.10B. However, in spite of this, we found a delay in Sox1 expression - Figure 6.3C - which implies that neural differentiation may be very sensitive to forces. It is interesting to note that, in more specialised stem cells - for example muscle stem cells (myoblasts) - LMNA expression is required for differentiation, with LMNA null or mutant mice displaying impaired differentiation kinetics and loss of potential (Frock *et al.* , 2006)(Perepelina *et al.* , 2017). A possible explanation for this may lie in the increasing importance of LMNA as a regulator of chromatin interactions at the nuclear periphery in more differentiated cell types (Solovei *et al.* , 2013) and the requirement for LMNA in cell types that undergo high mechanical strains (Swift *et al.* , 2013).

The overexpression of LBR was designed to strengthen the binding between LADs and the nuclear lamina, without modulating the forces transmitted to chromatin. We found, however, that LBR overexpression had

a rather drastic effect on nuclear morphology and the architecture of the nuclear envelope by, we believe, disassembling the nuclear lamina and reassembling it at sites of heterochromatin throughout the nucleus - Figures 5.5 and 5.6. A parallel may be drawn with the shape of granulocyte (neutrophil) nuclei which, albeit to a more extreme extent, are multi-lobed: a characteristic thought to aid them in squeezing through small spaces gaps as part of their function. It is known that sufficient levels of LBR are required for realising this shape (Hoffmann *et al.* , 2007)(Olins *et al.* , 2008) and it is possible that the overexpression LBR in our ES cell system is driving a similar process.

Given such drastic alterations in nuclear organisation upon LBR overexpression it is challenging to interpret the results of the bimodal distribution of Sox1 in the context of our hypothesis - forces on the nucleus are no longer required to move chromatin in proximity to the nuclear envelope to interact with the lamina because the nuclear lamina moves to the chromatin. It is therefore not possible to compare the phenotype in Sox1 from LBR overexpression to that of LMNA overexpression. We have shown, however, that when separated from effects due to cell density - Figure 6.6 - LBR overexpression negatively correlates with Sox1. The positive correlation of Sox1 and LBR can be explained as a density effect - if the amount of Sox1 or LBR remains constant in the nucleus, the mean intensity (measured) will rise as the projected nuclear area falls.

Chapter 7

General discussion and future directions

This final Chapter will first discuss current work: in particular, our preliminary results from decoupling the nucleus from the cytoskeleton with the overexpression of truncated nesprins that were introduced at the beginning of Chapter 5 in Figure 5.1. Our findings so far will then be summarised and discussed, and the directions in which this project might be taken presented.

7.1 Decoupling the nucleus from the cytoskeleton

The final set of perturbations are the overexpressions of truncated nesprins, depicted in Figure 5.1, designed to break the physical link between the cytoskeleton and the nucleus by out-competing endogenous nesprins for SUN1/2 protein binding at the inner nuclear membrane. Due to time constraints, these perturbations are not fully characterised and all experiments so far have been conducted using polyclonal lines. Figure 7.1, below, shows that the mRFP-SR-KASH proteins localise, as expected, to the nuclear envelope. There is a large dynamic range in the amount of protein expression: cells expressing high levels appear to be saturated at the nuclear envelope and the protein distributed throughout the cytoplasm while cells that express low levels show faint rings outlining the nucleus, or no signal at all.

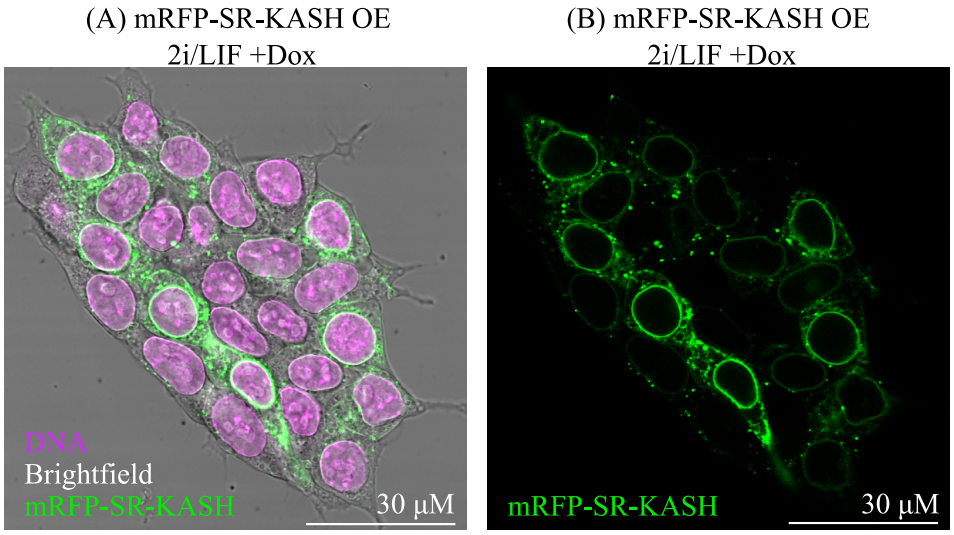

Figure 7.1: mRFP-SR-KASH localises to the nuclear envelope when overexpressed. Polyclonal mRFP-SR-KASH mouse ES cell line were cultured in 2i/LIF in ibidi dishes and doxycycline treated for 24 hours. The truncated spectrin repeat KASH domain containing proteins, fused to mRFP, localise to the nuclear envelope as expected. In cells containing high levels of the protein the nuclear envelope is saturated and the protein is distributed throughout the cytoplasm. In lower levels of expression, the protein is completely localised at the nuclear envelope.

7.2 Neural lineage capacity - preliminary results

In order to see whether reducing the forces transmitted to chromatin by breaking the LINC complex had an impact on ES cell differentiation towards the neural lineage we conducted immunofluorescent stains for Sox1 at days two, three and four after 2i/LIF withdrawal, the results of which are shown below in Figure 7.2. The details of the experimental setup and analysis can be found in Chapter 2. The results show that overexpression of mRFP-SR-KASH and mRFP-KASH, both of which act as dominant negatives for the endogenous nesprins, blocks the expression of Sox1 in the majority of cells after 3 days in N2B27 - Figure 7.2A and 7.2B, respectively. The overexpression of mRFP-KASHΔL, which acts as a control for the overexpressions of mRFP-SR-KASH and mRFP-KASH, also exhibits a bimodal response in Sox1 expression, however, the effect is much weaker and the majority of the cells express Sox1. The correlations of Sox1 intensity with mRFP-SR-KASH, mRFP-KASH and mRFP-KASHΔL are shown in Figure 7.3. The results show that, in cells that are expressing Sox1, overexpres-

sion of mRFP-SR-KASH and mRFP-KASH negatively correlates with Sox1 while overexpression of mRFP-KASHΔL shows no correlation. Of the cells that do not express Sox1, however, there is no correlation in the intensities of mRFP-SR-KASH, mRFP-KASH and mRFP-KASHΔL.

The preliminary results of the overexpression of the KASH constructs on the ability of mouse ES cells to differentiate towards the neural lineage are extremely encouraging. It appears that decoupling the nucleus and the cytoskeleton by breaking the LINC complex and, we hope, reducing the forces transmitted to chromatin is blocking neural differentiation. At this moment it is hard to say why there is proportion of cells, shown by the correlations in Figure 7.3, that do not express Sox1 or the KASH constructs (when induced). A possible explanation lies in the increased heterogeneity that comes from using polyclonal lines; the way of testing which will to be to use clonal lines in future experiments. These results, if reproducible, lend strength to the requirement of forces acting at the nuclear envelope in the process of mouse ES cell differentiation.

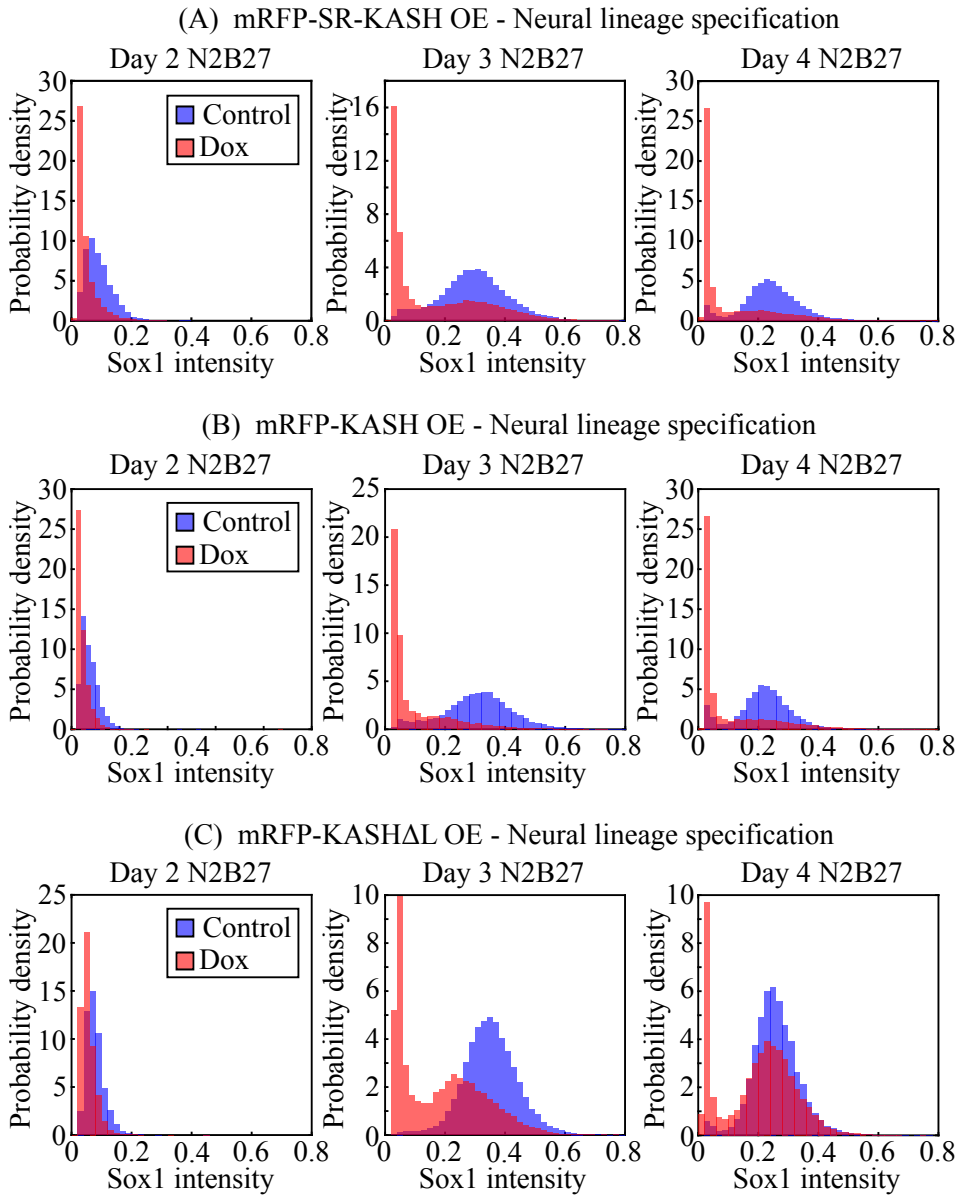

Figure 7.2: Decoupling of the LINC complex through expression of N-terminal truncated nesprins delays differentiation towards neuroectoderm in a bimodal fashion. Sox1 immunofluorescence in (A) mRFP-SR-KASH overexpressing (polyclonal), (B) mRFP-KASH overexpressing (polyclonal) and (C) mRFP-KASHΔL mouse ES cells differentiated towards neuroectoderm. Histograms for Sox1 intensity are shown at Day 2, Day 3 and Day 4 after 2i/LIF withdrawal, normalised so their total area is one. SR-KASH and KASH act as dominant negatives and outcompete endogenous nesprins for SUN1/2 binding. N = 1.

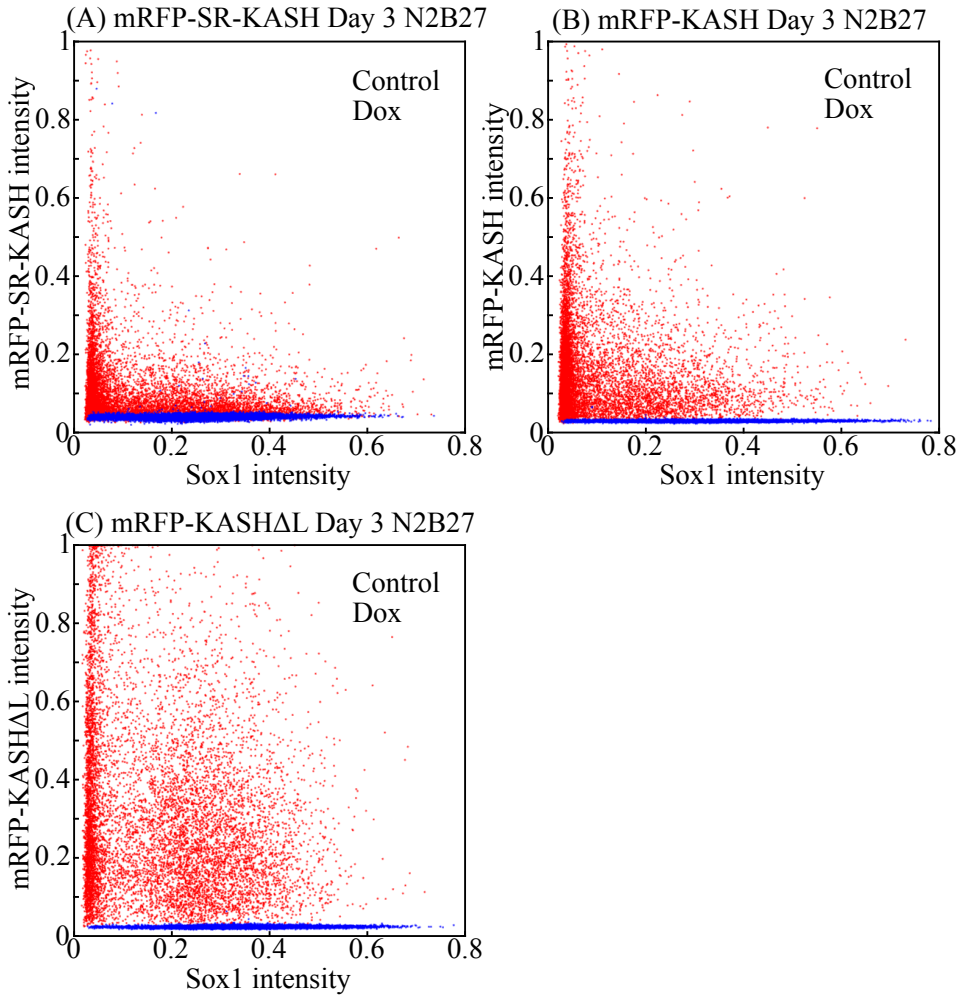

Figure 7.3: Intensity correlations between KASH construct proteins and Sox1 in KASH construct overexpressing cells. (A) Scatter plot of Sox1 intensity vs. mRFP-SR-KASH intensity by immunofluorescence in polyclonal mRFP-SR-KASH overexpressing mouse ES cells cultured in N2B27 for 72 hours. (B) Scatter plot of Sox1 intensity vs. mRFP-KASH intensity by immunofluorescence in polyclonal mRFP-KASH overexpressing mouse ES cells cultured in N2B27 for 72 hours. (C) Scatter plot of Sox1 intensity vs. mRFP-KASHΔL intensity by immunofluorescence in polyclonal mRFP-KASHΔL overexpressing mouse ES cells cultured in N2B27 for 72 hours. Cells that express Sox1 negatively correlate with the intensity of mRFP-SR-KASH and, to a lesser degree, mRFP-KASH but show no correlation with the intensity of mRFP-KASHΔL. N = 1.

7.3 Summary of results

Chapter 3 explored the mobility of H2B-eGFP in mES cells in the naive pluripotent state and during differentiation, using FRAP. We found that:

- The nuclei of mES cells undergo large, dynamic changes in shape - capable of moving chromatin on a bulk scale.
- There is a significant increase in the mobility of H2B-eGFP that is loosely bound to chromatin two hours after 2i/LIF withdrawal.

Chapter 4 investigated the role of the cytoskeleton in generating and propagating forces to the nucleus, using nuclear shape changes as a proxy. By developing two complementary methods of quantifying nuclear shape changes we have shown that:

- Nuclear shape changes are driven by actomyosin in the cytoskeleton: requiring both tension generated through non-muscle myosin II and the turnover of actin.
- Nuclear shape changes are not random but have a well-defined period of oscillation on the order of 200 seconds.
- The intensity of cortical actin also has a dominant oscillatory frequency on the order of 200s.
- There is a correlation between cortical actin intensity and local movements of the nuclear envelope: fluctuations in cortical actin intensity oscillate with a phase of π ahead of oscillations in nuclear envelope position.

Chapter 5 introduced the perturbations to our mouse embryonic stem cell system. We had two goals: to reduce the forces transmitted to chromatin and to modulate the interactions of chromatin at the nuclear periphery with the nuclear lamina. To reduce forces actin on chromatin we used two approaches. The first was to use the small molecule inhibitor Blebbistatin to block the phosphorylation of non-muscle myosin II in the cytoskeleton, inhibiting its action and, subsequently, its ability to generate forces. The second approach was to modify the structure of the nuclear envelope to modulate force transmission - the overexpressing LMNA was designed to stiffen the nucleus and the overexpression of N-terminal truncated nesprins to decouple the nucleus

and the cytoskeleton by breaking the LINC complex (discussed later). We also attempted to break the LINC complex at the inner nuclear membrane, by knocking down the SUN proteins. To alter the binding between peripheral chromatin and the nuclear lamina, we again targeted proteins in the nuclear envelope: the overexpressions of LMNA and LBR were designed to increase chromatin tethering to the nuclear lamina and the knockdown of LBR to reduce it. The results of the characterisation of our perturbations are as follows:

- Treatment with Blebbistatin, restricted to a low concentration of 2 µM to avoid blocking cellular proliferation, did not significantly affect nuclear shape changes but did affect nuclear morphology - increasing circularity.
- Overexpression of LMNA, which localised as expected to the nuclear envelope, reduced the effect of forces on the nucleus - evidenced by a reduction in nuclear shape changes and eccentricity.
- The overexpression of LBR had an unexpected and drastic effect on nuclear morphology - decreasing circularity and solidity - and chromatin organisation, by assembling nuclear lamina like structures within the nuclear interior.
- Knockdown of LBR had the opposite effect on nuclear morphology when compared with LBR overexpression - increasing circularity, solidity and reducing nuclear area.
- Treatment with 2 µM Blebbistatin or LMNA overexpression did not affect the frequency spectrum of oscillations in the nuclear boundary.
- Overexpression of LMNA reduced the relative fraction of H3K9me2 and increased the relative fraction of H3K27me3 at the nuclear envelope during differentiation (24 and 48 hours in N2B27).
- Overexpression of LBR reduced the relative fraction of H3K9me2 at the nuclear periphery during differentiation (24 and 48 hours in N2B27), but had no effect on the distribution of H3K27me3.
- We found evidence of possible mechanical regulation of H3K9me2 which shifts in distribution from upon cell spreading: in compact colonies H3K9me2 is enriched at the nuclear periphery, but not near cell-cell

junctions. When the colonies are more loosely bound and the cells spread, H3K9me2 forms a ring around the entire nuclear periphery.

Chapter 6 explored the effect of the perturbations introduced in the previous Chapter on the exit from the naive pluripotent state and differentiation towards the neural lineage. In particular, we were interested in looking for changes in differentiation kinetics or capacity. To begin with we looked at the kinetics of exit from naive pluripotency with a function assay: by differentiating cells in N2B27 and then replating back into 2i/LIF and counting the fraction of colonies recovered, we could determine what fraction of the population had irreversibly committed to differentiation. We then used qPCR to look at transcriptional changes that accompany the start of the differentiation process, at a population level, and then immunofluorescence to look at the distribution of the neuroectoderm specification marker Sox1 in more detail. The results are summarised below:

- Overexpression of LMNA or treatment with 2 µM Blebbistatin did not alter the kinetics of exit from the pluripotent state.
- Overexpression of LBR and LMNA created a bimodal distribution in Sox1, in which a significant fraction of the population does not express the neuroectoderm specification marker.
- Treatment with 2 µM Blebbistatin delayed upregulation of Sox1 in all cells.
- Knockdown of LBR had no effect on the distribution of Sox1, nor did knockdown of Sun1/2. It is likely, unfortunately, that the knockdown of Sun1 was not successful.
- Overexpression of LMNA negatively correlates with expression of Sox1, as does the overexpression of LBR when separated from density effects.

Lastly, this Chapter has presented preliminary results which show that decoupling the nucleus from the cytoskeleton through overexpression of N-terminal truncated nesprins blocks Sox1 expression in a bimodal fashion. Correlations of the KASH constructs with Sox1 expression show that, in cells expressing Sox1 - there is a negative correlation with the intensities of mRFP-SR-KASH and mRFP-KASH, but no correlation with the control mRFP-KASHΔL. This strongly indicates that the decoupling of the LINC complex is responsible for blocking neural specification.

7.4 General discussion

The goal of this research was to investigate the role of forces acting at the nuclear envelope in the context of mouse embryonic stem cell differentiation, specifically, whether they are important for exit from the naive pluripotent state and lineage specification. Our hypothesis was that forces are required to facilitate access to lineage specific genes, repressed and bound at the nuclear lamina. By modulating the forces transmitted to chromatin, or perturbing the interactions of chromatin at the nuclear periphery with the nuclear lamina, we hoped to alter the kinetics, or capacity, of mouse ES cells to differentiate. To a large extent we have met these goals.

At the beginning of the project we investigated the dynamic nature of H2B-eGFP using FRAP in the pluripotent state and during the early stages of differentiation. We sought to build upon the work done by Meshorer *et al.* (2006), who had shown that major architectural proteins (e.g. histone proteins) are dynamic and loosely bound to chromatin in ES cells, but become immobilised in ES cells that are lineage committed. The authors suggested that this 'hyperdynamic' binding of chromatin proteins was a hallmark of the pluripotent state and demonstrated that restricting the movement of histone H1 resulted in arrested differentiation. Using our *in vitro* embryonic stem cell culture system, which - through inhibition of GSK3 (CHIRON) and MEK activity (PD03) - has significantly less transcriptional heterogeneity within the population when compared with serum based culture (used in Meshorer *et al.* (2006)), we were able to explore changes in H2B-eGFP mobility during the early stages of differentiation. H2B-eGFP showed FRAP recovery kinetics present on two timescales, corresponding to two pools of H2B-eGFP with separate chromatin interactions. H2B-eGFP exhibited an initial rapid recovery, with an exponential profile and a time constant < 15 seconds, corresponding to a pool of freely diffusing H2B-eGFP. Recovery of H2B-eGFP intensity in the bleached region then occurred in a linear fashion with timescales > 15 seconds, corresponding to a pool of H2B-eGFP that is loosely bound to chromatin. This behaviour mirrors the findings of Meshorer *et al.* (2006).

The significant increase in the mobility of loosely bound H2B-eGFP observed two hours after 2i/LIF withdrawal suggests that chromatin organisation may be changing rapidly after release from the pluripotent state. This is consistent with rapid changes that have been shown to occur the transcriptional level; naive pluripotency factor mRNA declines by 70% within

4 hours of 2i/LIF withdrawal (Kalkan & Smith, 2014)(Leeb *et al.* , 2014). While performing the FRAP experiments we noticed that mES cell nuclei were undergoing large and dynamic changes in shape which were capable of moving chromatin on a bulk level. We sought to characterise and investigate the origin of these shape changes.

We have presented strong evidence for the necessity of both the polymerisation of actin and cytoskeletal tension, generated through non-muscle myosin II, in creating and propagating the forces that act on the nucleus - driving shape changes. There are a couple of possible mechanisms: The first requires a physical connection between the nucleus and the cytoskeleton. Pre-stress in the cytoskeleton allows forces, generated internally or applied externally to the cell, to be propagated over large distances (Jaalouk & Lammerding, 2009)(Wang *et al.* , 2009). If we inhibit the activity of non-muscle myosin II there is no tension to propagate forces to the nucleus, nor are there any forces generated in the cytoplasm. In addition, if we stabilise the polymerisation of actin then, while the cytoskeleton is capable of propagating forces, the forces on the nucleus are static. These effects would lead to a significant reduction in the amplitude of nuclear shape changes. The second mechanism requires a fluid flow around the nucleus, generated by actomyosin contractility. The flow of fluid would exert a dynamic pressure on the nucleus, with the physical connections of the cytoskeleton and the nucleus acting as local anchors, leading to shape changes. This mechanism has been postulated to explain rotations observed in the nuclei NIH 3T3 mouse embryonic fibroblasts (Kumar *et al.* , 2014). A path that could be taken to determine the relative contribution of each mechanism to driving nuclear shape changes in ES cells is presented in the next section.

The fluctuations in the nuclear envelope possess a well-defined period of oscillation of approximately 200 seconds. This compliments a previous study, which found fluctuations in the projected area of mES cells with an oscillatory period centred on 140 seconds (Talwar *et al.* , 2013). A novel finding of this research, however, is the presence of oscillations in local intensity of cortical actin, which possess the same period as the fluctuations in the nuclear boundary. Taking the cross-correlation between the local intensity of cortical actin and the local position of the nuclear envelope (radially inwards) revealed a clear relationship between the two, with cortical actin intensity fluctuating π radians out of phase with, and ahead of, the position of the nuclear boundary. This is strong evidence that the processes driving fluctuations in cortical actin are linked to the changes in nuclear shape. It

is thought that there is an optimum F-actin length and crosslinking density within the mesh (a function of F-actin density) for generating myosin II mediated contractility and subsequent force propagation (Chugh *et al.* , 2017). We can speculate that this may provide an explanation for hysteresis in the system and the phase lag of π between the movement of the nuclear boundary and the intensity of cortical actin. If F-actin density fluctuates about the optimum density for force generation, this would create a phase lag of π between the local force maximum and cortical F-actin intensity.

The first set of perturbations, designed to reduce forces transmitted to chromatin, was the overexpression of LMNA and treatment with 2 µM Blebbistatin - both of which altered nuclear morphology to be more circular, indicative of either a loss of tension on the nucleus or stiffening of the nuclear envelope. Only the overexpression of LMNA, however, significantly reduced nuclear shape changes, consistent with its role in stiffening the nucleus (Lammerding *et al.* , 2006)(Swift *et al.* , 2013). Neither of these perturbations altered the kinetics of exit from naive pluripotency, which implies that association with the nuclear lamina, while capable of actively silencing genes (Finlan *et al.* , 2008)(Reddy *et al.* , 2008), is not required to repress the genes that constitute the pluripotency network. We might have expected to find a delay in the exit from naive pluripotency with Blebbistatin treatment, which has been shown to promote self-renewal and increase the expression of the pluripotency factors Nanog and Oct4 (Walker *et al.* , 2010). A likely explanation for why we did not find this, however, is that the concentration of Blebbistatin used in our experiments - required for viability in long-term culture - was too low.

Overexpression of LMNA did, however, block mouse ES cells from committing to the neural linage - a significant fraction of the population did not express Sox1 at all, with those that did expressing the lowest levels of LMNA. Remarkably, despite not significantly reducing nuclear shape changes, treatment with 2 µM Blebbistatin delays Sox1 expression on a population level. The final perturbations designed to reduce forces transmitted to chromatin were the overexpressions of N-terminal truncated nesprins (KASH constructs), which act as dominant negatives for endogenous nesprins and decouple the nucleus from the cytoskeleton (Luxton *et al.* , 2011). Preliminary results are very promising - a significant fraction of the (overexpressing) population did not express Sox1, with the fraction that did negatively correlating with the level of overexpression. These results, when taken together, provide strong evidence that the process of mES cell lin-

eage specification may be very sensitive to, and require, forces acting at the nuclear envelope.

The perturbations designed to modulate the interactions between peripheral heterochromatin and the nuclear lamina were the overexpression of LMNA and the overexpression and knockdown of LBR. LMNA and LBR are thought to be components of two separate mechanical tethers that bind chromatin to the nuclear envelope (Solovei *et al.* , 2013) - association with which is correlated, although not exclusively, with transcriptional repression (Guelen *et al.* , 2008)(Peric-Hupkes *et al.* , 2010). While LMNA was correctly localised to the nuclear lamina, LBR - when overexpressed - was distributed throughout the nucleus and overlapped with regions of heterochromatin. Additionally, nuclear shape was significantly perturbed with large invaginations. Interestingly, although not as extreme, the shape resembles that of granulocytes - which possess a lobulated nuclei and require an adequate amount of LBR to form (Hoffmann *et al.* , 2007)(Olins *et al.* , 2008). We believe that LBR, which recognises and binds to chromatin with repressive histone modifications - notably H3K9me2 and H3K27me3 - is assembling nuclear lamina-like structures at sites of heterochromatin within the nucleus and changing their structure. Overexpression of LBR was found to block expression of Sox1 during differentiation. It is, however, challenging to interpret this result in the context of forces acting at the nuclear envelope in a meaningful way, because the nuclear lamina has moved to sites of heterochromatin, and not the other way around. Knockdown of LBR by siRNA, while it made nuclei more circular, did not affect the capacity for, or kinetics of, neural lineage specification.

To investigate whether overexpression of LMNA and LBR was altering chromatin interactions at the nuclear lamina we looked at the radial distributions of the repressive histone modifications H3K9me2 and H3K27me3, required for targeting and binding of chromatin to the nuclear lamina (Harr *et al.* , 2015), during differentiation. LMNA overexpression depleted H3K9me2 and enriched H3K27me3 at the nuclear periphery. LBR overexpression also depleted H3K9me2 at the nuclear periphery, but had no effect on the distribution of H3K27me3. Independent of the perturbations, the relative fraction of H3K9me2 dropped significantly at the nuclear periphery during differentiation - from 24 hours to 48 hours in N2B27, while the relative fraction of H3K27me3 increased. We expected to find an enrichment of both H3K9me2 and H3K27me3 at the nuclear periphery if genes were being restricted there. It was, therefore, surprising that the relative fraction of H3K9me2 at the nu-

clear periphery dropped with LMNA overexpression. Again, the results of the distributions of H3K9me2 and H3K27me3 with LBR overexpression are hard to interpret given the large effect LBR overexpression has on nuclear shape and unexpected localisation throughout the nucleus. It is possible that the enrichment of H3K27me3 is replacing the loss of H3K9me2 in a compensatory fashion - an effect that has been observed in epithelial stem cells (Le *et al.* , 2016). What remains to be reconciled with the Le *et al.* (2016) study, however, is that H3K9me2 enrichment at the nuclear periphery in epithelial stem cells was lost when the nuclei were placed under tension, stretching them - contrary to our system in which LMNA overexpression reduces the forces transmitted to chromatin. It is important to note, however, that the mechanism proposed for driving H3K9me2 depletion at the nuclear envelope in epidermal stem cells, when stretched, was traced to structural re-organisation of the cytoskeleton, the arrangements of which differ significantly from that of ES cells (epithelial stem cells possess more F-actin stress fibres and F-actin is not localised to the cortex). Nevertheless, our evidence does suggest that the distributions of H3K9me2 and H3K27me3 may be mechanosensitive in ES cells.

Finally, we observed additional evidence of possible mechanosensitivity of H3K9me2: the repressive histone modification was enriched at the periphery of nuclei on the edges of cells, but not when in close proximity with cell-cell junctions, creating a partial ring. This effect was lost during differentiation, where the nuclear periphery was enriched in H3K9me2 in a complete ring. Whether this was a result of the transcriptional changes that occur during differentiation, or tied to changes in cell morphology, notably cell spreading was unclear. As a preliminary experiment, we cultured mouse ES cells in 2i/LIF on gelatin and laminin, the former creating tight colonies and the latter colonies that were more spread. The spread colonies had complete rings of H3K9me2 whereas tight colonies had partial rings away from cell-cell junctions in nuclei at the edges of colonies. This suggests that H3K9me2 may be mechanically regulated as its distribution is tied to cellular morphology. It is interesting to note that H3K9me2 is preferentially enriched in areas of the nuclear periphery next to regions of the cytoskeleton that are highly contractile, which occurs in cells at the edges of colonies in 2i/LIF (Rosowski *et al.* , 2015).

To conclude, this project has characterised and uncovered novel relationships between the dynamics of nuclear shape changes in mouse embryonic stem cells and the components of the cytoskeleton responsible for creating

and propagating forces to the nucleus. We have demonstrated that forces acting on the nucleus are required for ES cell neural lineage specification, but not the exit from naive pluripotency. We have also found evidence that the repressive histone modifications H3K9me2 and H3K27me3, which modulate the interactions of chromatin with the nuclear lamina, are mechanosensitive. While we cannot conclude from this research that nuclear shape changes are responsible for facilitating the movements of lineage specific genes to and from the nuclear lamina, observed by Peric-Hupkes *et al.* (2010), we have made significant progress and laid the groundwork for tackling this question. In the next section I will discuss the next steps that could be taken.

7.5 Future directions

There are several ways in which this project can be developed. In the short term the most pressing goal is to fully characterise the KASH constructs; whether they are reducing nuclear shape changes, and therefore reducing forces on the nucleus, and to ensure that the neural lineage specification experiments are reproducible. Additionally, characterising the magnitude of the nuclear shape changes with the KASH constructs should provide an insight into how the forces are propagated to the nucleus. If forces are transmitted through the cytoskeleton directly to chromatin, then breaking the LINC complex should reduce nuclear shape changes. If, on the other hand, forces are being exerted on the nucleus by fluid flow in the cytoplasm, then breaking the LINC complex would likely not reduce the nuclear shape changes.

In the long term it will be important to show that genes are being misregulated at the nuclear envelope when forces that are transmitted to chromatin are perturbed. There are a few complementary approaches to this that could be taken. The first is to look at the physical location of important lineage genes (e.g. Sox1) in relation to the nuclear envelope during differentiation. The technique most suited for this is DNA fluorescence *in situ* hybridisation (FISH). FISH relies on the ability to create fluorescently labelled probes containing DNA sequences that are complementary to the DNA sequence in a region of interest in the genome. The probes are then applied to fixed cells and hybridise with the (physically intact) genome. The slides can then be imaged under fluorescence microscopy to locate the region of interest. We would hope to find that, when averaged across the population, the loci of lineage specific genes remain in closer proximity to the nuclear envelope

when compared with controls.

The second approach is to conduct RNA sequencing to find genes that are differentially regulated by forces acting at the nuclear envelope during differentiation. By comparing this list with the list of genes that are known to be enriched at the nuclear lamina, obtained through previously conducted DamID studies in ES cells, it will be possible to link spatial and transcriptional information. The hope would be to show that there is a positive correlation between genes that are enriched at the nuclear lamina and those that are differentially regulated during differentiation when forces on the nuclear envelope are perturbed.

Both experimental approaches would go a long way towards increasing our understanding of the role played by forces that act directly on chromatin in regulating transcriptional changes at the nuclear envelope.

Appendix A

A.1 Plasmids and oligonucleotides

Plasmids	
Name	**Origin**
pCAG LifeAct-TagRFP	Ibidi 60107
pCAG LifeAct-TagGFP-ires-Puro	Cloned into backbone Ibidi 60107
pCAG TagRPF-LMNB1	Cloned into backbone Ibidi 60107
pPB-EOS-GFP-ires-Puro	Gift from Silva lab
pPB-TAP IRI (TetO Hyg Dest)	Gift from Silva lab
pDONR221	Gift from Silva lab
pPB-CAG-rtTA	Gift from Silva lab
pCyL43 (PBase)	Gift from Silva lab
TetO Lmna Hyg	Gateway cloned
TetO Lbr Hyg	Gateway cloned
TetO mRFP-SR-KASH Hyg	Gateway cloned
TetO mRFP-KASH Hyg	Gateway cloned
TetO mRFP-KASHΔL Hyg	Gateway cloned

Table A.1: Plasmids used for cloning and transfections. Plasmids kindly gifted by the Silva lab can be found in Dos Santos *et al.* (2014).

Gateway Primers	
Name	**Sequence**
LMNA GATEWAY F	GGGGACAAGTTTGTACAAAAAAGC AGGCTTCGAAGGAGATAGAAC- CATGGAGACCCCGTCACA
LMNA GATEWAY R	GGGGACCACTTTGTACAAGAAAGC TGGGTCTTACATGATGCT- GCAGTTCTG
LBR GATEWAY F	GGGGACAAGTTTGTACAAAAAAAG CAGGCGCCACCATGCCAAGTAG- GAAGTTTGTTG
LBR GATEWAY R	GGGGACCACTTTGTACAAGAAAGC TGGGTATCAGTAAATG- TAGGGGAATATGCG
mRFP GATEWAY F	GGGGACAAGTTTGTACAAAAAAGC AGGCGCCACCATGGCCTCCTCC- GAG
KASH GATEWAY R	GGGGACCACTTTGTACAAGAAAGC TGGGTACTATGTGGGGGGTGGC
KASHΔL R	GGGGACCACTTTGTACAAGAAAGC TGGGTACTAGCAGCTG- TAGTCTTCTTCG
LMNB1 F IND	GGGGACAAGTTTGTACAAAAAAGC AGGCTCATTTTGGCAAAGAATTA- GATCC
LMNB1 R IND	GGGGACCACTTTGTACAAGAAAGC TGGGTCTCACATAATG- GCACAGCTT
LMNB1-tagRFP R IND	GGGGACCACTTTGTACAAGAAAGC TGGGTCTCAATTAAGTTTGTGC- CCC

Table A.2: Oligonucleotides used for Gateway cloning.

Sequencing Primers	
Name	**Sequence**
SR-KASH F1	GACAGCCCTTCCTGTCCCGA
SR-KASH F2	CGCTCATGCAGTGCCAGGAC
SR-KASH F3	CAGCTGCACTCAGGCCAACA
SR-KASH R1	TATAAGGGGTGCTGGACGCAGG
SR-KASH R2	TGAGCCTTCTGCCTCCGGTT
mRFP R1	CGCGCTCGTACTGTTCCACG
mRFP F1	GGCCAAGAAGCCCGTGCAG
LifeAct-GFP F1	GGCTTCTGGCGTGTGACC
LifeAct-GFP F2	TATCGAATTCCGCCCCTCTC
LifeAct-GFP F3	ACCACCAGGGCAAGGGTCT
LifeAct-GFP F4	TGCACGAGTGGGTTACATCG
LifeAct-GFP R1	CCGCCTTTGCAGGTGTATCT
LifeAct-GFP R2	TCTCATGAGCGGATACATA
LMNA SEQ R	AGCCCGCAGCTCCTG
LMNA SEQ R2	CCGTTATCGATCTCCACAA
LMNA SEQ F1	GGCAGGTAGCCAAGCTTG
LMNA SEQ F2	TGGCCCTGGACATGGA
GFP-IRES-Puro SeqR1	AGTTCTTGCAGCTCGGTGAC
GFP-IRES-Puro SeqF1	CCTGAGCAAAGACCCCAAC
tagRFP F1	CATGGGAGAGAGTCACCACA
tagRFP R1	CCTCGGATGTGCACTTGAAG
pCAG F1	TCCCCTTCTCCCTCTCCAG
LMNB1 SEQ1	TCAAGGCTCTCTACGAGACCG
LMNB1 SEQ2	GTACAAGCTGGCTCAAGCCC
LMNB1 SEQ3	GTCCTCCAGTCGCAGTGTG
LMNB1 SEQ4	GCACAGTCTTCAAGACCACCATAC
LBR R1	GGTCCTTCTGCCTGCACTG
LBR R2	TAAAAGGCCTGGAGGCTGTA
LBR F1	GGAAGGACTTGGAGTTTGGA
LBR F2	GAAGCACTGCTGACCTCCAT

Table A.3: Oligonucleotides used for sequencing.

InFusion Primers	
Name	**Sequence**
AmpR R INF	GTCCTGATAGCGGTCGGATCTTCA CCTAGATCCTTTTAA
AmpR F INF	CATCGATGATCTAGAAATGTGCGC GGAACC
GFP-IRES-Puro R	GGTTCCGCGCACATTTCTAGATCA TCGATGCATGG
GFP-IRES-Puro F	AAGGGGATCCACCGGTCGCCACCA TGGTGAGCAA
LMNB1 NTERM F	GTACCGGTCCCGCCATGGCGACCG CGACCCCCGT
LMNB1 NTERM F2	GTACCGGTCCCGCCATGGCGACCG CG
LMNB1 NTERM R	CGACCGGTCCTCCGCACATAATGG CACAGCTTTT
LMNB1 R INF	CATGGTGGCGACCGGTCCTCCGCA CATAATGGCACAGCTTTT
LMNB1 F INF	AATTAGATCCACCGGATGGCGACC GCG
LMNB1 F INF2	AATTAGATCCACCGGTCCCGCCAT GGCG
RFP-LMNB1 F INF	TCAGATCTCGAGCTCAAGCTTCGA TGGCGACCGCGAC
RFP-LMNB1 F INF2	TCAGATCTCGAGCTCAAGCTTCGA TGGCGCCGCGAC
RFP-LMNB1 R INF	GAGCTCGAGATCTGAGTCCGGAAT TAAGTTTGTGCCCCAG
LMNB1-VECT INF	ATCTAGAGTCGCGGCCTCACATAA TGGCACAGCT
LMNB1-VECT INF2	ATCTAGAGTCGCGGCCTCACATAA TGGCACAGCTTTTATTG
VECT-RFP INF	AGAATTAGATCTCGAGCCACCATG GTGTCTAAG

Table A.4: Oligonucleotides used for In-Fusion cloning.

A.2 Cell culture media

For 100 ml N2B27			
Reagent	**Conc. /µM**	**Conc. /mg ml^{-1}**	**Volume /ml**
Neurobasal Medium	-	-	49
DMEM F12 Ham	-	-	49
N2	-	-	0.5
B-27	-	-	1
L-Glutamine	2.2×10^3	-	-
2-Mercaptoethanol	1.1×10^2	-	-
For 100 ml 2i/LIF			
N2B27	-	-	100
CH99021 (Chiron)	3	-	-
PD0325901 (PD03)	1	-	-
LIF	-	1.0×10^{-2}	0.22

Table A.5: Cell culture media recipe.

For 10 ml N2		
Reagent	**Conc./mg ml^{-1}**	**Volume /ml**
DMEM F-12 Ham	-	5.36
Apotransferrin solution	10	-
Insulin	2.5	-
Sodium selenate solution	0.518	-
Putrescine solution	1.6	-
Progesterone solution	1.98×10^{-3}	
BSA	-	1

Table A.6: N2 components, made in-house.

A.3 Antibodies

Primary Antibodies		
Name	**Dilution**	**Catalogue no.**
Anti-Lamin B1	1/1000	Abcam ab16048
Anti-Lamin B Receptor	1/200	Abcam ab122919
Anti-Lamin C	?	Abcam ab8981
Anti-Emerin	?	Abcam ab156871
Anti-Nesprin 1	?	Abcam ab24742
Anti-SUN2	1/200	Abcam ab124916
Anti-SUN1	1/200	Abcam ab103021
Anti-Nuclear Pore Complex Proteins	?	Abcam ab50008
Tri-Methyl-Histone H3 (Lys4)	1/1000	Abcam ab8580
Di-Methyl-Histone H3 (Lys9	1/200	Abcam ab1220
Tri-Methyl-Histone H3 (Lys4)	1/400	CST 9751S
Tri-Methyl-Histone H3 (Lys27)	1/1600	CST 9733S
Tri-Methyl-Histone H3 (Lys9)	1/800	CST 13969P
Sox1	1/200	CST 4194S
Lamin A/C	1/200	CST 4777S
Tri-Methyl-Histone H3 (Lys27) Alexa Fluor 488 Conjugate	1/50	CST 5499S
Anti-Sox1	1/100	R&D Systems AF3369
Anti-Brachyury	1/200	R&D Systems AF2085
Lamin A	1/100	Santa Cruz SC-20680
Secondary Antibodies		
Goat anti-Rabbit Alexa Fluor 488	1/400	Thermo Fisher A11008
Goat anti-Mouse Alexa Fluor 488	1/400	Thermo Fisher A21121
Donkey anti-Mouse Alexa Fluor 488	1/400	Thermo Fisher A21202
Donkey anti-Rabbit Alexa Fluor 488	1/400	Thermo Fisher A21206
Donkey anti-Rabbit Alexa Fluor 555	1/400	Thermo Fisher A31572
Donkey anti-Goat Alexa Fluor 555	1/400	Thermo Fisher A21432
Donkey anti-Goat Alexa Fluor 647	1/400	Thermo Fisher A21447

Table A.7: Antibodies used for immunofluorescence.

A.4 siRNA knockdown

siRNA Knockdown		
siRNA	**Volume /µl**	**Catalogue no.**
ON-TARGETplus Mouse LBR	0.5	L-051330-01-0005
siGENOME Mouse Sun1	0.5	M-040715-00-0005
siGENOME Mouse Sun2	0.5	M-041247-01-0005
Scrambled	0.5	D-001810-10-05
RNAiMax Lipofectamine	0.5	See reagent list
2i/LIF or N2B27	100	-

Table A.8: Reagents for siRNA knockdown in 24-well plate format.

A.5 Taqman probes

Taqman Probes		
Gene	**Dye**	**Catalogue no.**
Nanog	FAM	Mm02384862_g1
Rex1	FAM	Mm03053975_g1
Oct4	FAM	Mm00658129_gH
Klf4	FAM	Mm00516104_m1
Tcfcp2l1	FAM	Mm00470119_m1
LMNB1	FAM	Mm00521949_m1
LMNA/C	FAM	Mm00497783_m1
Fgf5	FAM	Mm03053745_s1
Dnmt3b	FAM	Mm01240113_m1
Otx2	FAM	Mm00446859_m1
Sox1	FAM	Mm00486299_s1
Pou3f1	FAM	Mm00843534_s1
Brachyury	FAM	Mm01318252_m1
Sun1	FAM	Mm00659179_m1
Sun2	FAM	Mm01299500_m1
Lbr	FAM	Mm00522574_m1
GAPDH	VIC	4352339E

Table A.9: TaqMan probes used for qPCR.

A.6 Kits and reagents

Kits		
Name	**Manufacturer**	**Catalogue no.**
QIAquick Gel Extraction Kit	Qiagen	28704
QIAquick PCR Purification Kit	Qiagen	28104
QIAprep Spin Miniprep Kit	Qiagen	27104
RNeasy Mini Kit	Qiagen	74104
Plasmid Maxi Kit	Qiagen	12162
Plasmid Mini Kit	Qiagen	12123
RNase-Free DNase Set	Qiagen	79254
PureLink Plasmid Miniprep Kit	Invitrogen	K210010
Alkaline Phosphatase Kit	Millipore	SCR004
Reagents		
MicroAmp 96-Well Reaction Plate	Applied Biosystems	4346907
TaqMan Master Mix	Applied Biosystems	4352042
8-Strip PCR Caps	STARLAB	I1400-0900
Clear Polyolefin StarSeal	STARLAB	E2796-9793
Gateway BP Clonase II	Invitrogen	11789-020
Gateway LR Clonase II	Invitrogen	11791-020
SuperScript III First-Strand SS	Invitrogen	18080-051
Zeocin	Invitrogen	45-0430
Hygromycin B	Invitrogen	10687-010
Lipofectamine 2000 Reagent	Invitrogen	11668-030
Lipofectamine RNAiMAX Reagent	Invitrogen	13778-100
mLIF	Homemade	Biochem
N2	Homemade	SCI

Table A.10: Kits and reagents.

Reagents		
Name	**Manufacturer**	**Catalogue no.**
Neurobasal Medium	Gibco	21103-049
DMEM F-12 Ham	Gibco	21331-020
Geneticin G418	Gibco	10131-035
L-Glutamine	Gibco	25030-081
B-27 Supplement	Gibco	17504-044
2-Mercaptoethanol	Gibco	21985023
Q5 Hot Start HF DNA Polymerase	New England Biolabs	M0493S
μ-Dish 35mm, high	Ibidi	81156
E.cloni 10G DUOs	Lucigen	60107
Corning Fibronectin, Human	Fisher Scientific	354008
Jasplakinolide	Cambridge Bioscience	CAY11705-100
SiR-DNA (SiR-Hoechst)	Spirochrome AG	SC007
CH99021	Sigma-Aldrich	SML1046
PD0325901	Sigma-Aldrich	PZ0162
Laminin	Sigma-Aldrich	L2020
GMEM	Sigma-Aldrich	G5154
Dulbecco's Phosphate Buffered Saline	Sigma-Aldrich	D8537
Blebbistatin	Sigma-Aldrich	B0560
Nocodazole	Sigma-Aldrich	M1404
Y-27632	Sigma-Aldrich	Y0503
Hoechst 33342	Sigma-Aldrich	B2261

Table A.11: Reagents continued.

Bibliography

Annunziato, A. T. 2015. The fork in the road: Histone partitioning during DNA replication. *Genes*, **6**(2), 353–371.

Bannister, A. J., & Kouzarides, T. 2011. Regulation of chromatin by histone modifications. *Cell research*, **21**(3), 381–395.

Bian, Q., Khanna, N., Alvikas, J., & Belmont, A. S. 2013. β-Globin cis-elements determine differential nuclear targeting through epigenetic modifications. *The Journal of Cell Biology*, **203**(5), 767–783.

Brangwynne, C. P., MacKintosh, F. C., Kumar, S., Geisse, N. A., Talbot, J., Mahadevan, L., Parker, K. K., Ingber, D. E., & Weitz, D. A. 2006. Microtubules can bear enhanced compressive loads in living cells because of lateral reinforcement. *Journal of Cell Biology*, **173**(5), 733–741.

Burgess, R. J., & Zhang, Z. 2014. Histone chaperones in nucleosome assembly and human disease. *Nat Struct Mol Biol.*, **20**(1), 14–22.

Buxboim, A., Swift, J., Irianto, J., Spinler, K. R., Dingal, P. C. D. P., Athirasala, A., Kao, Y.-R. C., Cho, S., Harada, T., Shin, J. W., & Discher, D. E. 2014. Matrix elasticity regulates lamin-A,C phosphorylation and turnover with feedback to actomyosin. *Current Biology*, **24**(16), 1909–1917.

Cao, J., & Yan, Q. 2012. Histone ubiquitination and deubiquitination in transcription, DNA damage response, and cancer. *Frontiers in Oncology*, **2**, 1–9.

Carvajal, A. S., McKenna, T., Arzt, E. W., & Eriksson, M. 2015. Overexpression of lamin B receptor results in impaired skin differentiation. *PLoS ONE*, **10**(6), 1–14.

Cavey, M., & Lecuit, T. 2009. Molecular bases of cell-cell junctions stability and dynamics. *Cold Spring Harbor Perspectives in Biology*, **2**(26), 1–9.

Chang, Y.-C., Nalbant, P., Birkenfeld, J., Chang, Z.-F., & Bokoch, G. M. 2008. GEF-H1 couples nocodazole-induced microtubule disassembly to cell contractility via RhoA. *Molecular Biology of the Cell*, **19**(5), 2147–2153.

Chugh, P., Clark, A. G., Smith, M. B., Cassani, D. A. D., Dierkes, K., Ragab, A., Roux, P. P., Charras, G., Salbreux, G., & Paluch, E. K. 2017. Actin cortex architecture regulates cell surface tension. *Nat. Cell Biol.*, **19**(6), 689–697.

Constantinescu, D., Gray, H. L., Sammak, P. J., Schatten, G. P., & Csoka, A. B. 2006. Lamin A/C expression is a marker of mouse and human embryonic stem cell differentiation. *Stem cells*, **24**(1), 177–185.

Danowski, B. A. 1989. Fibroblast contractility and actin organization are stimulated by microtubule inhibitors. *Journal of Cell Science*, **93**(3280), 255–266.

Dixon, J. R., Jung, I., Selvaraj, S., Shen, Y., Jessica, E., Lee, A. Y., Ye, Z., Kim, A., Rajagopal, N., Diao, Y., Liang, J., Zhao, H., Lobanenkov, V. V., Ecker, J. R., Thomson, J., & Ren, B. 2015. Chromatin architecture reogranization during stem cell differentiation. **518**(7539), 331–336.

Dos Santos, Rodrigo L., Tosti, Luca, Radzisheuskaya, Aliaksandra, Caballero, Isabel M., Kaji, Keisuke, Hendrich, Brian, & Silva, José C R. 2014. MBD3/NuRD facilitates induction of pluripotency in a context-dependent manner. *Cell Stem Cell*, **15**(1), 102–110.

Eckersley-Maslin, M. A .and Bergmann, J. H., Lazar, Z., & Spector, D. L. 2013. Lamin A/C is expressed in pluripotent mouse embryonic stem cells. *Nucleus*, **4**(1), 53–60.

Engler, A. J., Sen, S., Sweeney, H. L., & Discher, D. E. 2006. Matrix elasticity directs stem cell lineage specification. *Cell*, **126**(4), 677–689.

Evans, M. J., & Kaufman, M. H. 1981. *Establishment in culture of pluripotential cells from mouse embryos.*

Finlan, L. E., Sproul, D., Thomson, I., Boyle, S., Kerr, E., Perry, P., Ylstra, B., Chubb, J. R., & Bickmore, W. A. 2008. Recruitment to the nuclear

periphery can alter expression of genes in human cells. *PLoS Genetics*, **4**(3).

Fletcher, D. A., & Mullins, R. D. 2010. Cell mechanics and the cytoskeleton. *Nature*, **463**(7280), 485–92.

Frock, R. L., Kudlow, B. A., Evans, A. M., Jameson, S. A., Hauschka, S. D., & Kennedy, B. K. 2006. Lamin A / C and emerin are critical for skeletal muscle satellite cell differentiation. *Genes & development*, **20**, 486–500.

Gaspar-Maia, A., Alajem, A., Meshorer, E., & Ramalho-Santos, M. 2011. Open chromatin in pluripotency and reprogramming. *Nature Reviews Molecular Cell Biology*, **12**(4), 273–273.

Gittes, F., Mickey, B., Nettleton, J., & Howard, J. 1993. Flexural rigidity of microtubules and actin filaments measured from thermal fluctuations in shape. *Journal of Cell Biology*, **120**(4), 923–934.

Guelen, L., Pagie, L., Brasset, E., Meuleman, W., Faza, M. B., Talhout, W., Eussen, B. H., de Klein, A., Wessels, L., de Laat, W., & van Steensel, B. 2008. Domain organization of human chromosomes revealed by mapping of nuclear lamina interactions. *Nature*, **453**(7197), 948–51.

Guo, F., Li, L., Li, J., Wu, X., Hu, B., Zhu, P., & Wen, L. 2017. Single-cell multi-omics sequencing of mouse early embryos and embryonic stem cells. **27**, 967988.

Hahn, C., & Schwartz, M. A. 2009. Mechanotransduction in vascular physiology and atherogenesis. *Nat Rev Mol Cell Biol*, **10**(1), 53–62.

Hampoelz, B., Azou-Gros, Y., Fabre, R., Markova, O., Puech, P.-H., & Lecuit, T. 2011. Microtubule-induced nuclear envelope fluctuations control chromatin dynamics in Drosophila embryos. *Development*, **138**(16), 3377–3386.

Harada, T., Swift, J., Irianto, J., Shin, J. W., Spinler, K. R., Athirasala, A., Diegmiller, R., Dingal, P. C. D. P., Ivanovska, I. L., & Discher, D. E. 2014. Nuclear lamin stiffness is a barrier to 3D migration, but softness can limit survival. *Journal of Cell Biology*, **204**(5), 669–682.

Harr, J. C., Luperchio, T. R., Wong, X., Cohen, E., Wheelan, S. J., & Reddy, K. L. 2015. Directed targeting of chromatin to the nuclear lamina

is mediated by chromatin state and A-type lamins. *The Journal of Cell Biology*, **208**(1), 33–52.

Hoffmann, K., Sperling, K., Olins, A. L., & Olins, D. E. 2007. The granulocyte nucleus and lamin B receptor: Avoiding the ovoid. *Chromosoma*, **116**(3), 227–235.

Hudspeth, A. J. 2014. Integrating the active process of hair cells with cochlear function. *Nat Rev Neurosci*, **15**(9), 600–614.

Inoué, S., & Salmon, E. D. 1995. Force generation by microtubule assembly/disassembly in mitosis and related movements. *Molecular biology of the cell*, **6**(12), 1619–40.

Jaalouk, D. E., & Lammerding, J. 2009. Mechanotransduction gone awry. *Nature Reviews Molecular Cell Biology*, **10**(1), 63–73.

Janson, M. E., & Dogterom, M. 2004. A bending mode analysis for growing microtubules: evidence for a velocity-dependent rigidity. *Biophysical journal*, **87**(4), 2723–36.

Kalkan, T., & Smith, A. 2014. Mapping the route from naive pluripotency to lineage specification. *Philosophical transactions of the Royal Society of London. Series B, Biological sciences*, **369**(1657), 20130540–.

Kind, J., Pagie, L., Ortabozkoyun, H., Boyle, S., De Vries, S. S., Janssen, H., Amendola, M., Nolen, L. D., Bickmore, W. A., & Van Steensel, B. 2013. Single-cell dynamics of genome-nuclear lamina interactions. *Cell*, **153**(1), 178–192.

Kumar, A., Maitra, A., Sumit, M., Ramaswamy, S., & Shivashankar, G. V. 2014. Actomyosin contractility rotates the cell nucleus. *Scientific reports*, **4**, 3781.

Lammerding, J., Fong, L. G., Ji, J. Y., Reue, K., Stewart, C. L., Young, S. G., & Lee, R. T. 2006. Lamins A and C but not lamin B1 regulate nuclear mechanics. *Journal of Biological Chemistry*, **281**(35), 25768–25780.

Lanzuolo, C., Sardo, F. L., Orlando, V., & Drosophila, I. 2012. Concerted epigenetic signatures inheritance at PcG targets through replication. *Cell Cycle*, **11**(7), 1296–1300.

Le, H. Q., Ghatak, S., Yeung, C.-Y. C., Tellkamp, F., Günschmann, C., Dieterich, C., Yeroslaviz, A., Habermann, B., Pombo, A., Niessen, C. M., & Wickström, S. A. 2016. Mechanical regulation of transcription controls Polycomb-mediated gene silencing during lineage commitment. *Nature Cell Biology*, **18**(8), 864–875.

Leeb, M, Dietmann, S, Paramor, M., Niwa, H., & Smith, A. 2014. Genetic Exploration of the exit from self-renewal using haploid embryonic stem cells. *Cell Stem Cell*, **14**, 385–393.

Li, Y., Lovett, D., Zhang, Q., Neelam, S., Kuchibhotla, R. A., Zhu, R., Gundersen, G. G., Lele, T. P., & Dickinson, R. B. 2015. Moving cell boundaries drive nuclear shaping during cell spreading. *Biophysical Journal*, **109**(4), 670–686.

Liao, F.-F, Xu, H., Torrey, N., Road, P., & Jolla, L. 2015. HHS Public Access. *Nat. Rev. Mol. Cell Biol.*, **2**(74), 519–532.

Lieberman-Aiden, E., van Berkum, N. L., Williams, L., Imakaev, M., Ragoczy, T., Telling, A., Amit, I., Lajoie, B. R., Sabo, P. J., Dorschner, M. O., Sandstrom, R., Bernstein, B., Bender, M. A., Groudine, M., Gnirke, A., Stamatoyannopoulos, J., Mirny, L. A., Lander, E. S., & Dekker, J. 2009. Comprehensive mapping of long-range interactions reveals folding principles of the human genome. *Science*, **326**(5950), 289–293.

Lowe, M., Hostager, R., & Nobuaki, K. 2016. Preservation of epigenetic memory during DNA replication matthew. *J Stem Cell Res Ther*, **8**(12), 1699–1712.

Luxton, G. W. G., Gomes, E. R., Folker, E. S., & Worman, H. Gunderson G. G. 2011. TAN lines: a novel nuclear envelope structure involved in nuclear positioning. *Nucleus*, **2**(3), 173–81.

Martin, G. R. 1981. Isolation of a pluripotent cell line from early mouse embryos cultured in medium conditioned by teratocarcinoma stem cells. *Proc Natl Acad Sci U S A*, **78**(12), 7634–7638.

Martinac, B. 2004. Mechanosensitive ion channels: molecules of mechanotransduction. *Journal of cell science*, **117**(12), 2449–2460.

Mattila, P. K., & Lappalainen, P. 2008. Filopodia: molecular architecture and cellular functions. *Nature Reviews: Molecular Cell Biology*, **9**, 446–454.

May, R. C., & Machesky, L. M. 2001. Phagocytosis and the actin cytoskeleton. *Journal of cell science*, **114**(Pt 6), 1061–1077.

McBeath, R., Pirone, D. M., Nelson, C. M., Bhadriraju, K., & Chen, C. S. 2004. Cell shape, cytoskeletal tension, and RhoA regulate stem cell lineage commitment. *Developmental Cell*, **6**(4), 483–495.

Meshorer, E., Yellajoshula, D., George, E., Scambler, P. J., Brown, D. T., & Misteli, T. 2006. Hyperdynamic plasticity of chromatin proteins in pluripotent embryonic stem cells. *Developmental Cell*, **10**(1), 105–116.

Mitchison, T, & Kirschner, M. 1984. Dynamic instability of microtubule growth. *Nature*, **312**(5991), 237–42.

Miyake, Y., Inoue, N., Nishimura, K., Kinoshita, N., Hosoya, H., & Yonemura, S. 2006. Actomyosin tension is required for correct recruitment of adherens junction components and zonula occludens formation. *Experimental Cell Research*, **312**(9), 1637–1650.

Moldovan, G. L., Pfander, B., & Jentsch, S. 2007. PCNA, the maestro of the replication fork. *Cell*, **129**(4), 665–679.

Morgani, S. M., Canham, M. A., Nichols, J., Sharov, A. A., Migueles, R. P., Ko, M. S. H., & Brickman, J. M. 2013. Totipotent embryonic stem cells arise in ground-state culture conditions. *Cell Reports*, **3**(6), 1945–1957.

Nagano, T., Lubling, Y., Stevens, T. J., Schoenfelder, S., & Yaffe, E. 2014. Europe PMC funders group single cell Hi-C reveals cell-to-cell variability in chromosome structure. **502**(7469).

Nichols, J., & Smith, A. 2012. Pluripotency in the embryo and in culture. *Cold Spring Harbor Perspecti ves in Biology*, **4**, 1–15.

Oakes, P. W., Beckham, Y., Stricker, J., & Gardel, M. L. 2012. Tension is required but not sufficient for focal adhesion maturation without a stress fiber template. *Journal of Cell Biology*, **196**(3), 363–374.

Olins, A, Zwerger, M., Herrmann, H., Zentgraf, H., Simon, A., Monestier, M., & Olins, D. 2008. The human granulocyte nucleus: Unusual nuclear

envelope and heterochromatin composition. *European Journal of Cell Biology*, **87**(5), 279–290.

Pajerowski, J. D., Dahl, K. N., Zhong, F. L., Sammak, P. J., & Discher, D. E. 2007. Physical plasticity of the nucleus in stem cell differentiation. *Proceedings of the National Academy of Sciences of the United States of America*, **104**(40), 15619–15624.

Pellegrin, S., & Mellor, H. 2007. Actin stress fibres. *Journal of cell science*, **120**(20), 3491–9.

Peng, X., Nelson, E. S., Maiers, J. L., & Demali, K. A. 2015. Histone-modifying enzymes, histone modifications and histone chaperones in nucleosome assembly: Lessons learned from Rtt109 histone acetyltransferases. *Crit. Rev. Biochem. Mol. Biol.*, **50**(1), 31–53.

Perepelina, K. I., Smolina, N. A., Zabirnik, A. S., Dmitrieva, R. I., Malashicheva, A. B., & Kostareva, A. A. 2017. The role of LMNA mutations in myogenic differentiation of C2C12 and primary satellite cells. *Cell and Tissue Biology*, **11**(3), 213–219.

Peric-Hupkes, D., & van Steensel, B. 2010. Role of the nuclear lamina in genome organization and gene expression. *Cold Spring Harbor Symposia on Quantitative Biology*, **75**(4), 517–524.

Peric-Hupkes, D., Meuleman, W., Pagie, L., Bruggeman, S. W. M., Solovei, I., Brugman, W., Gräf, S., Flicek, P., Kerkhoven, R. M., van Lohuizen, M., Reinders, M., Wessels, L., & van Steensel, B. 2010. Molecular maps of the reorganization of genome-nuclear lamina interactions during differentiation. *Molecular Cell*, **38**(4), 603–613.

Phair, R. D., Scaffidi, P., Elbi, C., Vecerová, J., Dey, A., Ozato, K., Brown, D. T., Hager, G., Bustin, M., & Misteli, T. 2004. Global nature of dynamic protein-chromatin interactions in vivo: three-dimensional genome scanning and dynamic interaction networks of chromatin proteins. *Molecular and cellular biology*, **24**(14), 6393–6402.

Prokocimer, M., Davidovich, M., Nissim-Rafinia, M., Wiesel-Motiuk, N., Bar, D. Z., Barkan, R., Meshorer, E., & Gruenbaum, Y. 2009. Nuclear lamins: key regulators of nuclear structure and activities. *Journal of cellular and molecular medicine*, **13**(6), 1059–1085.

Rajgor, D., & Shanahan, C. M. 2013. Nesprins: from the nuclear envelope and beyond. *Expert reviews in molecular medicine*, **15**(e5), 1–17.

Reddy, K. L., Zullo, J. M., Bertolino, E., & Singh, H. 2008. Transcriptional repression mediated by repositioning of genes to the nuclear lamina. *Nature*, **452**(7184), 243–7.

Riedl, J., Crevenna, A. H., Kessenbrock, K., Yu, J. H., Bista, M., Bradke, F., Jenne, D., Holak, T. A., Werb, Z., Sixt, M., Wedlich-Soldner, R., Klopferspitz, A., Avenue, P., & Francisco, S. 2010. Lifeact: a versatile marker to visualize F-actin. *Nat. Methods*, **5**(7), 1–8.

Rosowski, K. A., Mertz, A. F., Norcross, S., Dufresne, E. R., & Horsley, V. 2015. Edges of human embryonic stem cell colonies display distinct mechanical properties and differentiation potential. *Scientific Reports*, **5**(1), 14218.

Schreiner, S. M., Koo, P. K., Zhao, Y., Mochrie, S. G. J., & King, M. C. 2015. The tethering of chromatin to the nuclear envelope supports nuclear mechanics. *Nature Communications*, **6**, 7159.

Semrau, S., Goldmann, J., Soumillon, M., Tarjei, S., Jaenisch, R., & Oudenaarden, A. V. 2016. Dynamics of lineage commitment revealed by single-cell transcriptomics of differentiating embryonic stem cells. 1–31.

Shewan, A. M. 2005. Myosin 2 Is a key Rho Kinase target cecessary for the local concentration of E-Cadherin at cell-cell contacts. *Molecular Biology of the Cell*, **16**(10), 4531–4542.

Shin, J.-W., Spinler, K. R., Swift, J., Chasis, J. A., Mohandas, N., & Discher, D. E. 2013. Lamins regulate cell trafficking and lineage maturation of adult human hematopoietic cells. *Proceedings of the National Academy of Sciences of the United States of America*, **110**(47), 18892–18897.

Smutny, M., Cox, H. L., Leerberg, J. M., Kovacs, E. M., Conti, M. A., Ferguson, C., Hamilton, N. A., Parton, R. G., Adelstein, R. S., & Yap, A. S. 2010. Myosin II isoforms identify distinct functional modules that support integrity of the epithelial zonula adherens. *Nature Cell Biology*, **12**(7), 696–702.

Solovei, I., Wang, A. S., Thanisch, K., Schmidt, C. S., Krebs, S., Zwerger, M., Cohen, T. V., Devys, D., Foisner, R., Peichl, L., Herrmann, H., Blum,

H., Engelkamp, D., Stewart, C. L., Leonhardt, H., & Joffe, B. 2013. LBR and lamin A/C sequentially tether peripheral heterochromatin and inversely regulate differentiation. *Cell*, **152**(3), 584–598.

Swift, J., Ivanovska, I. L., Buxboim, A., Harada, T., Dingal, P. C. D. P., Pinter, J., Pajerowski, J. D., Spinler, K. R., Shin, J.-W., Tewari, M., Rehfeldt, F., Speicher, D. W., & Discher, D. E. 2013. Nuclear lamin-A Scales with tissue stiffness and enhances matrix-directed differentiation. *Science*, **341**(6149), 1240104–1240104.

Tajik, A., Zhang, Y., Wei, F., Sun, J., Jia, Q., Zhou, W., Singh, R., Khanna, N., Belmont, A. S., & Wang, N. 2016. Transcription upregulation via force-induced direct stretching of chromatin. *Nature Materials*, **15**(12), 1287–1296.

Takahashi, K., & Yamanaka, S. 2006. Induction of pluripotent stem cells from mouse embryonic and adult fibroblast cultures by defined factors. *Cell*, **126**(4), 663–676.

Talwar, S., Kumar, A., Rao, M., Menon, G. I., & Shivashankar, G. V. 2013. Correlated spatio-temporal fluctuations in chromatin compaction states characterize stem cells. *Biophysical Journal*, **104**(3), 553–564.

Towbin, B. D., González-Aguilera, C., Sack, R., Gaidatzis, D., Kalck, V., Meister, P., Askjaer, P., & Gasser, S. M. 2012. Step-wise methylation of histone H3K9 positions heterochromatin at the nuclear periphery. *Cell*, **150**(5), 934–947.

Vogel, M. J., Peric-Hupkes, D., & van Steensel, B. 2007. Detection of in vivo protein-DNA interactions using DamID in mammalian cells. *Nature protocols*, **2**(6), 1467–78.

Walker, A., Su, H., Conti, M. A., Harb, N., Adelstein, R. S., & Sato, N. 2010. Non-muscle myosin II regulates survival threshold of pluripotent stem cells. *Nature Communications*, **1**(6), 1–9.

Walter, M., Teissandier, A., Pérez-Palacios, R., & Bourc'his, D. 2016. An epigenetic switch ensures transposon repression upon dynamic loss of DNA methylation in embryonic stem cells. *eLife*, **5**(9), 1689–1699.

Wang, N., Tytell, J. D., & Ingber, D. E. 2009. Mechanotransduction at a distance: mechanically coupling the extracellular matrix with the nucleus. *Nature reviews. Molecular cell biology*, **10**(1), 75–82.

Wen, L., & Tang, F. 2016. Single-cell sequencing in stem cell biology. *Genome Biology*, **17**(71), 1–12.

Wiche, G. 1998. Role of plectin in cytoskeleton organization and dynamics. *Journal of cell science*, **111**, 2477–2486.

Ying, Q. L., Nichols, J., Chambers, I., & Smith, A. 2003. BMP induction of Id proteins suppresses differentiation and sustains embryonic stem cell self-renewal in collaboration with STAT3. *Cell*, **115**(3), 281–292.

Ying, Q. L., Wray, J., Nichols, J., Batlle-Morera, L., Doble, B., Woodgett, J., Cohen, P., & Smith, A. 2008. The ground state of embryonic stem cell self-renewal. *Nature*, **453**(7194), 519–523.

Zhang, Y., Ng, H. H., Erdjument-Bromage, H., Tempst, P., Bird, A., & Reinberg, D. 1999. Analysis of the NuRD subunits reveals a histone deacetylase core complex and a connection with DNA methylation. *Genes and Development*, **13**(15), 1924–1935.

Zullo, J. M., Demarco, I. A., Piqué-Regi, R., Gaffney, D. J., Epstein, C. B., Spooner, C. J., Luperchio, T. R., Bernstein, B. E., Pritchard, J. K., Reddy, K. L., & Singh, H. 2012. DNA sequence-dependent compartmentalization and silencing of chromatin at the nuclear lamina. *Cell*, **149**(7), 1474–1487.